

UNIVERSITY OF OKLAHOMA

GRADUATE COLLEGE

PERFORMANCE EVALUATION OF THE THIRD GENERATION

TD-SCDMA SYSTEM

A Dissertation

SUBMITTED TO THE GRADUATE FACULTY

in partial fulfillment of the requirements for the

degree of

Doctor of Philosophy

By

SHUQING LIU  
Norman, Oklahoma  
2004

UMI Number: 3120036

### INFORMATION TO USERS

The quality of this reproduction is dependent upon the quality of the copy submitted. Broken or indistinct print, colored or poor quality illustrations and photographs, print bleed-through, substandard margins, and improper alignment can adversely affect reproduction.

In the unlikely event that the author did not send a complete manuscript and there are missing pages, these will be noted. Also, if unauthorized copyright material had to be removed, a note will indicate the deletion.

**UMI**<sup>®</sup>

---

UMI Microform 3120036

Copyright 2004 by ProQuest Information and Learning Company.

All rights reserved. This microform edition is protected against unauthorized copying under Title 17, United States Code.

ProQuest Information and Learning Company  
300 North Zeeb Road  
P.O. Box 1346  
Ann Arbor, MI 48106-1346

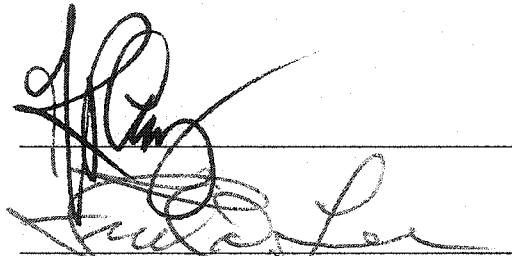
© Copyright by SHUQING LIU 2004

All Rights Reserved

PERFORMANCE EVALUATION OF THE THIRD GENERATION  
TD-SCDMA SYSTEM

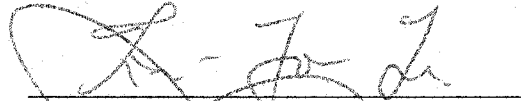
A Dissertation APPROVED FOR THE  
SCHOOL OF ELECTRICAL AND COMPUTER ENGINEERING

BY



Handwritten signature of the author, appearing to be 'Kerem Aslan', written over a horizontal line.

Kerem Aslan



Handwritten signature of the advisor, appearing to be 'T. J. Li', written over a horizontal line.



Handwritten signature of the advisor, appearing to be 'T. J. Li', written over a horizontal line.

## ACKNOWLEDGEMENTS

Firstly, I would like to express my sincere gratitude to my advisor, Dr. J. R. Cruz, for his guidance, encouragement and support throughout my Ph.D. studies. It is his technical expertise and wisdom that helped make this work possible. His valuable teaching and advice, both academic and non-academic, will benefit me forever.

Secondly, I would like to thank Dr. John Cheung, Dr. Kevin Grasse, Dr. Fred Lee and Dr. Tianyou Yu for their support and their time serving on my committee. I am blessed to have such a wonderful committee.

I am also appreciative of Dr. Rohani Kamyar, who used to work at the Motorola Research Center, for his precious help on the cooperative projects with Motorola. His passing away was a great loss.

I also thank my other lab mates in the Communications Signal Processing Laboratory for the helpful discussions and their friendship.

Finally, I would like to thank Motorola, Inc. for support this research project.

*To my wonderful husband Hongxin and our lovely son Jeffrey*

# TABLE OF CONTENTS

<b>ABSTRACT</b> .....	<b>xiii</b>
<b>1 INTRODUCTION</b> .....	<b>1</b>
1.1 What is TD-SCDMA?.....	1
1.2 Research Background.....	3
1.3 Overview of the Dissertation.....	4
<b>2 THE TD-SCDMA SYSTEM</b> .....	<b>6</b>
2.1 Introduction .....	6
2.2 Transmitter Structure.....	7
2.3 Channel Modeling .....	18
2.3.1 Multi-path Propagation Model.....	18
2.3.2 Doppler Spread Mobile Channel.....	20
2.3.3 AWGN Channel .....	23
2.4 Base-station Receiver .....	23
2.4.1 General Function Blocks.....	23
2.4.2 Viterbi Decoder .....	25
2.4.2.1 Definitions.....	25
2.4.2.2 Viterbi Algorithm.....	27
2.4.2.3 Viterbi Algorithm Structure .....	30
2.4.2.3.1 Hard Decoder Structure.....	31
2.4.2.3.2 Soft Decoder Structure .....	33
2.4.2.4 Simulation of the Viterbi Decoder .....	36

<b>3 SYNCHRONIZATION PERFORMANCE OF THE UPLINK .....</b>	<b>40</b>
3.1 Introduction .....	40
3.2 Uplink Synchronous Transmission .....	41
3.2.1 Synchronous Scheme .....	42
2.4.2.1 Synchronization Acquisition .....	43
2.4.2.1 Synchronization Tracking .....	44
3.2.2 Channel Model .....	44
3.3 Synchronization Performance Analysis .....	45
3.3.1 Main Path Estimation .....	45
3.3.2 Synchronization and Code Cross-Correlation Properties .....	48
3.3.3 Performance and Code Auto-Correlation Properties .....	50
3.3.4 Synchronization and Interference.....	52
3.4 Simulation Results and Discussion .....	53
3.5 Conclusion.....	60
<b>4 CHANNEL ESTIMATION AND EQUALIZATION FOR THE UPLINK .....</b>	<b>61</b>
4.1 Introduction .....	61
4.2 RAKE Receivers .....	62
4.2.1 RAKE Receiver Models.....	62
4.2.1.1 Tapped-Delay-Line Channel Model.....	64
4.2.1.2 Maximal Ratio Combiner.....	65
4.2.1.3 Channel Estimation .....	66
4.2.1.3.1 Cross-correlation Channel Estimation .....	67
4.2.1.3.2 MMSE Channel Estimation .....	76
4.2.2 Simulation of the Uplink RAKE Receivers .....	85

4.3 MMSE Equalizer.....	87
4.3.1 MMSE Equalizer Model .....	87
4.3.1.1 Fully Spaced Equalizer.....	89
4.3.1.2 Fractionally Spaced Equalizer.....	90
4.3.2 Simulation Results.....	91
4.4 Conclusion.....	98
<b>5 ANTENNA ARRAYS .....</b>	<b>100</b>
5.1 Introduction .....	100
5.2 System Model for the Adaptive Antenna Array.....	101
5.2.1 Sensor Array.....	102
5.2.2 Pattern-Forming .....	105
5.2.3 Control Unit for Weight Adjustment .....	107
5.2.3.1 Data Stream in the Control Unit.....	107
5.2.3.2 Algorithm in the Control Unit— DMI .....	109
5.2.4 Array Performance Limits.....	111
5.3 Simulations Results .....	112
5.3.1 Array Beam Pattern.....	114
5.3.2 Performance Comparison.....	120
5.4 Discussion and Conclusion .....	122
<b>6 CONCLUSIONS .....</b>	<b>123</b>
<b>REFERENCES .....</b>	<b>126</b>

## LIST OF TABLES

TABLE 2.1	Signal Constellation for QPSK .....	13
TABLE 2.2	Signal Constellation for 8PSK .....	14
TABLE 2.3	Channel Models for Channel A.....	19
TABLE 2.4	Channel Models for Channel B.....	19
TABLE 2.5	Simulation Parameters for the Viterbi Decoder .....	37
TABLE 3.1	Simulation Parameters for System Validation .....	54
TABLE 4.1	Parameters for RAKE Receivers.....	72
TABLE 4.2	Parameters for MMSE Receivers.....	92
TABLE 5.1	Parameters for System with Antenna Array.....	113

## LIST OF FIGURES

Fig. 2.1. Reverse system for TD-SCDMA.....	6
Fig. 2.2. Mobile transmitter for TD-SCDMA .....	8
Fig. 2.3. Code tree for generation of OVSF codes .....	15
Fig. 2.4. Waveform of the pulse-shaping filter. ....	17
Fig. 2.5. Channel fast fading waveform.....	21
Fig. 2.6. Autocorrelation function of the channel waveform.....	22
Fig. 2.7. Base-station RAKE receiver for TD-SCDMA .....	24
Fig. 2.8. Four stages of a two-state trellis diagram.....	27
Fig. 2.9. Trellis representation at stage n for rate-1/2 convolutional coding in TD-SCDMA .....	28
Fig. 2.10. Convolutional encoder with 1/2-rate and length nine (256-states) .....	29
Fig. 2.11. Decision regions for signal detection.....	32
Fig. 2.12. Soft data detection showing soft values .....	34
Fig. 2.13. Performance of QPSK constellation for the TD-SCDMA system.....	38
Fig. 2.14. Performance of 8PSK constellation for the TD-SCDMA system.....	39
Fig. 3.1. Synchronized reverse system for TD-SCDMA. ....	42
Fig. 3.2. The TD-SCDMA subframe structure. ....	43
Fig. 3.3. Burst structure. ....	44
Fig. 3.4. Uplink synchronization in a multipath environment. ....	45
Fig. 3.5. Cross-correlation functions for the OVSF code-pairs.....	50
Fig. 3.6. Auto-correlation functions for some OVSF codes. ....	51

<b>Fig. 3.7. Performance Comparison of main path time delay estimators for ITU channel models.....</b>	<b>55</b>
<b>Fig. 3.8. Comparison of synchronized and unsynchronized systems. ....</b>	<b>57</b>
<b>Fig. 3.9. Performance comparison of synchronized and unsynchronized systems with a small time-shift using code pair 3 and 5. ....</b>	<b>59</b>
<b>Fig. 4.1. Basic system model with RAKE receiver for TD-SCDMA uplink.....</b>	<b>63</b>
<b>Fig. 4.2. Tapped delay line channel model for RAKE receiver.....</b>	<b>65</b>
<b>Fig. 4.3. Maximal-ratio-combiner in TD-SCDMA.....</b>	<b>66</b>
<b>Fig. 4.4. Channel Tap weight estimation with cross-correlation method. ....</b>	<b>67</b>
<b>Fig. 4.5. Performance of cross-correlation based RAKE receiver with different number of fingers. ....</b>	<b>75</b>
<b>Fig. 4.6. MMSE channel estimation in a RAKE receiver. ....</b>	<b>77</b>
<b>Fig. 4.7. Performance of MMSE-based RAKE receiver with different tap-delays. ....</b>	<b>81</b>
<b>Fig. 4.8. Performance of MMSE-based RAKE receiver.....</b>	<b>84</b>
<b>Fig. 4.9. Comparison of Cross-correlation / MMSE based receivers under ITU channel models.....</b>	<b>86</b>
<b>Fig. 4.10. Illustration of the MMSE equalizer.....</b>	<b>88</b>
<b>Fig. 4.11. Linear transversal filter for MMSE equalizer.....</b>	<b>88</b>
<b>Fig. 4.12. Comparison of MMSE equalizers with different equalizer length N. ....</b>	<b>94</b>
<b>Fig. 4.13. Comparison of MMSE equalizers with differently spaced taps.....</b>	<b>96</b>
<b>Fig. 4.14. Comparison of MMSE equalizers with differently rates. ....</b>	<b>98</b>

<b>Fig. 5.1. Functional diagram of a four-element adaptive array system. ....</b>	<b>101</b>
<b>Fig. 5.2. Four-element equispaced linear array.....</b>	<b>103</b>
<b>Fig. 5.3. Two-element linear array patterns .....</b>	<b>104</b>
<b>Fig. 5.4. Four-element linear array directivity pattern with <math>d = \lambda/2</math> and <math>\delta = \pi/6</math> in the upper, <math>\delta = 0</math> in the lower .....</b>	<b>106</b>
<b>Fig. 5.5. Functional diagram of a four-element adaptive array system. ....</b>	<b>107</b>
<b>Fig. 5.6. Data burst structure. ....</b>	<b>109</b>
<b>Fig. 5.7. Array beam pattern using DMI for two-user system.....</b>	<b>115</b>
<b>Fig. 5.8. Array beam pattern using DMI for three-user system with arriving angles of 0 (desired user), -0.4, and 0.3 radians.....</b>	<b>116</b>
<b>Fig. 5.9. Array beam pattern using DMI for four-user system with arriving angles of 0 (desired user), -0.4, 0.3, and 0.6 radians.....</b>	<b>117</b>
<b>Fig. 5.10. Array beam pattern using DMI for five and eight-user system .....</b>	<b>119</b>
<b>Fig. 5.11. Performance of two-user TD-SCDMA system with an antenna array....</b>	<b>121</b>
<b>Fig. 5.12. Performance of a four and eight-user TD-SCDMA system with an antenna array.....</b>	<b>121</b>

## ABSTRACT

Among all the third generation (3G) systems, time-division duplex synchronous code-division multiple access (TD-SCDMA) system is a unique system and has a lot advantages. The performance of the TD-SCDMA system is evaluated using both link level computer simulations and analysis. This dissertation is focused on the performance evaluation and improvement from the receiver model perspective, including Viterbi decoding algorithms, receiver structures, channel estimation algorithms, channel equalization algorithms, and smart antenna techniques.

Firstly, a basic reverse TD-SCDMA system is setup, including a transmitter, a receiver and a channel. Within the receiver model, a specific soft Viterbi decoding algorithm is developed. Secondly, the system synchronization requirements and their impact on its performance under realistic conditions are evaluated. The need for uplink synchronization is established and the sensitivity of the system performance to time misalignment is qualified. To mitigate multipath fading, a RAKE receiver and a minimum mean-square-error (MMSE) receiver are considered. Two RAKE receivers are compared and it is observed that the MMSE-based RAKE receiver always outperforms the cross-correlation based RAKE receiver. An MMSE receiver, including fully or fractionally spaced equalizer is also considered. MMSE receivers do improve the performance for some channels, but not in others. Fractionally spaced equalizers outperform the fully spaced equalizer.

Finally, the performance of the system with an antenna array consisting of a linear array of four equally spaced omni-directional antenna elements, and a direct matrix inversion algorithm (DMI) using the MMSE criterion, was also evaluated.

# Chapter 1

## Introduction

### 1.1 What is TD-SCDMA?

The demand for wireless communication services has rapidly increased, not only because of the growth in the number of users, but also because of the changing nature of the traffic. Data traffic which until recently represented a small segment of the wireless services is growing dramatically. The major services that the second generation of mobile systems provided is limited to voice and low rate data. These systems no longer satisfy the ever-increasing demand for high-speed data transmission. Third generation (3G) mobile systems are currently being deployed worldwide, and will deliver a variety of data services [1].

Time-division duplex synchronous code-division multiple access (TD-SCDMA) is one of the 3G systems. Among all the 3G systems being proposed, the advantages of TD-SCDMA lie in their outstanding spectrum efficiency, low transmission power [2], low cost, and flexibility for asymmetric traffic.

TD-SCDMA is based on a combination of two multiple-access techniques--time division multiple access (TDMA) and synchronous CDMA (SCDMA) [3], which uses a much wider transmission bandwidth compared to the data rate of the users. This spread spectrum technique allows for the simultaneous operation of many signals at the same carrier frequency simultaneously, as well as suppress the interfering noise. It uses smart antennas, a synchronous scheme and software radio techniques to increase system capacity by reducing co-channel interference, combating multipath fading, and reducing transmission power requirements. This system uses a time-division duplex (TDD) mode. It inherits all the advantages of TDD systems [4] such as,

- Use of various frequency resources without a need to pair frequencies,
- Suitable for asymmetrical transmission [5],
- Easy to utilize new signal processing techniques, and
- Low cost.

TD-SCDMA is unique in its uplink synchronization technique, which, together with joint detection algorithms, enhances the coverage of a base station and allows TD-SCDMA deployments for macro, micro and pico cell applications. Its uplink synchronization technique ensures signal orthogonality among traffic channels. All signals coming from each terminal will be synchronous at the input of the base station demodulator. This feature is important to guarantee orthogonality of the spreading

codes and to decrease multiple access interference from other code channels in the same radio frequency (RF) channel. All of these signals are to be synchronized at  $1/8$  of a code chip using a closed loop and an open loop control, which should hold even for a fast moving user. Because of this synchronization, the orthogonality of the signals for each code channel is insured and the co-channel interference is reduced to small levels, within the same cell.

## **1.2 Research Background**

Performance evaluation is always very useful and helpful to equipment makers and service providers. There are many research results published about other 3G systems. An interference evaluation of the UMTS Terrestrial Radio Access (UTRA) TDD is presented in [6]. In [7], the authors analyze the performance of the reverse link of the CDMA2000 system. The performance optimization of single frequency broadcast systems in FDD-CDMA has been investigated in [8]. There are many other papers published about CDMA2000 [9] [10], UTRA TDD [11] [12], wideband CDMA (WCDMA), and UTRA FDD. In [13], the authors briefly introduce the network structure of TD-SCDMA and its air interface. In [14], the authors give a more detailed overview of the TD-SCDMA system, including the design motivation, technical content, frame structures, etc. There are, however, few research results published on TD-SCDMA systems, and most are from the same source, the group who proposed the standard [15]-[18], thus receiving very limited independent

confirmation. In this work we evaluated the uplink performance of this TD-SCDMA system and discussed possible improvements.

### **1.3 Scope of the Dissertation**

The research is based on the TD-SCDMA standard, released by China Wireless Telecommunication Standards (CWTS), one member of the 3rd Generation Partnership Project (3GPP). The TD-SCDMA standard defines the transmitter structure, but leaves the receiver design open. The receiver model is critical to the performance of the system. This dissertation focused on the performance evaluation and improvement from the receiver model perspective, including the Viterbi decoding algorithms, receiver structures, channel estimation algorithms, channel equalization algorithm, and smart antenna techniques.

Chapter 2 gives an overview of the TD-SCDMA system, including transmitter, channel model, and receiver. Specifically, because of the specific signal constellation of the system, a specific soft word generation algorithm needed to be developed for the soft decoder. A comparison between the hard decision Viterbi decoder and the soft decision Viterbi decoder is presented.

In Chapter 3, the system synchronization requirements and their impact on its performance under realistic conditions are evaluated. Further, the relationship

between the synchronization performance and the correlation properties of the spreading codes is discussed. To validate the analytical results, a simulation of the TD-SCDMA is carried out.

Several channel estimation and equalization methods for the TD-SCDMA system are considered in Chapter 4. The methods are used to combat multipath degradation, therefore improving the system performance. channel estimation methods are included in the RAKE receiver model, which can provide diversity for multipath channels. The channel equalization methods are also included in the MMSE receiver, which can compensate for channel distortion.

A smart antenna array was included in the system, which substantially improves its performance as discussed in Chapter 5. RAKE and MMSE receivers can only compensate for multipath degradation in certain situations. Antenna arrays can not only compensate for multipath degradation, but also improve the performance of a multiuser system by enhancing the detection and reception of certain desired signals and suppressing the interfering signals.

Finally, some discussion on TD-SCDMA system and a conclusion are presented in Chapter 6.

## Chapter 2

### The TD-SCDMA System

#### 2.1 Introduction

TD-SCDMA is one of the approved 3G wireless standards. Among all other 3G systems, TD-SCDMA is unique in its uplink synchronization technique. In order to evaluate the system performance, a basic realistic reverse TD-SCDMA system (shown in Fig. 2.1) is set up, including the mobile transmitter according to the standard [20], [21], the base-station receiver, and the multi-path channel based on ITU models.

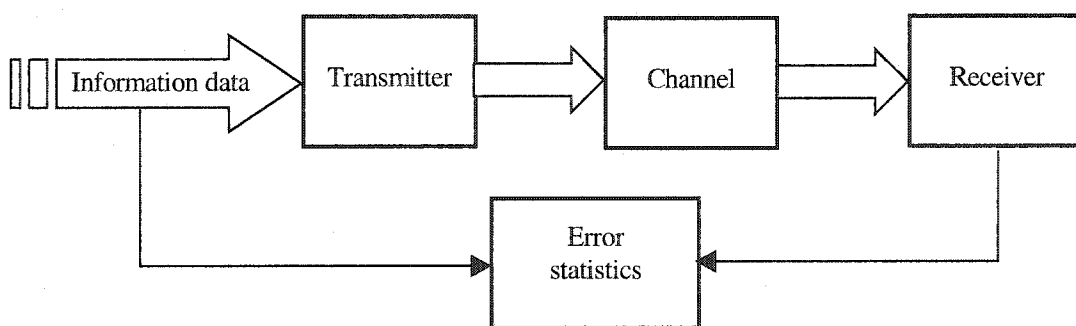


Fig. 2.1. Reverse system for TD-SCDMA.

The system is simulated mainly using C++ programs, and using some MATLAB programs. Most of the function blocks are implemented at chip-level, but some of the function blocks are implemented at the sample-level of eight times the chip-rate, because of the synchronization component of this system in which the minimum timing adjustment in the up-link is  $1/8$  chip.

Within the receiver model, the Viterbi algorithm (VA) plays a very important role. A common VA can be used for decoding of the convolutional code in the TD-SCDMA receiver, either for soft or hard decoders. But because of the specific signal constellation in the system, a specific soft word generation algorithm is developed for the soft decoder. Therefore, we also used the data sequence to generate a specific soft decoder and compare their performances.

## **2.2 Transmitter Structure**

The mobile transmitter structure is shown in Fig. 2.2 for a TD-SCDMA system. Data arrives at the transmitter unit in the form of transport block sets, once every transmission time interval (TTI). The TTI is from a set of {10ms, 20ms, 40ms, and 80ms}. The data stream goes through all the function blocks in the transmitter, and then through the air interface. The component blocks are discussed in the following.

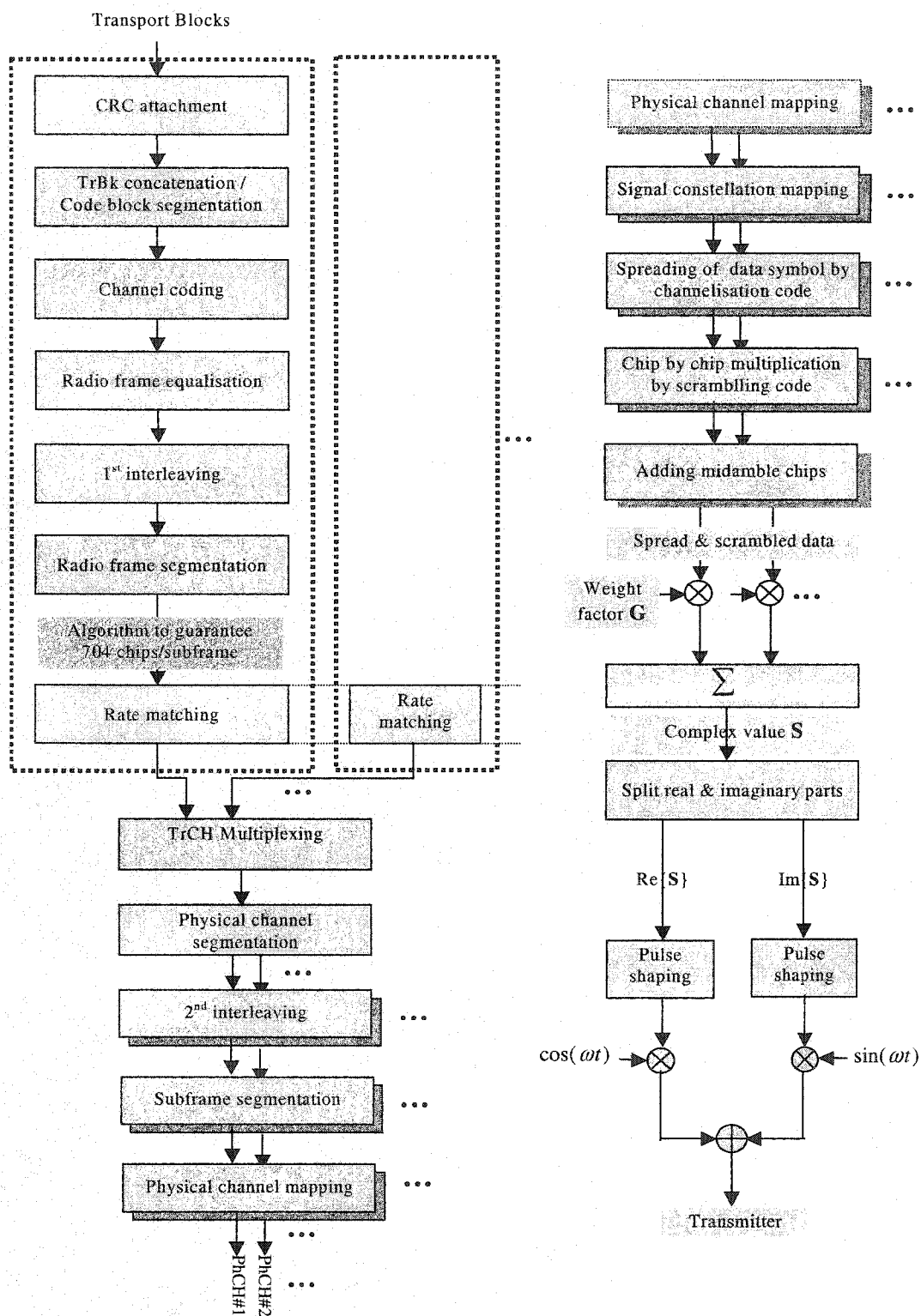


Fig. 2.2. Mobile transmitter for TD-SCDMA.

### ***CRC attachment***

Error detection is provided on transport blocks through a cyclic redundancy check (CRC). The CRC is 24, 16, 8, or 0 bits. Like the 16-bit CRC-CCITT, the CRC in TD-SCDMA is the CRC of the left-shifted message. The parity bits are generated by one of the following cyclic generator polynomials:

$$g_{CRC24}(D) = D^{24} + D^{23} + D^6 + D^5 + D + 1 \quad (2.1)$$

$$g_{CRC16}(D) = D^{16} + D^{12} + D^5 + 1 \quad (2.2)$$

$$g_{CRC8}(D) = D^8 + D^7 + D^4 + D^3 + D + 1 \quad (2.3)$$

### ***TrBk concatenation/Code block segmentation***

All transport blocks (TrBk) including their CRC parity bits in a TTI need to be concatenated. If the number of bits during a TTI is larger than the maximum size of a code block, code block segmentation is performed after the concatenation. The maximum size  $Z$  for a convolutional code is:

$$Z = 512 - K_{tail} = 512 - 8 = 504. \quad (2.4)$$

### ***Channel coding***

Code blocks are delivered to the Channel Coding block, which can be convolutional coding, turbo coding, or no channel coding. The convolutional code is rate 1/2 with a constraint length of nine. The generator functions for the rate 1/2 code are  $G_0 = 561$  (octal) and  $G_1 = 753$  (octal). The generator functions for the rate 1/3 code are  $G_0 = 557$  (octal),  $G_1 = 663$  (octal), and  $G_2 = 711$  (octal).

### ***Radio frame size equalization***

This unit is padding the input bit sequence in order to ensure that the output can be segmented in fixed data segments of the same size.

### ***1<sup>st</sup> interleaving***

The first interleaving is a block inter-leaver with inter-column permutations. Four algorithms for interleaving are available depending on the interleaving span (the duration of TTI, which can be any one in the set {10ms, 20ms, 40ms, and 80ms}).

### ***Radio frame segmentation***

When the TTI is larger than 10ms, the input bit sequence is segmented and mapped onto consecutive radio frames.

### ***Rate matching***

In this block bits on a transport channel are repeated or punctured. The number of bits on a transport channel can vary between different TTIs. The rate-matching algorithm is performed to ensure that the total bit rate after the second multiplexing is identical to the total channel bit rate of the allocated dedicated physical channels.

### ***Transport channel (TrCH) multiplexing***

Every 10ms, a radio frame from each transport channel is delivered to TrCH multiplexing. These radio frames are serially multiplexed into a coded composite transport channel (CCTrCH).

### ***Physical channel (PhCH) segmentation***

When more than one physical channel (PhCH) is used, physical-channel-segmentation divides the bits among the different PhCHs.

### ***2<sup>nd</sup> interleaving***

The 2<sup>nd</sup> interleaving can be applied to all data bits transmitted during one frame, or separately within each timeslot, on which the CCTrCH is mapped, according to the selection from a higher layer.

### ***Sub-frame segmentation***

This unit is between the 2<sup>nd</sup> interleaving and the physical channel mapping. The rate-matching algorithm already guarantees the bit stream number to be even and can be divided into two sub-frames.

### ***Physical channel mapping***

The bit stream from the sub-frame segmentation is mapped onto code channels of time slots. The mapping is performed like block interleaving, writing the bits into the columns. But a PhCH with an odd number is filled in forward order, while a PhCH with an even number is in reverse order.

### ***Signal constellation mapping***

This unit maps bits onto a signal point constellation. A certain number of CDMA codes can be assigned to either a single user or different users who are simultaneously transmitting data bursts in the same time slot and the same frequency. Before assigning a code to a data stream, the data stream is converted to complex symbols. For QPSK modulation, the data symbols are generated from two consecutive data bits from the output of the physical channel mapping procedure, as shown in Table 2.1. In the table,  $b_{m,n}^{(k,i)}$  refers to the real ( $i=1$ ) or imaginary ( $i=2$ ) part of the  $m$ th ( $m=1,2$ ) bit of  $n$ th symbol with  $k$ th user. For 8PSK modulation, the data symbols from three consecutive bits are as shown in Table 2.2.

TABLE 2.1

SIGNAL CONSTELLATION FOR QPSK

<b>Consecutive Binary Bit Pattern</b>	<b>Complex Symbol</b>
$b_{1,n}^{(k,1)} b_{2,n}^{(k,1)}$	$\underline{d}_n^{(k,i)}$
00	+j
01	+1
10	-1
11	-j

TABLE 2.2

## SIGNAL CONSTELLATION FOR 8PSK

Consecutive Binary Bit Pattern	Complex Symbol
$b_{1,n}^{(k,i)} b_{2,n}^{(k,i)} b_{3,n}^{(k,i)}$	$\underline{d}_n^{(k,i)}$
000	$\cos(11\pi/8) + j \sin(11\pi/8)$
001	$\cos(9\pi/8) + j \sin(9\pi/8)$
010	$\cos(5\pi/8) + j \sin(5\pi/8)$
011	$\cos(7\pi/8) + j \sin(7\pi/8)$
100	$\cos(13\pi/8) + j \sin(13\pi/8)$
101	$\cos(15\pi/8) + j \sin(15\pi/8)$
110	$\cos(3\pi/8) + j \sin(3\pi/8)$
111	$\cos(\pi/8) + j \sin(\pi/8)$

*Channelization code spreading*

Each data symbol is spread with a complex-valued spreading code  $\mathbf{c}_Q$  of length  $Q$ . Spreading codes  $\mathbf{c}_Q$  are generated from the binary codes  $\mathbf{a}_Q$ , which are orthogonal variable spreading factor (OVSF) codes, allowing to mix in the same timeslot channels with different spreading factors while preserving orthogonality. The OVSF codes can be defined using the code tree of Fig. 2.3, where  $Q \in \{1, 2, 4, 8, 16\}$ .

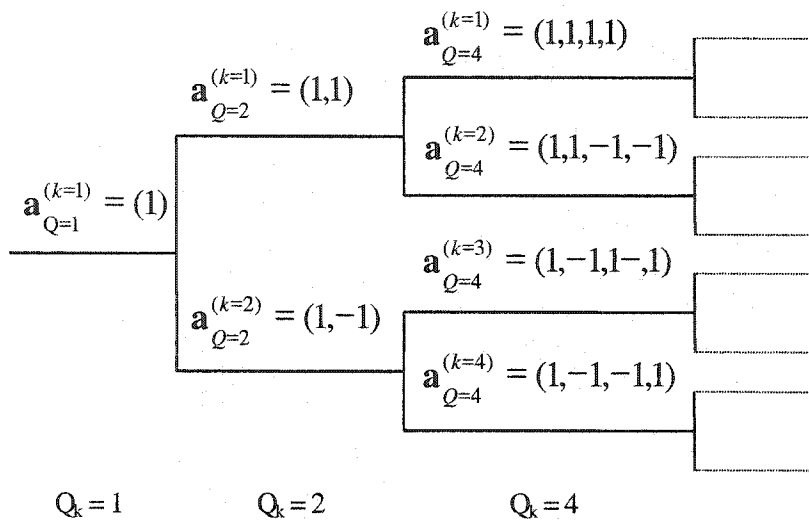


Fig. 2.3. Code tree for generation of OVSF codes.

### *Data symbol scrambling*

The spreading of data by a code of length  $Q$  is followed by a cell specific scrambling sequence  $V$  of length  $Q_{\max} = 16$ . Before the scrambling, the length matching needs to be performed. There are a total of 128 scrambling sequences, which are divided in groups of four sequences. Every group is defined by the downlink synchronization code used by the base station.

### ***Adding midamble chips***

A physical channel in TDD is a burst, which is transmitted, in a particular time slot within allocated radio frames. A burst has the duration of one time slot of combination of a data part, a mid-amble and a guard period. The midamble part of the burst is of length 144 chips. The midambles, i.e., training sequences of different users active in the same cell and same time slot are cyclically shifted versions of one single basic mid-amble code. There are 128 different basic mid-amble codes with length 128 for the whole system. All traffic time slots on a carrier must have the same basic mid-amble code. For each user in the same time slot, the mid-amble chips are calculated individually.

### ***Summing unit***

Up to two different physical reverse channels are combined within one time slot. Each spread and scrambled channel with complex value is separately weighted by a weight factor and combined using complex addition.

### ***Pulse shaping***

The pulse shaping filtering is applied to each chip at the transmitter. The impulse response of the filter is a root-raised cosine. The overall filter function at the receiver

should also be a root-raised cosine. The corresponding raised cosine impulse  $h(t)$  is defined as:

$$h(t) = \frac{\sin\left(\pi \frac{t}{T_c}(1-\alpha)\right) + 4\alpha \frac{t}{T_c} \cos\left(\pi \frac{t}{T_c}(1+\alpha)\right)}{\pi \frac{t}{T_c} \left(1 - \left(4\alpha \frac{t}{T_c}\right)^2\right)}, \quad (2.5)$$

where, the roll-off factor is  $\alpha = 0.22$  and  $T_c$  is the chip duration. The waveform for this filter is shown in Fig. 2.4.

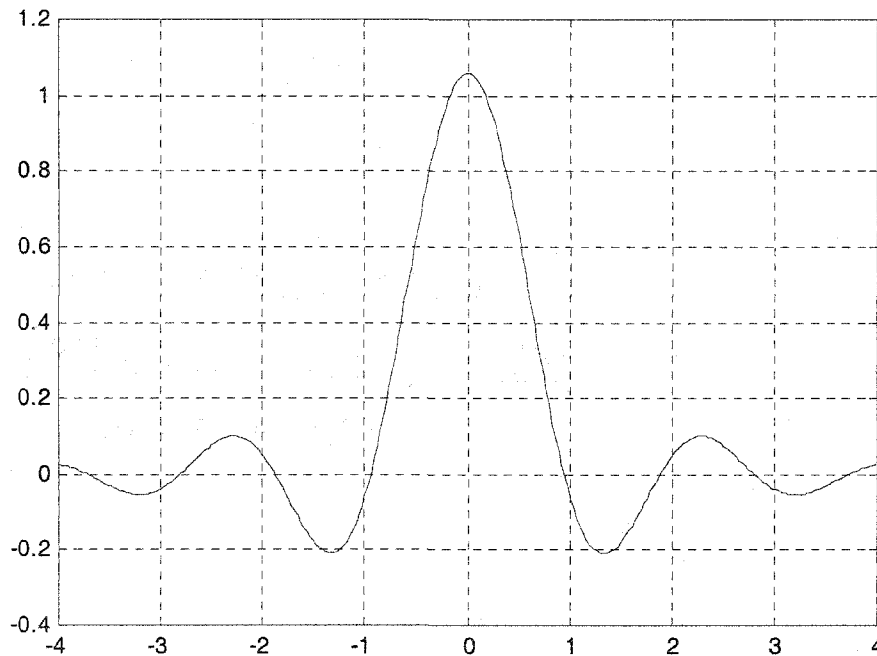


Fig. 2.4. Waveform of the pulse-shaping filter.

A root-raised cosine filter is not the same as a raised cosine filter. It is generated by splitting a raised cosine filter between two filters, one at the transmitter, with transfer function denoted by  $h_T(t)$ , and the other at the receiver, with transfer function denoted

by  $h_R(t)$ . In the frequency domain, we have  $H_T(f)H_R(f)$  as the transfer function of a raised cosine filter. It can be shown [22] that, in the relatively simple case where we have an additive noise source at the receiver input, this splitting can optimize the SNR at the receiver output.

## 2.3 Channel Modeling

We set up the multi-path channel structure using the ITU models [23]. In every path, we use Jakes' fading model [24] to simulate the Doppler spread, and all data sequences are contaminated by additive white Gaussian noise (AWGN).

### 2.3.1 Multi-path Propagation Model

The multi-path propagation channels are set up according to the ITU.1225 models for 3G, shown in Tables 2.3 and 2.4. These channels represent different quantities of the delay-spread values. Channel A is a low delay spread case that occurs frequently. Channel B is a median delay spread case that also occurs frequently. Each of these two channels is expected to be encountered for some percentage of time in a given test environment.

TABLE 2.3

## CHANNEL MODELS FOR CHANNEL A

Indoor		Indoor to Outdoor and Pedestrian		Vehicular	
Relative Delay [ns]	Average Power [dB]	Relative Delay [ns]	Average Power [dB]	Relative Delay [ns]	Average Power [dB]
0	0.0	0	0.0	0	0.0
50	-3.0	110	-9.7	310	-1.0
110	-10.0	190	-19.2	710	-9.0
170	-18.0	410	-22.8	1090	-10.0
290	-26.0			1730	-15.0
310	-32.0			2510	-20.0

TABLE 2.4

## CHANNEL MODELS FOR CHANNEL B

Indoor		Indoor to Outdoor and Pedestrian		Vehicular	
Relative Delay [ns]	Average Power [dB]	Relative Delay [ns]	Average Power [dB]	Relative Delay [ns]	Average Power [dB]
0	0.0	0	0.0	0	-2.5
100	-3.6	200	-0.9	300	-0.0
200	-7.2	800	-4.9	8900	-12.8
300	-10.8	1200	-8.0	12900	-10.0
500	-18.0	2300	-7.8	17100	-25.2
700	-25.2	3700	-23.9	20000	-16.0

These tables describe the tapped-delay-line parameters for each of the terrestrial test environments. For each tap of the channels two parameters are given: the time delay relative to the first tap and the average power relative to the strongest tap.

Multi-path mobile channels are set up according to these models. Within every path the Jakes' fading model for Doppler spread is used.

### 2.3.2 Doppler Spread Mobile Channel

The Jakes fading model is a deterministic method for simulating time-correlated Rayleigh fading waveforms. This model assumes that uniformly distributed rays with equal-strength arrive at a moving receiver, such that every ray experiences a Doppler shift. The revisited model further gives multiple non-correlated waveforms. The maximum Doppler shift is

$$\omega_{MAX} = 2\pi f v / c , \quad (2.6)$$

where  $v$  is the vehicle speed,  $f$  is the carrier frequency, and  $c$  is the speed of light. The simulation will thus produce an RF spectrum, which is a discrete approximation to the Doppler spread form [25]

$$\left[ 1 - \left( \frac{f - f_c}{f_m} \right)^2 \right]^{-1/2}, \quad (2.7)$$

where,  $f_c$  is the carrier frequency and  $f_m$  is the maximum Doppler spread.

In this model, fading is mainly determined by the speed of the user equipment. If the speed is high, both the amplitude and the phase of the channel impulse change fast, and vice versa. This can be observed in Fig. 2.5, which shows the channel waveforms during one second.

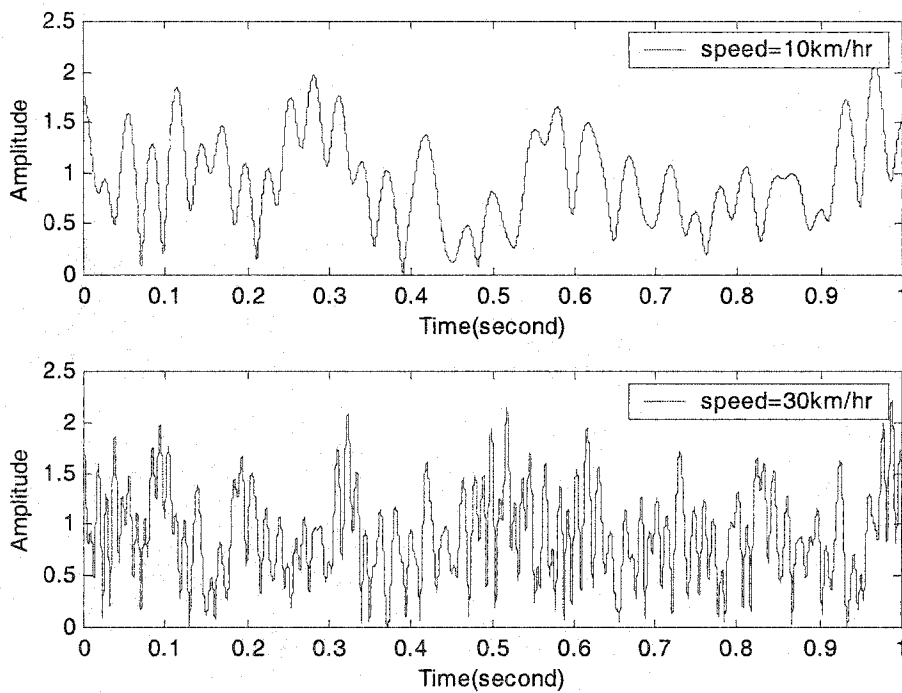


Fig. 2.5. Channel fast fading waveform.

To test the autocorrelation function of the channel model, a complex baseband waveform was generated using eight oscillators and Doppler frequency  $\omega_{MAX} = 2 * \pi * 55.5$ . Then, 1,000,000 samples were generated using a sampling period of  $200 \mu s$ . It is shown in the upper panel of Fig. 2.6 that the autocorrelation function agrees well with theoretical values. Compared with the real part of the autocorrelation function, the cross-correlation function of the real part and imaginary part of the channel fading waveform is very small, which is represented by the imaginary part of the autocorrelation function, shown in the lower panel of Fig. 2.6. This is a good Rayleigh fading model.

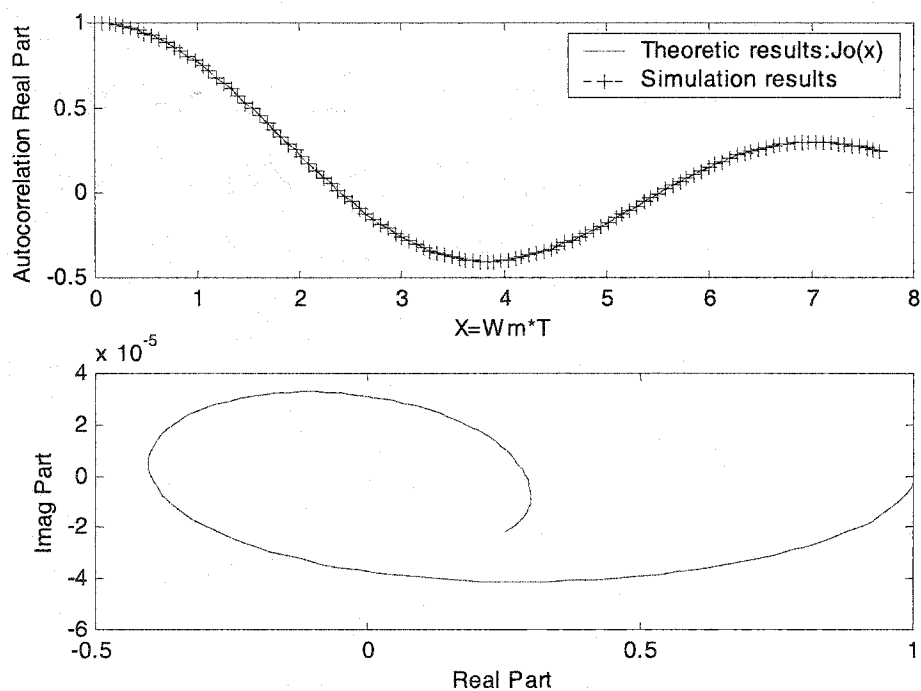


Fig. 2.6. Autocorrelation function of the channel waveform.

### **2.3.3 AWGN Channel**

To implement the AWGN channel, a sequence of uniform distributed random numbers in (0,1) is first generated according to the Wichiman-Hill algorithm [26]. In this algorithm, three inferior linear multiplicative, congruential generators are used and result in an excellent generator having a period of  $7.5e13$ . Then Gaussian random numbers are generated using the polar method. Complex-valued AWGN channels are generated afterward.

## **2.4 Base-Station Receiver**

The TD-SCDMA standard, like all standards, leaves the receiver model open. We use a typical RAKE receiver, and specific functions for the TD-SCDMA system, as shown in Fig. 2.7.

### **2.4.1 General Function Blocks**

Many function blocks in this receiver accomplish the reverse tasks of the transmitter. After going through the matched filters, the data sequence enters the combining block with time-delays and phases adjustments, and then goes through all the function blocks in Fig. 2.7.

Because of the special role the Viterbi decoder plays in the receiver, in the next subsection we describe it in more detail.

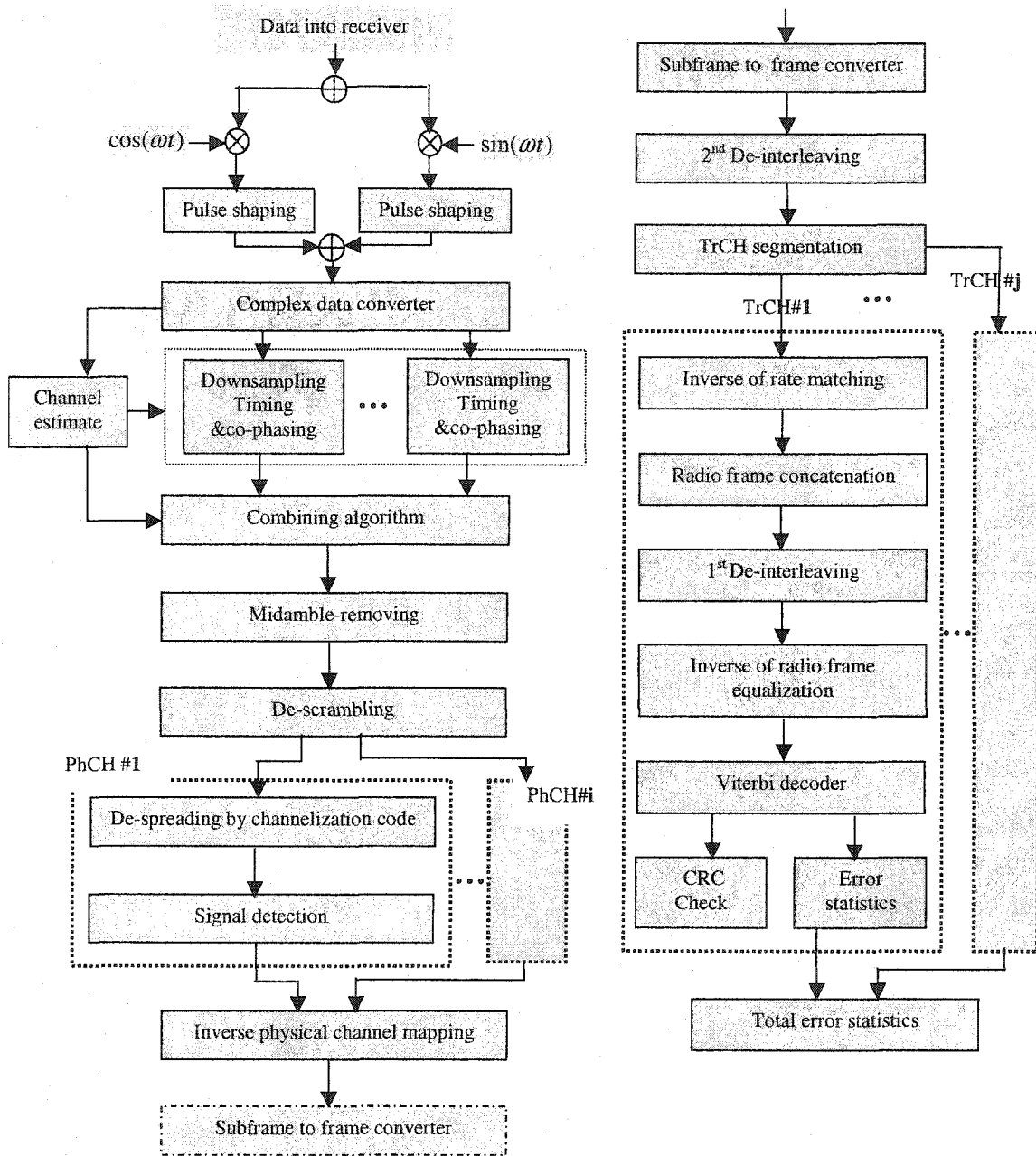


Fig. 2.7. Base-station RAKE receiver for TD-SCDMA.

## 2.4.2 Viterbi Decoder

The Viterbi algorithm (VA) is widely used for estimation and detection in digital communications and signal processing [19]. The VA can recursively find the most-likely state transition sequence according to the statistics theory of maximum-likelihood (ML). Therefore, the VA can be used to find the noiseless finite-state sequence according to the ML criterion, given a sequence of finite-state signals contaminated by noise.

In this basic structure, it is used to decode the convolution codes to enhance the performance of the TD-SCDMA system. Given a received sequence of symbols corrupted by AWGN, the Viterbi algorithm finds the sequence that is closest in distance to the received sequence [19]. The distance can be Euclidean distance [27] or Hamming distance. The resulted sequence is the global most likely sequence. Before describing the Viterbi algorithm in the system, some definitions are presented in the following.

### 2.4.2.1 Definitions

*Survivor path:* for a given state, the survivor path is the sequence of symbols entering the state, which is the closest in distance to the received noisy sequence.

**Path metric:** for a given state  $i$  at time- $n$  (stage- $n$ ), the path metric is the distance between the survivor path and the received noisy sequence. It is denoted as  $M_{i,n}$ .

**Branch metric:** branch metric is the distance between the received noisy symbol,  $y_n$ , and the ideal noiseless output symbol at time- $n$  (stage- $n$ ) when state  $i$  transits to state  $j$ . We denote the branch metric as  $B_{i,j,n}$ .

**Trellis diagram:** a finite-state diagram by a time-indexed equivalent, which can visualize the transitions from state to state [27].

### **Example**

Let us assume a trellis with two states  $0$  and  $1$ , as shown in Fig. 2.8. With this four stages' representation, we can see there are four symbols in the input or output sequence. Assume that the received sequence is  $\{0, 1.5, -0.4, 1.1\}$ . At the end of stage 2, the survivor path for state 1 is the solid path indicated in the figure. Then, the new path metric  $M_{1,2}$  for state 1 at stage 2 is the distance between the output sequence  $\{0, 1, 0\}$  and the received sequence  $\{0, 1.5, -0.4\}$ . The branch metric  $B_{0,1,2}$  is the distance between the output symbol 0 and the received symbol  $-0.4$ .

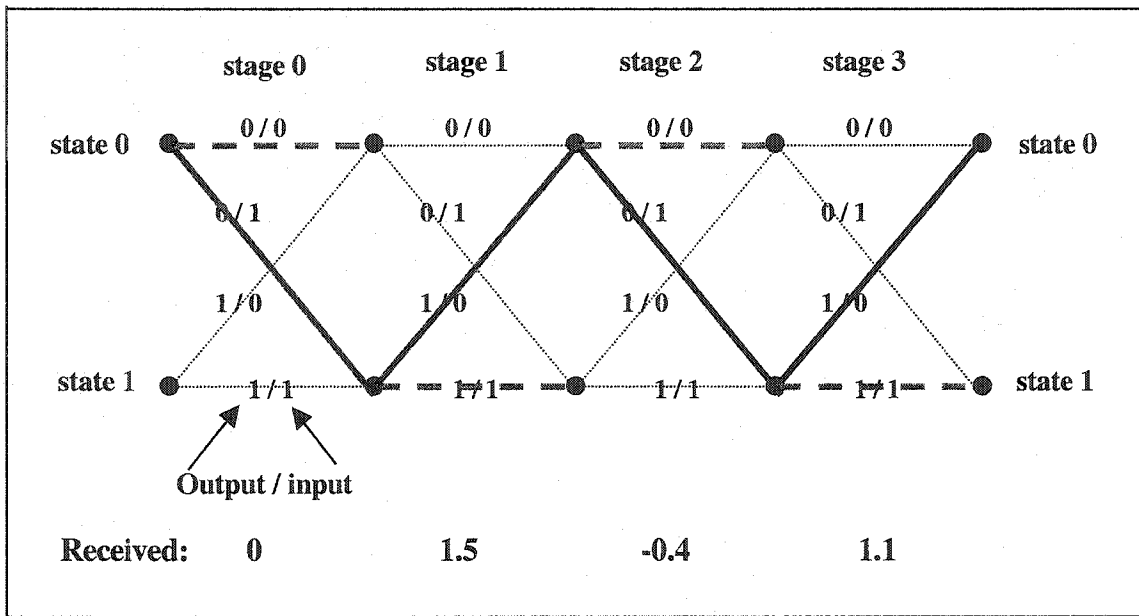


Fig. 2.8. Four stages of a two-state trellis diagram.

### 2.4.2.2 Viterbi Algorithm

Except for the distance measure, the procedure to search for the most likely sequence is the same for both hard and soft decision decoders. In TD-SCDMA, the standard uses convolutional coding with rate 1/2 or 1/3, 256-state, 512-stage, initial state 0, and 8 tail bits to let the register return to state 0 after block coding. The part of trellis-representation at stage  $n$  for 1/2-rate convolutional coding is shown in Fig. 2.9. In this trellis, all the output / input pairs from state  $i$  to state  $j$  can be calculated from the convolutional encoder shown in Fig. 2. 10.

The aim of the algorithm is to search for the most-likely sequence. To compute the sequence, the algorithm recursively compute the survivor path for each state at each stage. At the last stage, the algorithm selects the survivor path, which has the minimum path metric to be the global most-likely path. After acquiring the global most-likely path, all the input / output sequence can be obtained.

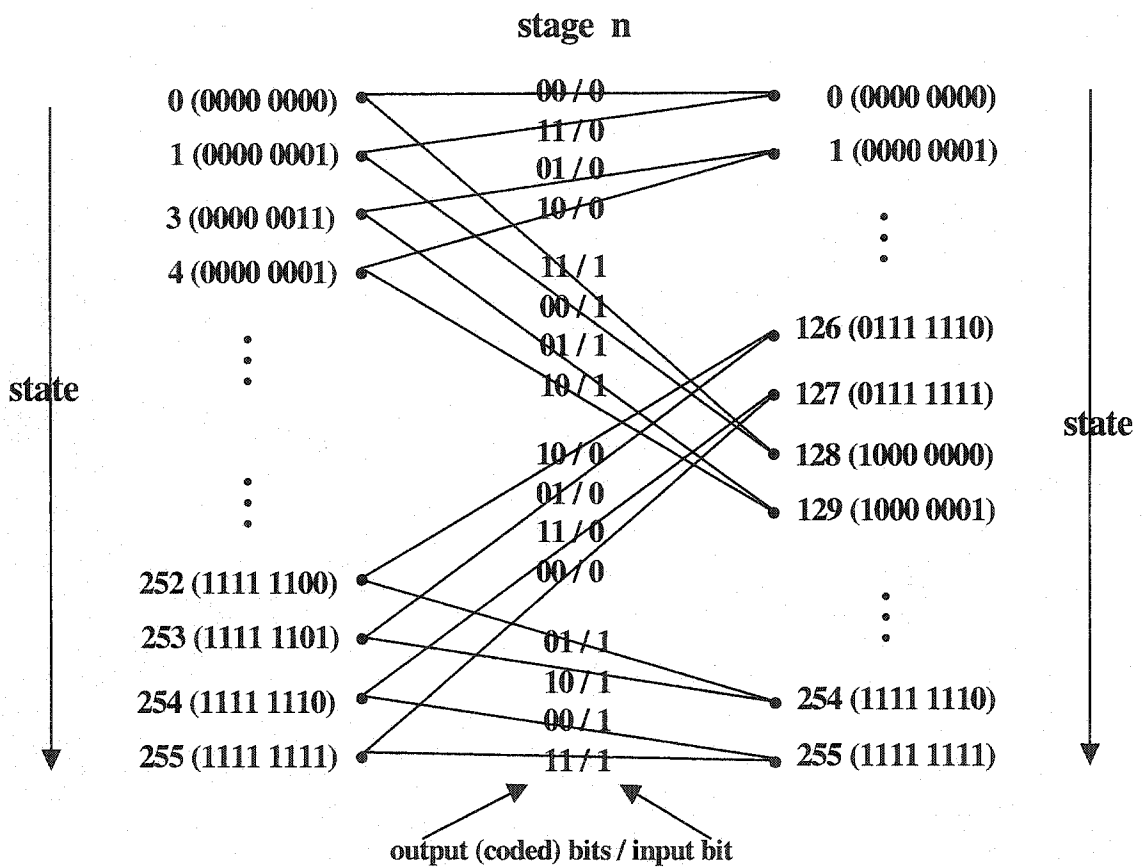


Fig. 2.9. Trellis representation at stage n for rate-1/2 convolutional coding in TD-SCDMA.

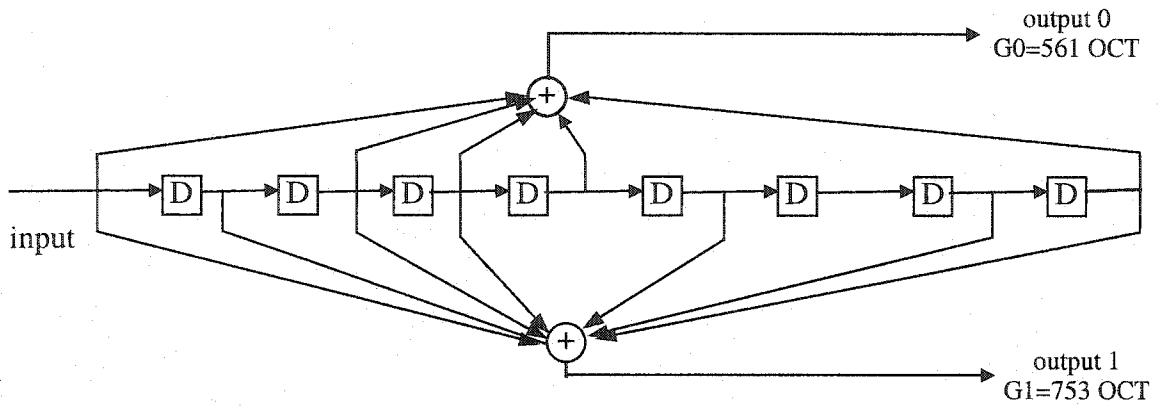


Fig. 2.10 Convolutional encoder with 1/2-rate and length nine (256-states).

There are three major steps in this algorithm.

**1) Initial setting for the algorithm**

Since the initial state of the shift register is state-0, we set the initial path metric as follows

$$\begin{aligned}
 M_{0,0} &= 0 \\
 M_{i,0} &= \infty, \quad (i = 1, \dots, 255)
 \end{aligned}
 \tag{2.8}$$

**2) Recursive calculation for stage- $n$  ( $n = 0, \dots, 511$ )**

This step includes branch and path metric calculation and survivor path update.

Every branch metric  $B_{i,j,n}$  ( $i, j \in \{0, \dots, 255\}, n \in \{0, \dots, 511\}$ ) for all transitions given in

the trellis diagram in Fig. 9 is generated first according to the definition. Then the path metric is computed as following

$$M_{i,n} = \min_{j \in \{0, \dots, 255\}} [M_{j,n-1} + B_{j,i,n}], \quad (i = 0, \dots, 255). \quad (2.9)$$

Finally, the survivor path for each state is updated.

### ***3) The global most-likely path trace back***

From the convolutional coding in the standard, we know that the register state returns back to state-0 at the end. Then we do not need to select the survivor path with minimum path metric as is commonly done. We only need to pick the survivor path for state-0 at stage-511 as the global most-likely sequence. After obtaining the path, we can trace back all the transitions in all stages to get the input / output sequence. The input sequence is what we want for the information symbol sequence.

#### **2.4.2.3 Viterbi Decoder Structure**

The basic structure for soft and hard decision decoding is the same (see Fig. 2.7). But the data types between function blocks “Signal Detection” and “Viterbi Decoder” are different: the data stream is floating type for the soft decoder and a short integer type for the hard decoder. Also, the algorithms for the three function blocks “Signal

Detection”, “Inverse of Rate Matching” and “Viterbi Decoder” need to be matched to each other.

#### **2.4.2.3.1 Hard Decoder Structure**

For hard decision decoding, each noisy symbol in the received sequence is detected by the block “Signal Detection”, and is already mapped to a bit sequence of 0/1. After inverse rate matching adjustment, the data sequence is used to calculate the path metric by quasi-Hamming distance to decide the most-likely sequence.

##### ***Signal Detection***

The detection process involves identifying the nearest Gray-coded constellation point to each received complex vector using the ML rule. With a QPSK constellation, each received symbol maps to two bits, which are determined by the decision regions shown in Fig. 2.11a. With an 8-PSK constellation, each received symbol maps to three bits, which are determined by the decision regions shown in Fig. 2.11b. Thus, the data sequence after detection is a sequence of 0/1.

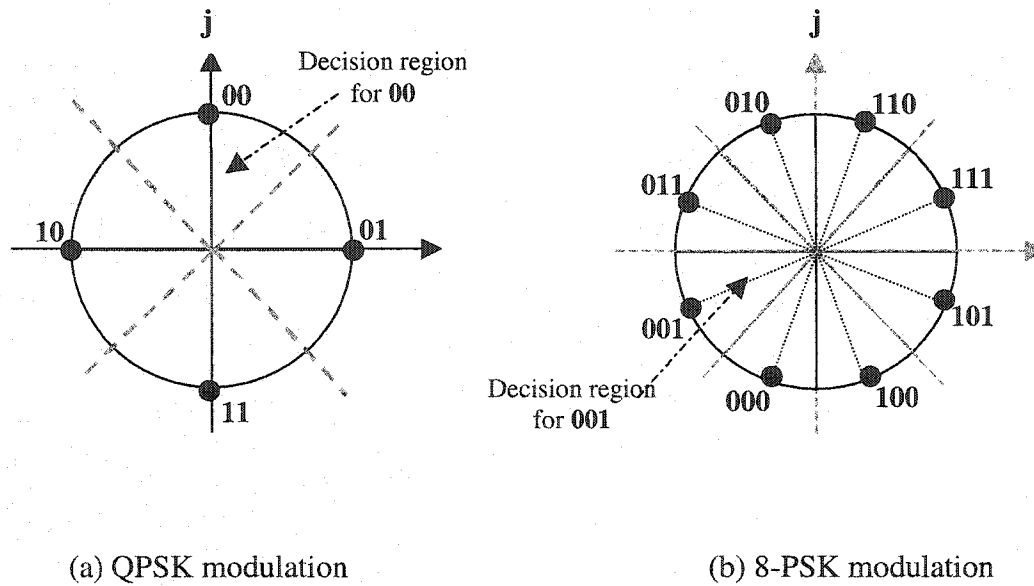


Fig. 2.11. Decision regions for signal detection.

### *Inverse of Rate Matching*

In this block, the input sequence from  $\{0,1\}$  is mapped to the output sequence from  $\{0, 0.5, 1\}$ . The mapping algorithm is as follows:

- The punctured bits, which are discarded at the transmitter, will be replaced by 0.5. Because these bits are assumed by the algorithm, not to give any information about the channel, we make them have the same distance to bits 0/1.
- The repeated bits in the transmitter will be averaged during the repeated duration, instead of being discarded at the receiver, because all of them provide channel information.

### ***Viterbi Decoder Block***

The distance used in hard decision Viterbi decoding is the Hamming distance except for those punctured or repeated bits, which might differ from bits 0/1. The Hamming distance is the number of bits in which the two sequences differ. This quasi-Hamming distance is used both in the path and branch metrics. The branch metric for the transition from state- $i$  to state- $j$  at stage- $n$  can be described as

$$B_{i,j,n} = \sum_{k=0}^m |y_{k,n} - c_{k,i,j}|, \quad (2.10)$$

where  $m = 1$  for 1/2-rate coding and  $m = 2$  for 1/3-rate coding, and

$c_{k,i,j} \in \{0,1\}$  is the output symbol in output- $k$  at the transition from state- $i$  to state- $j$  (referring to Fig. 2.10), and

$y_{k,n} \in \{0,0.5,1\}$  is the received symbol corresponding to stage- $n$  in output- $k$ .

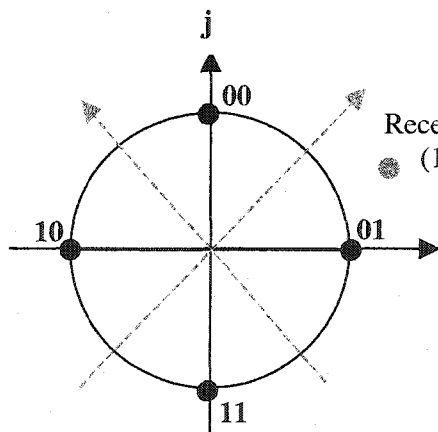
#### **2.4.2.3.2 Soft Decoder Structure**

For soft decision decoding, the noisy symbols detected by “Signal Detection” will not be mapped to the bit sequence of 0/1, but to a sequence of signed one-dimensional distance values, and then, used to calculate every Euclidean distance as its path metric for every path.

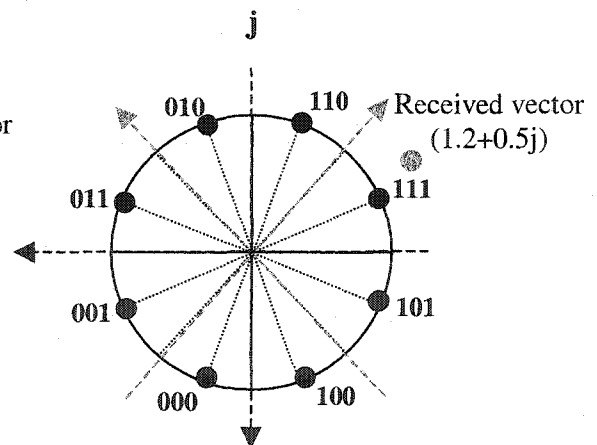
### Signal Detection

Because of the signal constellations shown in Fig. 2.12, the soft words cannot be generated directly as in other standards [28]. The aim is to generate the soft words for decoder use. For QPSK, when we receive symbol vector  $a + bj$ , we rotate it  $-45^\circ$  to get  $(a + bj) * (\cos(45^\circ) - j \sin(45^\circ))$ , say  $c + dj$ . Then the real part of the rotated vector will be the soft value for the first bit, and the imaginary part for the second bit. For example,

- The received vector is  $1.2 + 0.5j$ .
- The rotated vector will be  $1.202 - 0.495j$ .
- The soft value for the first bit is 1.202, and the soft value for the second bit is  $-0.495$ .



a) QPSK constellation.



(b) 8PSK constellation.

Fig. 2.12. Soft data detection showing soft values.

For 8PSK, when a symbol vector  $a + bj$  is received, it will be rotated  $180^\circ$  to get  $-a - bj$ . Then the real part of the rotated vector will be the soft value for the first bit, and the imaginary part for the second bit. As for the third bit, we rotate it  $-45^\circ$ , and use the real part times the imaginary part as the soft value. For example,

- The received vector is  $1.2 + 0.5j$ .
- The  $-45^\circ$  rotated vector will be  $1.202 - 0.495j$ .
- The soft value for the third bit is  $1.202 * (-0.495) = -0.595$ .
- The 180-degree rotated vector will be  $-1.2 - 0.5j$ .
- The soft value for the first bit is  $-1.2$ , and the soft value for the second bit is  $-0.5$ .

### *Inverse of Rate Matching*

In this block, the input sequence from  $\{0,1\}$  is mapped to the output sequence from  $\{0, 0.5, 1\}$ . The mapping algorithm is as follows:

- The punctured bits, discarded at the transmitter, are replaced by 0. Because in this algorithm, the value-0 is not in favor of bit-0 or bit-1.
- The repeated bits in the transmitter will be averaged during the repeated duration, instead of being discarded at the receiver, because all of them provide channel information.

### ***Viterbi Decoder Block***

The distance used in the soft decision Viterbi decoder is the Euclidean distance. The branch metric for the transition from state- $i$  to state- $j$  at stage- $n$  can be described as

$$B_{i,j,n} = \sum_{k=0}^m (y_{k,n} - c_{k,i,j})^2, \quad (2.11)$$

where  $m = 1$  for 1/2-rate coding and  $m = 2$  for 1/3-rate coding, and

$c_{k,i,j} \in \{-1,1\}$  is the output symbol in output- $k$  at the transition from state- $i$  to state- $j$ , and

$y_{k,n}$  is the received symbol corresponding to stage- $n$  in output- $k$ .

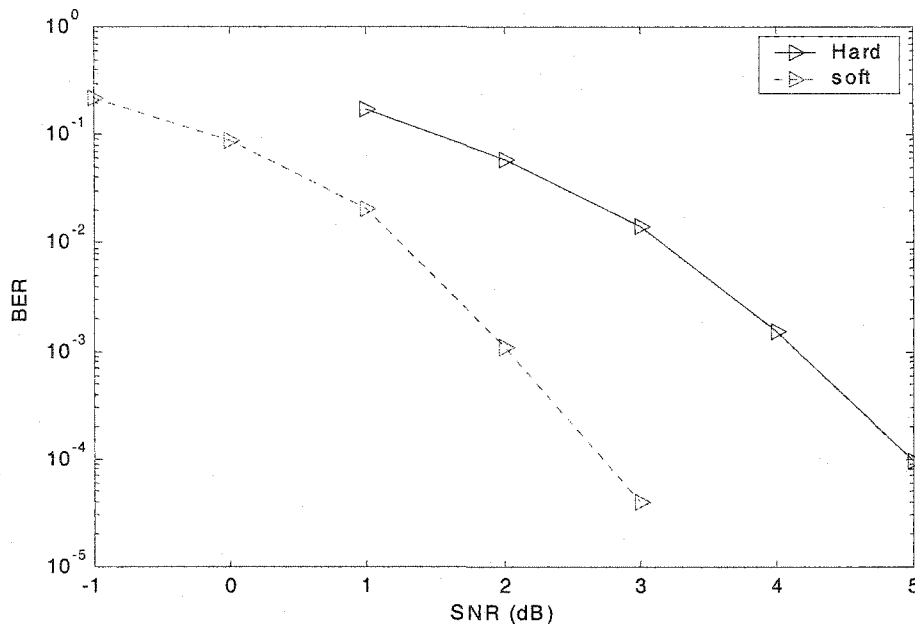
#### **2.4.2.4 Simulation of the Viterbi Decoder**

For the purpose of comparing the soft and hard Viterbi decoders, the uplink bit-error-rate (BER) simulation is carried out according to the parameters shown in Table 2.5. The BER performance comparisons are shown in Figs 2.13 and 2.14. We observe that the BER performance difference between soft / hard decision Viterbi decoding with a 1/2 code-rate is about 2-dB no matter whether QPSK (Fig 2.13(a)) or 8PSK (Fig. 2.14(a)) is used. The BER performance difference for the 1/3 code-rate is much less.

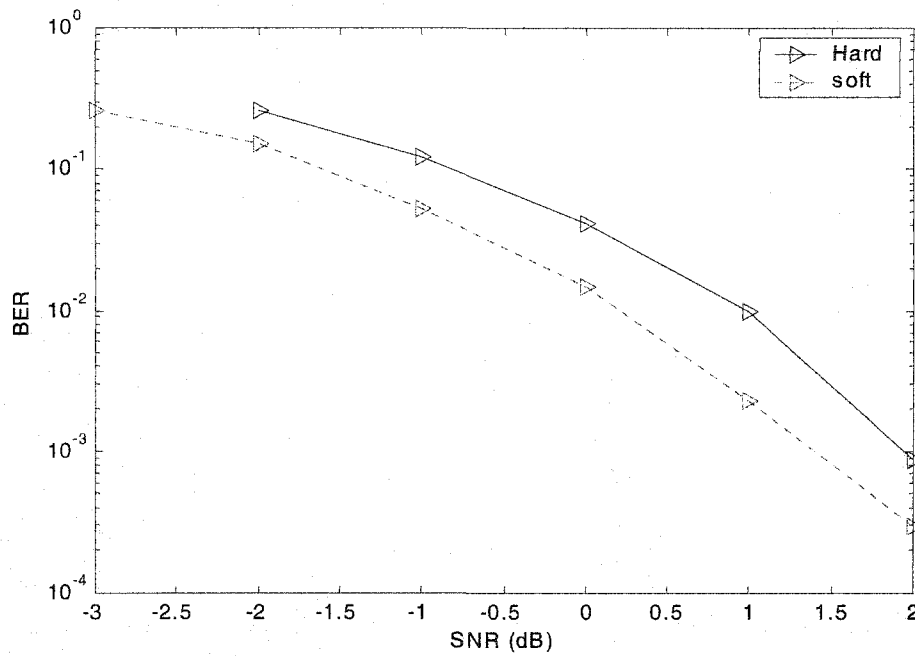
TABLE 2.5

## SIMULATION PARAMETERS FOR THE VITERBI DECODER

Parameter	Data	Units
Carrier Frequency	2000	MHz
Information Bit Source	Random	
FEC Code Rate	1/2, or 1/3	
Channel Model	AWGN	
Vehicle Speed	0	
Signal Constellation	QPSK, or 8PSK	
Spreading Factor	16	
Transmission Time Interval (TTI)	10	ms
Channelization Code	1	

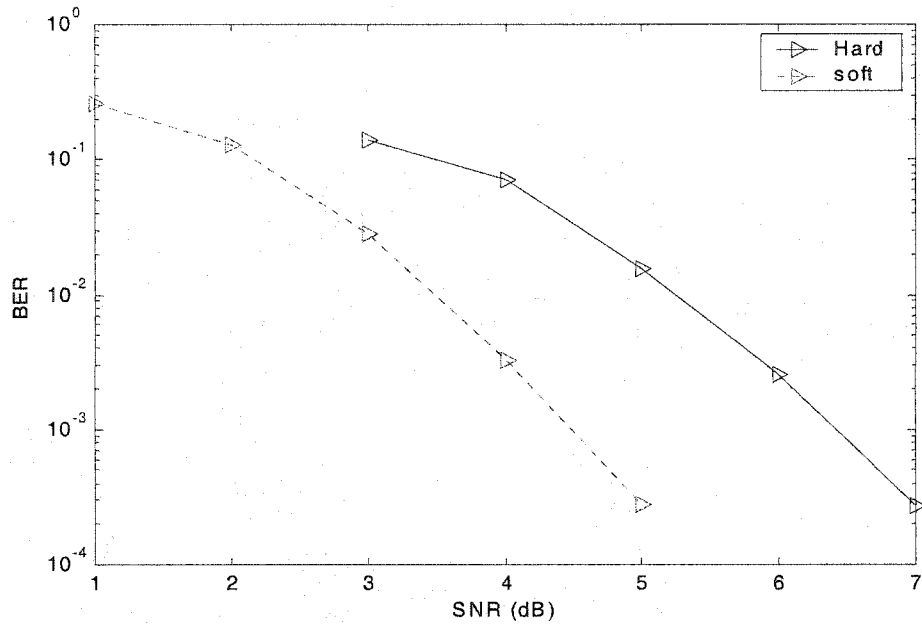


(a) BER versus SNR for 1/2 code-rate system.

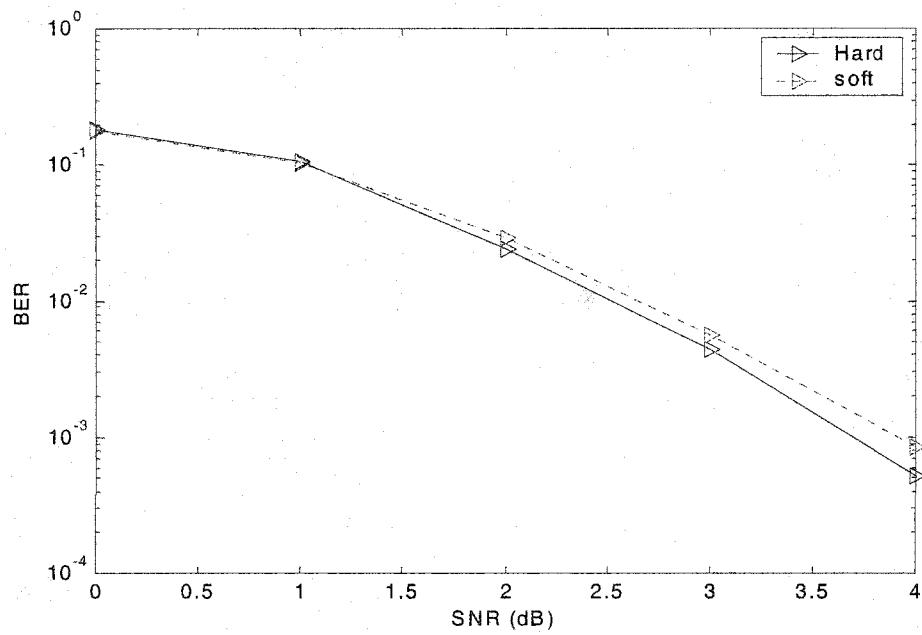


(b) BER versus SNR for 1/3 code rate system.

Fig. 2.13 Performance of QPSK constellation for the TD-SCDMA system.



(a) BER versus SNR for 1/2 code-rate system.



(b) BER versus SNR for 1/3 code rate system.

Fig. 2.14 Performance of 8PSK constellation for the TD-SCDMA system.

## Chapter 3

### Synchronization Performance of the Uplink

#### 3.1 Introduction

Among all the 3G systems being approved, TD-SCDMA is unique in its uplink synchronization technique, which, together with joint detection algorithms, enhances the coverage of a base station and allows TD-SCDMA deployments for macro, micro and pico cell applications. This synchronization is responsible for its good performance, which is reported to be better than any other 3G systems by ensuring signal orthogonality among traffic channels [3]. All signals coming from each terminal will be synchronous at the input of the base station demodulator. This synchronization is important to guarantee orthogonality of the spreading codes and to decrease multiple access interference from other code channels in the same RF channel. All of these signals are to be synchronized at  $1/8$  of a code chip using a closed loop and an open loop control, which should hold even for a fast moving user. Because of this synchronization, the orthogonality of the signals for each code channel is insured and the co-channel interference is reduced to small levels, within

the same cell. In this chapter we evaluate the system synchronization requirements and their impact on its performance under realistic conditions.

Most CDMA systems do not require synchronous operation, since the spreading codes commonly used for multiple-access have good cross-correlation properties [29]. The question of why synchronization is required for the recently proposed TD-SCDMA system and its impact on performance is the central concern of this chapter.

### **3.2 Uplink Synchronous Transmission**

TD-SCDMA is a system based on a combination of two multiple-access techniques--time division multiple access (TDMA) and synchronous CDMA (SCDMA) [3]. In this system, the spreading codes are OVSF codes, which can preserve orthogonality in the same timeslot while using different spreading factor codes. This orthogonality property ensures a good performance, i.e., low interference from other users. But this performance comes at the expense of very strict uplink synchronization requirements.

These synchronization requirements in an operational environment using realistic simulations of a single cell with two users were evaluated. Details of the mobile transmitter are shown in Fig. 2.2, including all the function blocks as called for in the standard [20], [21]. Some of which are at the chip-level, while others are done at the sample-level (1 chip = 8 samples). A typical RAKE receiver is shown in Fig. 2.7.

Many function blocks in this receiver accomplish the reverse tasks of the transmitter. The synchronization procedure according to the standard [20], [30], is outlined in Fig. 3.1.

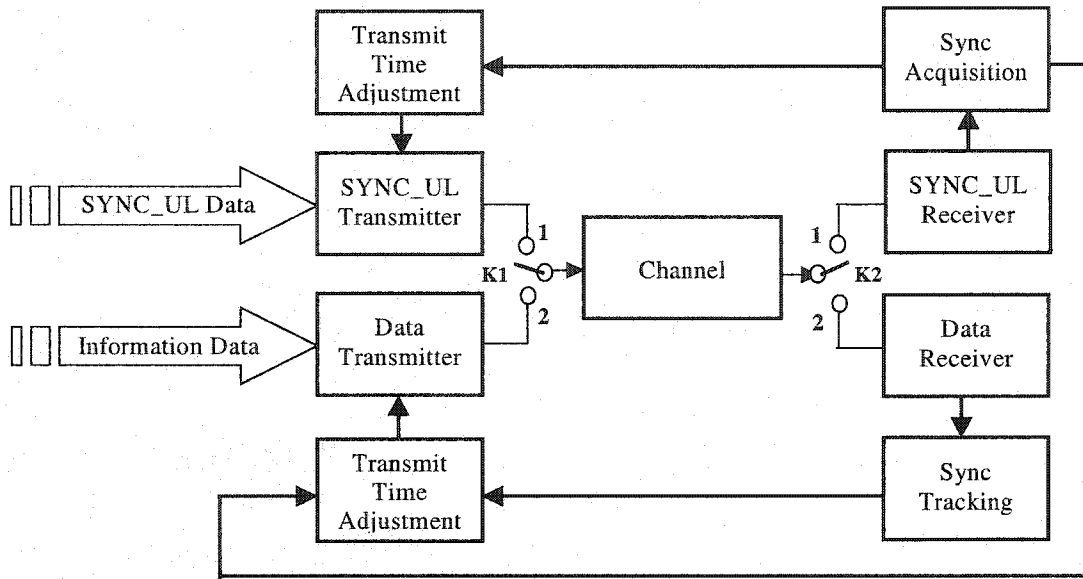


Fig. 3.1. Synchronized reverse system for TD-SCDMA.

### 3.2.1 Synchronous Scheme

The uplink synchronous transmission scheme can reduce uplink intra-cell interference by making the base-station receive orthogonalized signals from the mobile stations. This synchronization scheme includes two steps: acquisition and tracking as shown in Fig. 3.1.

### 3.2.1.1 Synchronization Acquisition

The acquisition mode is shown in Fig. 3.1 when both switches **K1** and **K2** are in position 1. When the user power is on, it first needs to establish the downlink synchronization with the cell. Once the downlink synchronization is established, the user can start establishing uplink synchronization. Though the user can obtain the downlink synchronization, the distance to the base station is still uncertain which may lead to an unsynchronized uplink transmission. The first transmission in the uplink direction is in a special time-slot UpPTS (referred to subframe structure in Fig. 3.2) to reduce the interference in the normal time-slots. The user transmits the access signature SYNC\_UL for uplink synchronization. On receiving the signal, the base station estimates the synchronization time shift, and feeds it back to the user, who in turn adjusts its transmitting time. The base station estimates and feeds back the time shift one more time, before synchronization is established.

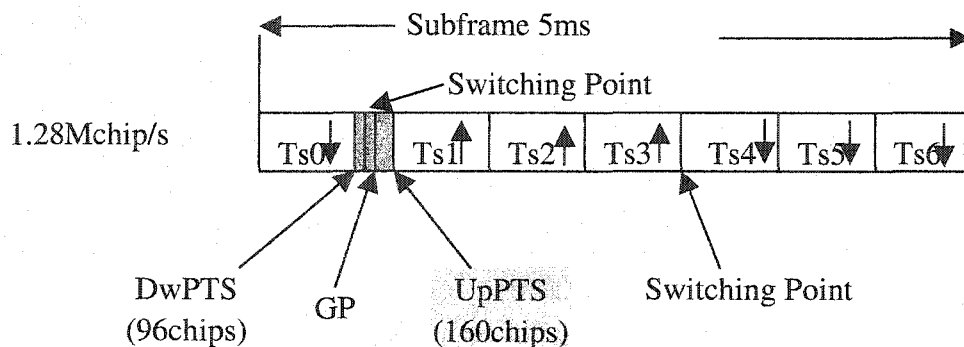


Fig. 3.2. The TD\_SCDMA subframe structure.

### 3.2.1.2 Synchronization Tracking

The tracking mode is shown in Fig. 3.1 when both switches **K1** and **K2** are in position **2**. After acquiring synchronization, the transmitter sends the information data including a midamble training sequence in a data burst, shown in Fig. 3.3. From the midamble information, the base station estimates the synchronization time shift, and feeds it back to the user transmitter. The user can adjust the transmitting time of the next transmission. Thus, the midamble training sequence included in the data burst is the technique used to maintain synchronization.

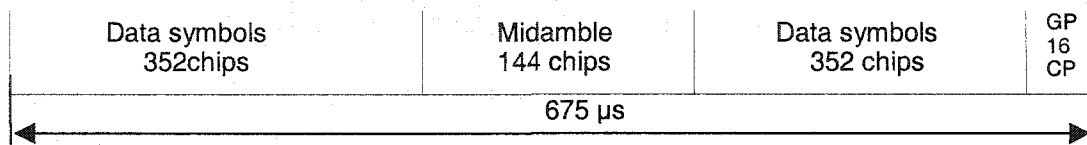


Fig. 3.3. Burst structure. (GP denotes the guard period and CP the chip period)

### 3.2.2 Channel Model

The multi-path propagation channels are set up according to the ITU.1225 models for 3G, shown in Tables 2.3 and 2.4. In every path, we use the Jakes' fading model [24] to simulate the Doppler spread. The transmitted sequence is also contaminated with AWGN.

### 3.3 Synchronization Performance Analysis

In a multipath environment, uplink synchronization means that the main paths are synchronized at the base station (see Fig. 3.4). In a real situation, synchronization may not be strictly achieved. In this section, the issues of main path estimation and performance sensitivity to time misalignment are addressed.

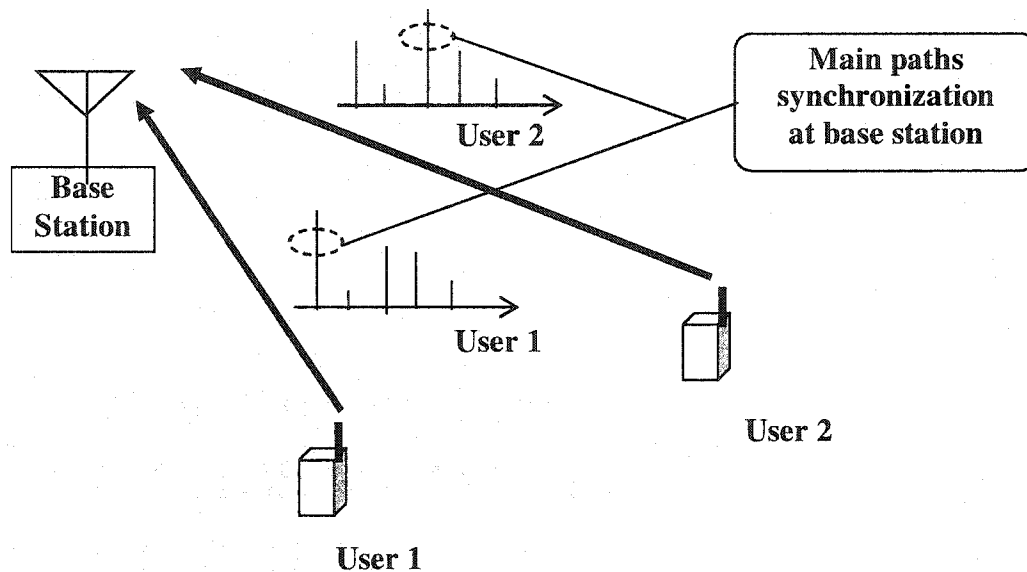


Fig. 3.4. Uplink synchronization in a multipath environment.

#### 3.3.1 Main Path Estimation

Synchronization is a critical issue in a TD-SCDMA system. In an operational environment signals go through a multi-path propagation channel and not all multi-

path components can be synchronized. Only the main path from each mobile in the cell can be synchronized, as illustrated in Fig. 3.4. The estimation of the main-path time delay stands out to be a decisive factor in determining system performance.

In the middle of every timeslot, there is a training sequence—the midamble, which occupies 144-chips. We can use this sequence to estimate the time delay of the main path. In this section, we first consider a cross-correlator to identify the time delay, and later we add a minimum-mean-square-error (MMSE) estimator to refine the time delay estimate.

### *1) Correlation estimator*

Under the assumption that during one time slot the channel remains unchanged, we can estimate the main path time delay by correlating the received midamble signal with the transmitted training signal. Cross-correlation is defined as the integral

$$h(\tau) = \int_{-\infty}^{\infty} s(t) \cdot r(t - \tau) \cdot dt, \quad (3.1)$$

which is a measure of the similarity between the transmitted midamble signal  $s(t)$  and the received midamble signal  $r(t)$  with time advance  $\tau$ . By locating the largest peak of the cross-correlation function  $h(\tau)$ , we can estimate the time delay of the main

path. All these computations are in the discrete time domain—sample-level, and the summation operation  $\sum$  replaces the integral operation  $\int$ .

## 2) Correlation and MMSE estimator

An alternative approach is to refine the sliding correlator estimate with an MMSE estimator, i.e., the correlation estimator is first used to coarsely identify the main path time delay, and the MMSE estimator is then employed to finely locate the time delay.

Let

$$\mathbf{S} * \mathbf{h} = \mathbf{r}, \quad (3.2)$$

where  $\mathbf{S}$  is the mid-amble information matrix,  $\mathbf{h}$  is the channel coefficients vector, and  $\mathbf{r}$  is the received mid-amble vector. In particular, for a ten-tap delay-line channel model, the matrix and vectors are given by

$$\mathbf{S} = \begin{bmatrix} s(0) & 0 & \dots & 0 \\ s(1) & s(0) & \dots & 0 \\ s(2) & s(1) & \dots & 0 \\ s(3) & s(2) & \dots & 0 \\ \dots & \dots & \dots & \dots \\ s(1151) & s(1150) & \dots & s(1142) \end{bmatrix}, \quad (3.3)$$

$$\mathbf{h} = [h(-4) \quad h(-3) \quad \dots \quad h(0) \quad \dots \quad h(4) \quad h(5)]^T, \quad (3.4)$$

$$\mathbf{r} = [r(-4) \quad r(-3) \quad r(-2) \quad r(-1) \quad \dots \quad r(1147)]^T. \quad (3.5)$$

In this model,  $s(k)$  is the mid-amble symbol transmitted during the  $k$ th sample interval,  $h(j)$  is the channel coefficient for the  $j$ th path ( $h(0)$  denotes the strongest path identified by the correlation estimator), and  $r(p)$  is the received mid-amble symbol for the  $p$ th sample interval. The mid-amble sequence in our system consists of 1152 samples. We use the MMSE criterion to estimate  $\mathbf{h}$ , as

$$\mathbf{h} = (\mathbf{S}^H * \mathbf{S})^{-1} * \mathbf{S}^H * \mathbf{r}. \quad (3.6)$$

After solving for  $\mathbf{h}$ , we can further identify the index  $j$  corresponding to the largest  $h(j)$  value (largest amplitude). This  $j$  provides an estimate of the main path time delay.

### 3.3.2 Synchronization and Code Cross-Correlation Properties

Codes commonly used in CDMA to allow for the multiple access of several signals at the same carrier frequency have cross-correlation functions that are uniformly low, especially when the time-shift between different users is small, leading to low levels

of interference from different coded channels. Usually, CDMA systems do not require time synchronization [29].

Let us check the spreading codes used in the TD-SCDMA standard. The codes used are OVSF codes and scrambling codes. All the users in the same timeslot share the same scrambling code within a cell. Then the properties of the spreading code are mainly determined by the OVSF codes, which can preserve orthogonality while using different spreading factors in the same timeslot. The orthogonality property assumes perfect synchronization. We are interested in investigating what happens in the presence of some time-shift. For that we need to look at the cross-correlation function of different OVSF codes. Consider, for example, scrambling code 1 and OVSF codes with a spreading factor of 16. The cross-correlation functions are periodic with period 16 chips, and are shown in Fig. 3.5. We see from Fig. 3.5 that code-pairs 3 and 5 and 2 and 4 are good because the cross-correlation is very low for small time-shifts. This indicates that performance should not be very sensitive to time-misalignment for these pairs. The code-pair 3 and 7 is very poor with a large cross-correlation value for a small time-misalignment, and should lead to large performance losses for small time-shifts. The code-pair 5 and 13 is somewhere in-between the two previous examples.

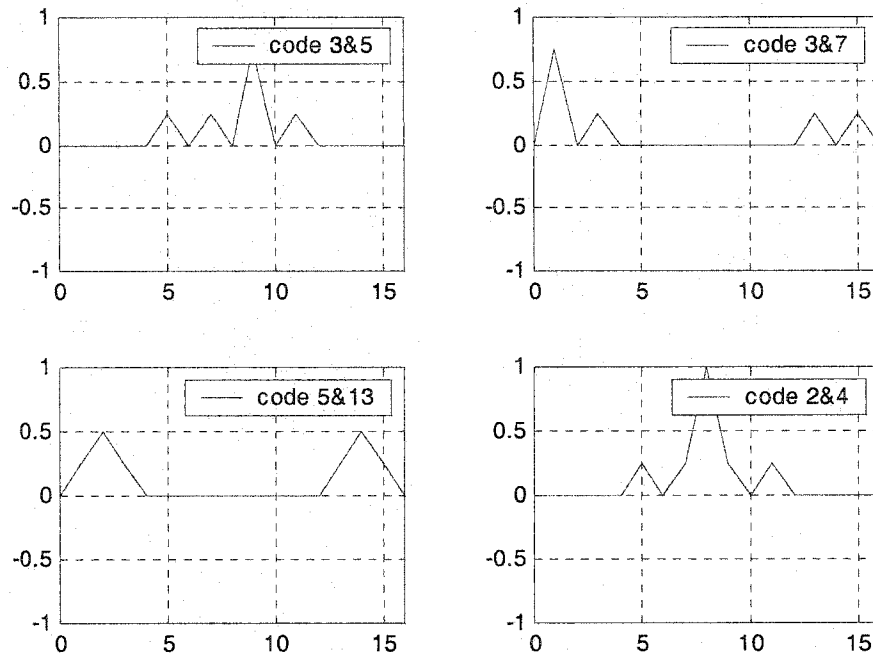


Fig. 3.5. Cross-correlation functions for some OVSF code-pairs.

### 3.3.3 Performance and Code Auto-Correlation Properties

Both autocorrelation and cross-correlation are critical in wireless spread spectrum communication system. Autocorrelation is a measure of the similarity between a signal and a phase-shifted replica of itself [31]. Autocorrelation is of most interest in choosing code sequences that give the least probability of false synchronization, which means that the autocorrelation function should only have one peak and the peak should be narrow and high valued. When the auto-correlation function has more side peaks, some energy will spill out in multi-path environments, causing more

interference. Thus system performance will degrade by using these codes. Consider, for example, scrambling code 1 and OVSF codes with a spreading factor of 16. The auto-correlation functions are periodic with period 16 chips, and are shown in Fig. 3.6. We can see that these OVSF codes have good auto-correlation properties. This ensures good performance just by using standard techniques

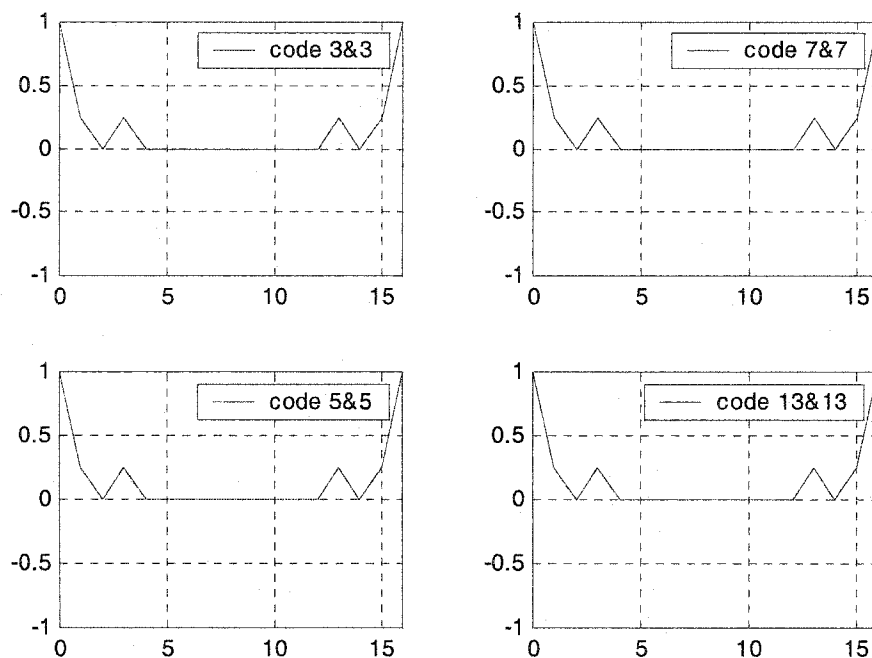


Fig. 3.6. Auto-correlation functions of some OVSF codes.

### 3.3.4 Synchronization and Interference

The aim of the synchronization operation is to orthogonalize all the users at the base station, thus to reduce the interference from other users. The question of whether or not the synchronization always reduces the interference is an important issue.

The interference from other user is mainly decided by two factors—the cross-correlation value and the interfering user energy. As discussed in Section 3.3.2, the cross-correlation function is the deciding factor when the correlation value is not very small, and the interfering user energy can be ignored. But the interfering energy cannot be ignored when the cross-correlation value is very small, say zero, which means the interfering signal is orthogonal to the desired one. Just like AWGN, more energy brings in more interference.

For a TD-SCDMA system in a multipath environment, uplink synchronization means that the main paths are synchronized at the base station (see Fig. 3.4). For the desired user, the main path with less interference is critical to meet performance. Synchronization may bring in more interfering user energy to the main path of the desired user. With some code-pairs, such as code-pair 3 and 5 in Fig. 3.5, they are always orthogonal to each other for small time misalignments. But small time misalignment may offset the interfering user energy from the main path, thus bringing in less interference to the desired user at the main path. This will lead to better

performance than the strictly synchronized case. In this situation, the interfering signal is just like AWGN to the desired user, and less AWGN energy leads to less interference. To validate our analysis, we carried out some computer simulations.

### **3.4 Simulation Results and Discussion**

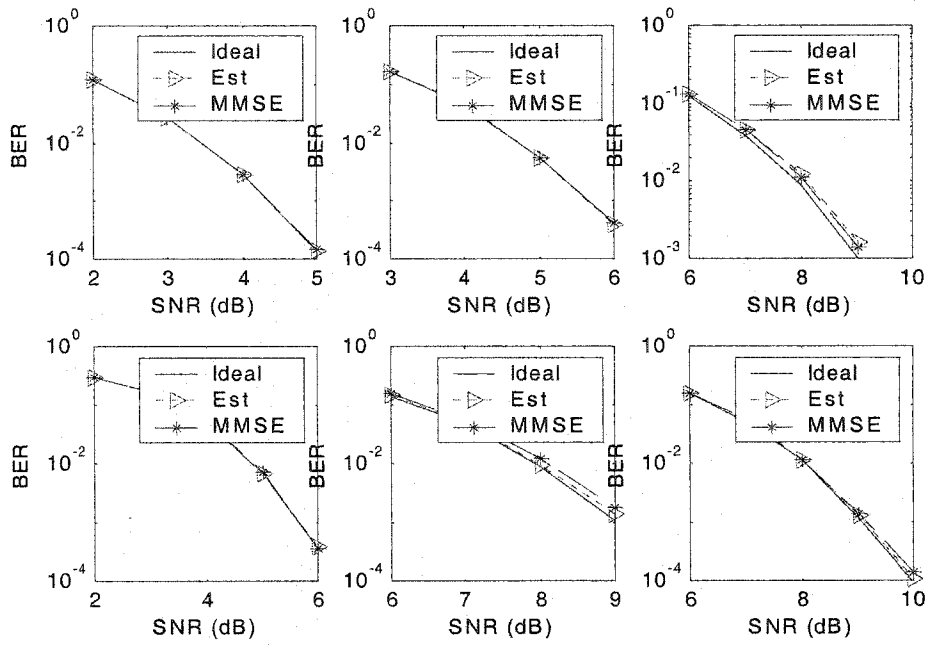
For the TD-SCDMA system validation, the uplink BER simulation is carried out according to the parameters shown in Table 3.1. We consider a two-user system synchronized at the main path with an ideal RAKE receiver having known path parameters, namely time delay and coefficients. We compare the performance using different time delay estimators as shown in Fig. 3.7, where “ideal” means perfect time delay estimate, “Est” stands for correlation estimator, and “MMSE” indicates the use of the sliding correlator and the MMSE estimator. We chose code-pairs 5 and 13 and 3 and 7 because accurate synchronization is needed for these pairs as explained above.

From Fig. 3.7, we can see that the performance loss due to the estimation errors of the main path time delay is very small.

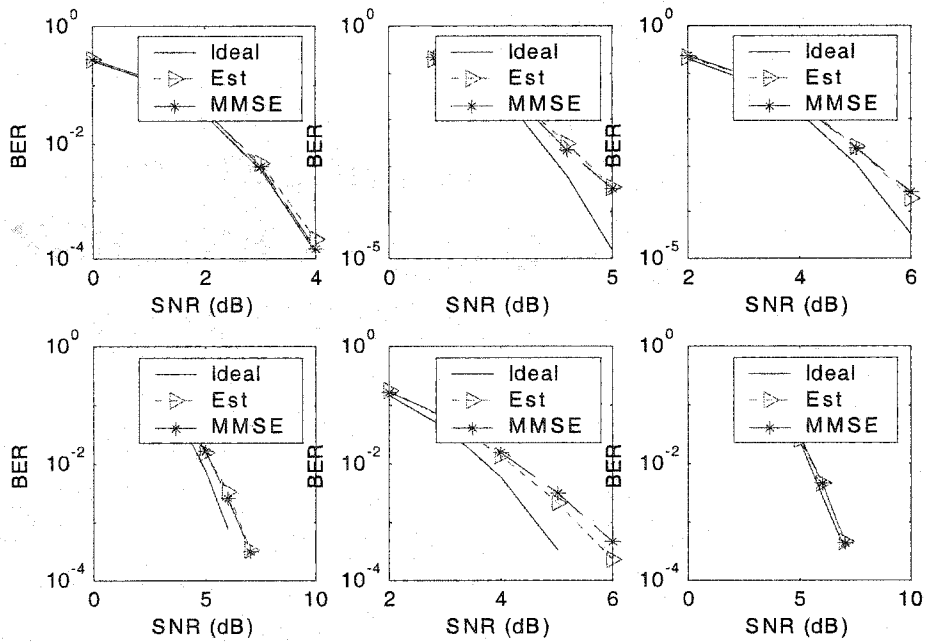
TABLE 3.1

## SIMULATION PARAMETERS FOR SYSTEM VALIDATION

Parameter	Data	Units
Carrier Frequency	2000	MHz
Gross Data Rate	17600	bps
Information Bit Source	Random	
FEC Code Rate	1/2	
Channel Fading	Rayleigh	
Vehicle Speed	0	
Signal Constellation	QPSK	
Spreading Factor	16	
Synchronization Step-Size	1/8	chip
No. of Paths (Fingers)	Up to 6 according to ITU model	
Transmission Time Interval (TTI)	10	ms



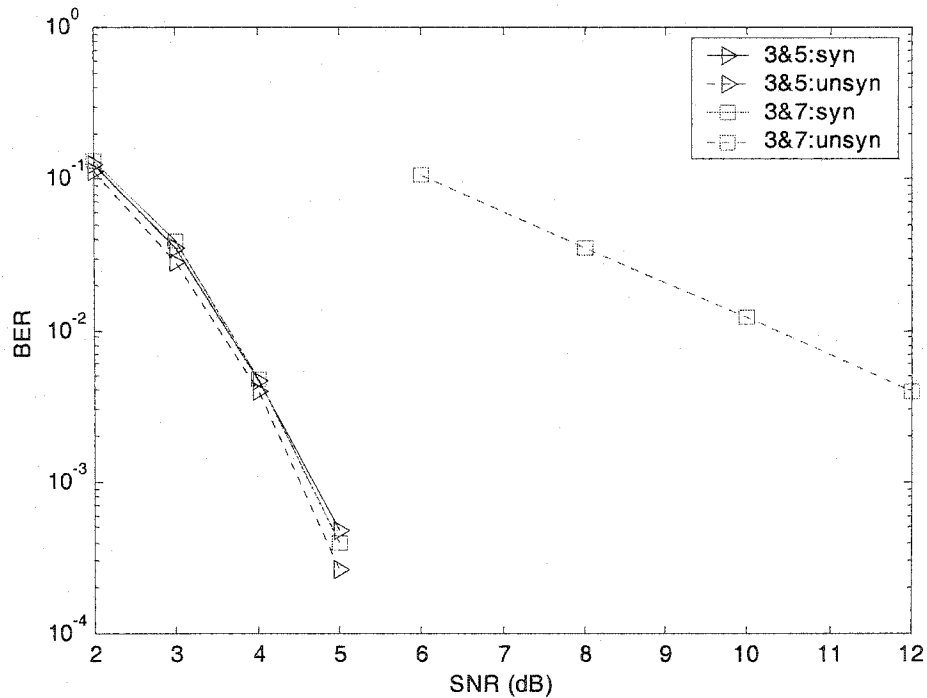
(a) Code-pair 5 and 13.



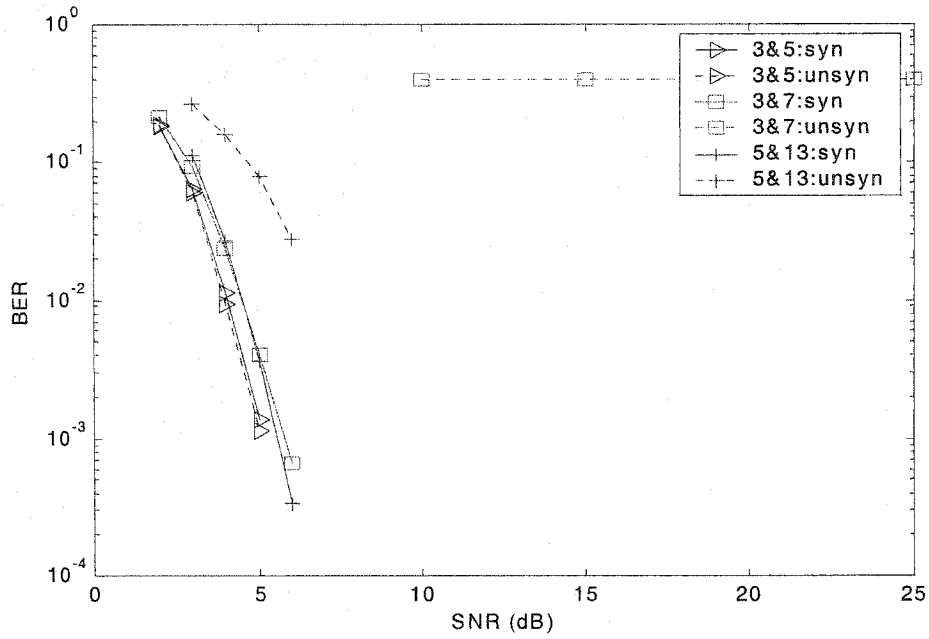
(b) Code-pair 3 and 7.

Fig. 3.7. Comparison of main path time delay estimators for ITU channel models.

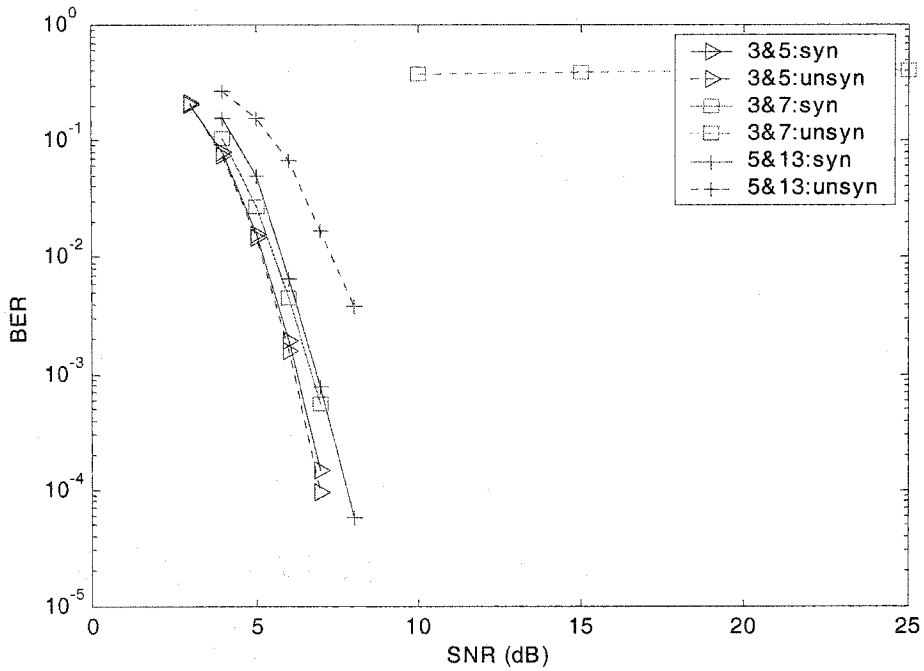
We also compare a synchronized system with an unsynchronized one having a small time-shift, as shown in Fig. 3.8. We can see that the performance loss for the unsynchronized system is heavily dependent on the particular code-pair used and very large for code-pair 3 and 7 as shown in Fig. 3.8. There are relatively large performance losses for time misalignments with code-pair 5 and 13, while code-pair 3 and 5 is not very sensitive to time-misalignment as shown in Fig. 3.8. These results are in agreement with our analysis.



(a) Single path channel



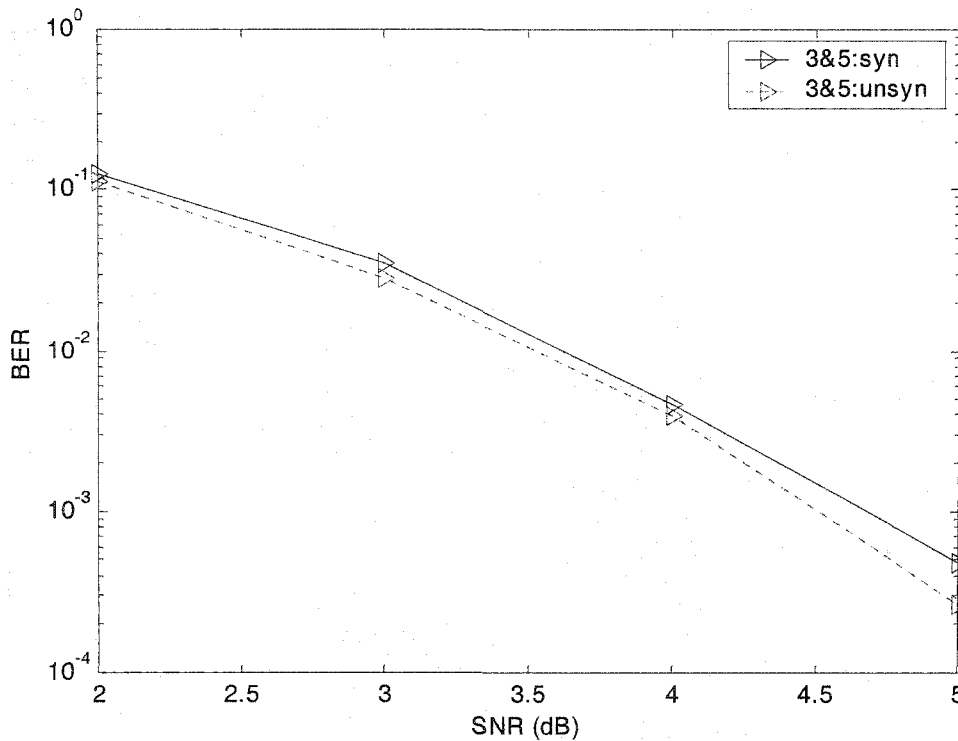
(b) ITU Channel-A-indoor model



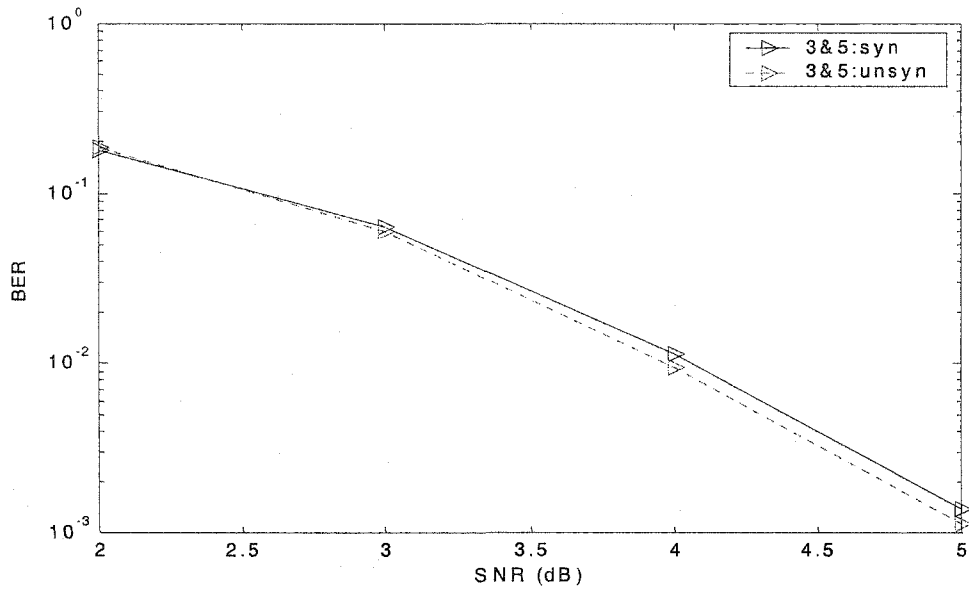
(c) ITU Channel-A-indoor-to-outdoor model.

Fig.3.8. Performance comparison of synchronized and unsynchronized systems.

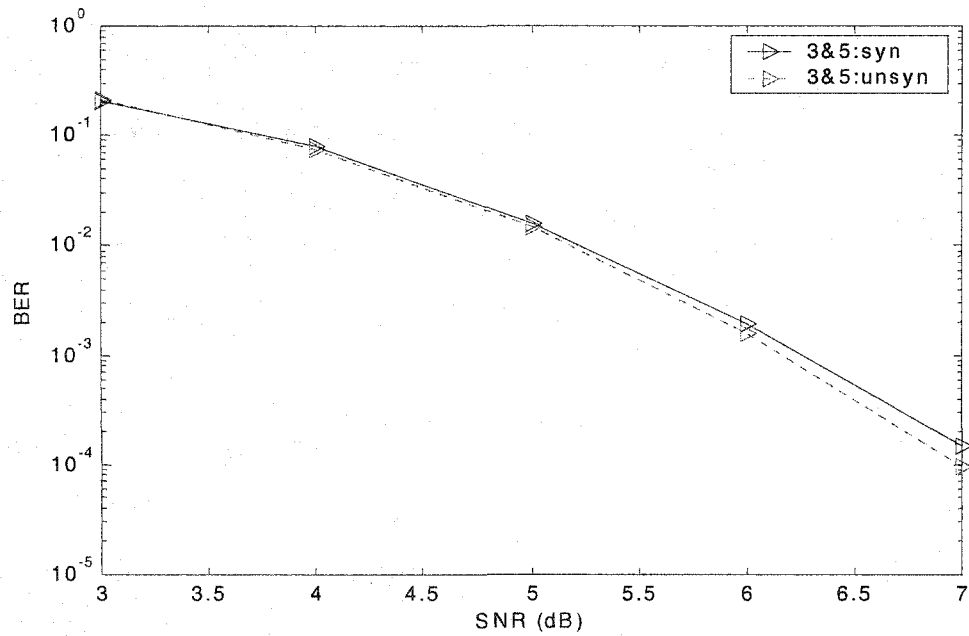
For the case where signals remain orthogonal for a small time misalignment, as in code-pair 3 and 5, it is interesting to determine the performance without synchronization. The simulation results are given in Fig. 3.9. From the figure, we can see that the unsynchronized system works even slightly better than the synchronized one, which is against our intuition, but in agreement with our analysis. This gain is very small, and it can be ignored compared to the large loss with other code pairs requirements such as pair 3 and 7 in Fig. 3.8. For the system to meet the performance, the synchronization operation is necessary.



(a) Single path channel



(b) ITU Channel-A-indoor model



(c) ITU Channel-A-indoor-to-outdoor model.

Fig. 3.9. Performance comparison of synchronized and unsynchronized systems with a small time-shift using code-pair 3 and 5.

### **3.5 Conclusion**

We evaluated the synchronization performance of the TD-SCDMA standard recently proposed by CWTS using realistic simulation scenarios involving two users within a cell. The need for synchronization was traced to the usage of the OVSF codes and it was shown that while for some pairs of codes the performance loss due to time misalignment is small, for some pairs there even exists a very small gain, and other pairs it is very sensitive to small time shifts. For the system to meet performance specifications synchronization is necessary, and can be achieved using standard techniques without introducing significant performance losses. The spreading OVSF codes used in this standard are the main reason for the need for uplink synchronization. These codes were selected because they preserve the orthogonality property in the same timeslot while using different spreading factors.

## Chapter 4

### Channel Estimation and Equalization for the Uplink

#### 4.1 Introduction

SCDMA techniques possess inherent protection against coherent interference since the orthogonal spreading OVSF codes are used. However, after going through mobile wireless communications channel, which is characterized by time-varying multi-path channel fading [32], the signals lose their orthogonal property. This will lead to a performance loss due to increased cross correlation. To prevent performance degradation, channel estimation or channel equalization is needed to improve the detection.

One way to compensate for multi-path fading is diversity [33]. In this chapter, we provide diversity using a RAKE receiver, whose performance is based on accurate channel multipath estimation. When we supply to the receiver several replicas of the same information signal transmitted over independently fading channels and combine the signals using a maximum-ratio-combining (MRC) algorithm, the probability that the combined signal will fade is reduced considerably, thus, performance is improved.

From another perspective, channel distortion results in intersymbol interference (ISI), which causes high error rates [33]. One solution for this ISI problem is to design a receiver that employs an algorithm for compensating the ISI in the received signal. The compensator for the ISI is an equalizer. Our equalization method will be based on the use of a linear filter with adjustable coefficients. The MMSE criterion is used to optimize the equalizer coefficients.

## **4.2 RAKE Receivers**

### **4.2.1 RAKE Receiver Models**

The RAKE receiver is designed to operate in a multipath environment. The midamble sequence (also called training sequence or pilot sequence) in every timeslot of the TD-SCDMA system is very valuable for estimating the multipath fading-channel parameters (including amplitude and phase). It is beneficial for detecting multipath rays so that the RAKE fingers can efficiently combine multipath components for coherent reception [34]. Accurate channel estimation is critical to reliable coherent communications [35].

The basic idea of the RAKE receiver is to use the pseudo-noise property of the signal to resolve the multipath components, and then to combine the multipath components

using certain combining algorithm. The basic system model for a RAKE receiver is given in Fig. 4.1. In this system, we assume that there are  $L$  diversity channels, carrying the same information-bearing signal, and the  $L$  channels are mutually statistically independent. Thus, the equivalent low-pass received signals for the  $L$  channels can be expressed as

$$\begin{aligned} r_k(t) &= \alpha_k s_k(t) + n_k(t) \\ &= |\alpha_k| e^{-j\phi_k} s_k(t) + n_k(t), \quad k = 1, 2, \dots, L \end{aligned} \quad (4.1)$$

where,  $\{|\alpha_k| e^{-j\phi_k}\}$  represent the attenuation factors and phase shifts for the  $L$  channels,  $s_k(t)$  denotes the signal transmitted on the  $k$ th channel, and  $n_k(t)$  denotes the AWGN on the  $k$ th channel.

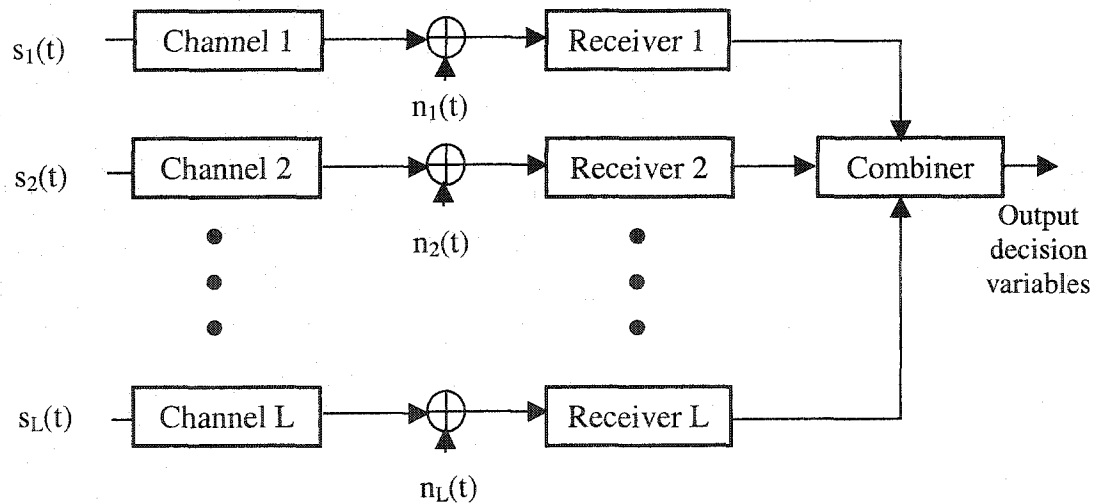


Fig. 4.1. Basic system model with RAKE receiver for TD-SCDMA uplink.

In the system with a RAKE receiver, we need to address three issues:

- Model for the multipath components.
- Combining algorithm for good performance.
- Estimation methods for multipath parameters.

#### 4.2.1.1 Tapped-Delay-Line Channel Model

If the channel is assumed to be slowly fading, then the noiseless received signal through the multipath channel can be expressed as

$$r(t) = \sum_k \alpha_k(t) s(t - kT), \quad (4.2)$$

where,  $\alpha_k(t)$  is the complex-valued channel parameter in the  $k$ th channel, including attenuation and phase shift, and  $s(t)$  is the transmitted signal. We assume that the total multipath spread is  $T_m$ . Then the tapped delay line model for the channel can be truncated at  $L = T_m / T + 1$  taps, where  $T$  is the chip duration of 781.25 ns since the chip rate is 1.28 Mcps for the TD-SCDMA system. The truncated tapped delay line channel model is shown in Fig. 4.2.

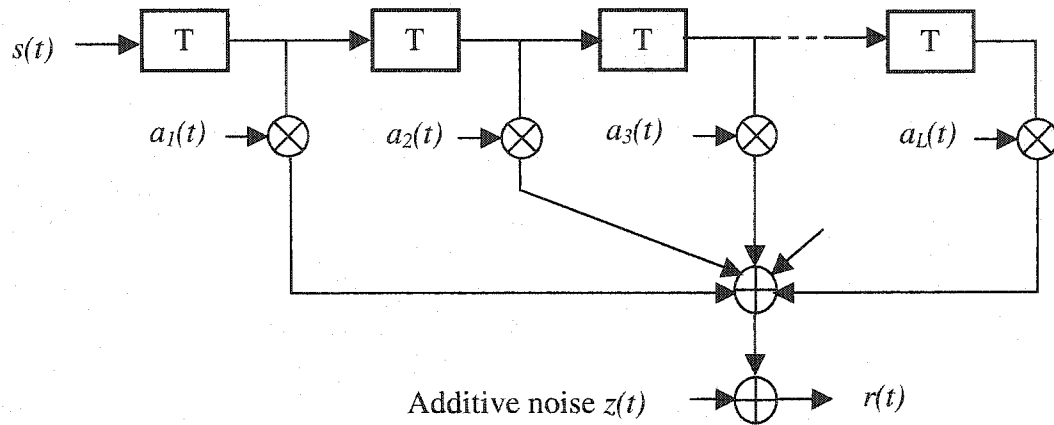


Fig. 4.2. Tapped delay line channel model for RAKE receiver.

In the channel model, energy distribution among different channel is done according to ITU model, shown in Tables 2.3 and 2.4. The time-variant effect in every coefficient is model by Jakes fading model [24].

#### 4.2.1.2 Maximal Ratio Combiner

The combining algorithm in the RAKE receiver for the TD-SCDMA system is the maximum ratio combining shown in Fig. 4.3. This combiner achieves the best performance in which each matched filter output is multiplied by the conjugate of the complex-valued channel gain  $|\alpha_k|e^{-j\phi_k}$  [33]. The effect of this multiplication is to compensate for the phase shift in the channel and to weight the signal by a factor that is proportional to the signal strength. Thus, a strong signal carries a larger weight than a weak signal. This optimum combiner assumes that the channel parameters as attenuation  $\{|\alpha_k|\}$  and phase shift  $\{\phi_k\}$  are perfectly known. In the real TD-SCDMA

system, the estimation of channel parameters will not be ideal. There may be some performance loss due to estimation error.

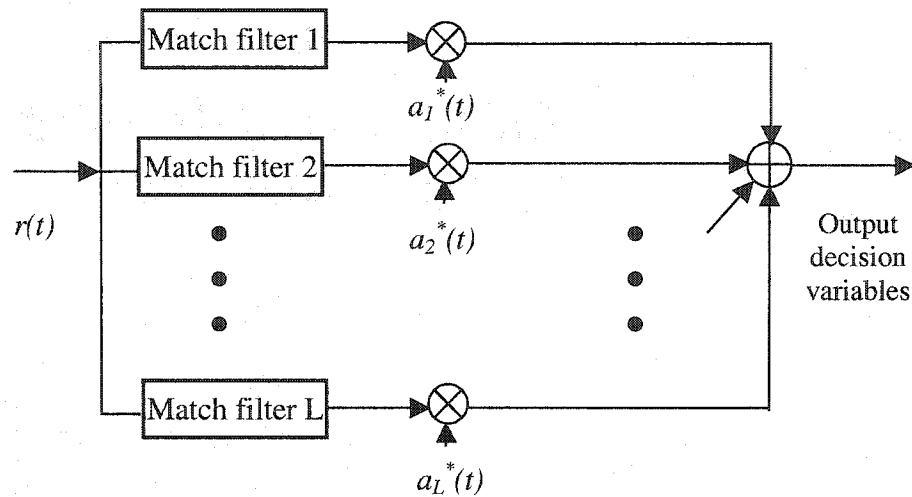


Fig. 4.3. Maximal-ratio-combiner in TD-SCDMA.

#### 4.2.1.3 Channel Estimation

In a practical system, relatively good estimates can be obtained when the channel fading is sufficiently slow. In this section, we consider two methods to estimate the channel coefficients: cross-correlation estimation and linear minimum-mean-square-error (MMSE) estimation.

#### 4.2.1.3.1 Cross-correlation Channel Estimation

This method uses the property that the midamble sequence for every user has a noise-like autocorrelation function to estimate every tap weight of the channel path. Fig. 4.4 illustrates this method for estimating the tap weights in TD-SCDMA. In the figure,  $r_m(t)$  is the received midamble signal,  $s_m^*(t)$  is the conjugate of the transmitted midamble signal, and  $\hat{a}_k(t)$  is the estimated value of the  $k$ th path coefficient.

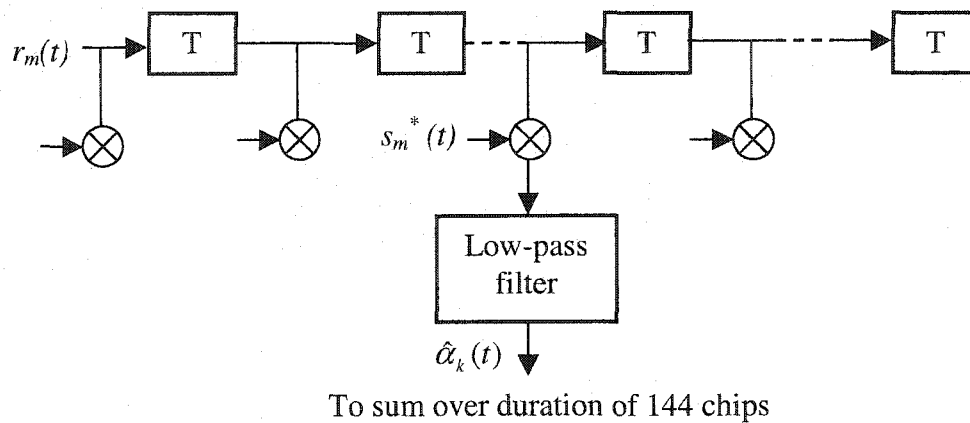


Fig. 4.4. Channel tap weight estimation with cross-correlation method.

#### A. Tap weight calculation

We can derive the coefficient estimates  $\hat{\alpha}_k(t)$  under the assumption that the channel remains unchanged during one time slot, including the 144 chips of the midamble

signal. We know that the received noise midamble signal  $r_m(t)$  at the output of the multipath channel can be expressed as

$$r_m(t) = \sum_k \alpha_k(t) s_m(t - kT) + n(t), \quad (4.3)$$

where  $\alpha_k(t)$  denotes the  $k$ th channel coefficients. After sampling all the signals at the chip-rate, we got

$$r_m(nT) = \sum_k \alpha_k(nT) s_m(nT - kT) + n(nT), \quad n = 0, 1, \dots, 144, \quad (4.4)$$

which can be simplified to

$$r_m(n) = \sum_k \alpha_k(n) s_m(n - k) + n(n), \quad n = 0, 1, \dots, 144. \quad (4.5)$$

Considering that  $\alpha_k(t)$  remains constant during 144 chips of the midamble signal, (4.5) can be written as,

$$r_m(n) = \sum_k \alpha_k s_m(n - k) + n(n), \quad n = 0, 1, \dots, 144. \quad (4.6)$$

Using vectors, (4.6) can be rewritten as

$$\mathbf{r}_m = \sum_k \alpha_k \mathbf{s}_m(k) + \mathbf{n}, \quad (4.7)$$

where  $\mathbf{r}_m$  represent the vector  $[r_m(0) \ r_m(1) \ \dots \ r_m(143)]^T$ ,  $\mathbf{s}_m(k)$  represents the vector  $[s_m(-k) \ s_m(1-k) \ \dots \ s_m(143-k)]^T$ , and  $\mathbf{n}$  denotes the noise vector  $[n(0) \ n(1) \ \dots \ n(143)]^T$ . Hereafter, in the matrix-vector notation,

- $T$  denotes the transpose operation.
- $H$  denotes the Hermition operation.
- $*$  denotes the conjugate operation.

We can derive  $\alpha_M$  from (4.7) when  $k=M$

$$\begin{aligned}
\mathbf{r}_m^T \mathbf{s}_m^*(M) &= \left( \sum_k \alpha_k \mathbf{s}_m(k) + \mathbf{n} \right)^T \mathbf{s}_m^*(M) \\
&= \sum_k \alpha_k \mathbf{s}_m(k)^T \mathbf{s}_m^*(M) + \mathbf{n}^T \mathbf{s}_m^*(M) \\
&= \alpha_M \mathbf{s}_m(M)^T \mathbf{s}_m^*(M) + \sum_{k \neq M} \alpha_k \mathbf{s}_m(k)^T \mathbf{s}_m^*(M) + \mathbf{n}^T \mathbf{s}_m^*(M)
\end{aligned} \tag{4.8}$$

Because of the good autocorrelation function of the midamble sequence the second term goes to zero, and due to the low correlation value of the noise vector  $\mathbf{n}$  and midamble sequence vector  $\mathbf{s}_m(M)$  the third term also goes to zero. Let  $\delta$  denote a very small sum of the 2<sub>nd</sub> and 3<sub>rd</sub> terms, then the equation can simplify to

$$\begin{aligned}
\mathbf{r}_m^T \mathbf{s}_m^*(M) &= \alpha_M \mathbf{s}_m(M)^T \mathbf{s}_m^*(M) + \delta \\
&= \alpha_M \|\mathbf{s}_m(M)\|^2 + \delta \\
\alpha_M &= (\mathbf{r}_m^T \mathbf{s}_m^*(M) - \delta) / \|\mathbf{s}_m(M)\|^2 \\
&= c \cdot \mathbf{r}_m^T \mathbf{s}_m^*(M) + \sigma
\end{aligned} \tag{4.9}$$

where  $c$  denotes a constant,  $\sigma$  represents  $c \cdot \delta$ . Now we derive the estimate for  $\alpha_M$

$$\hat{\alpha}_M = c \cdot \mathbf{r}_m^T \mathbf{s}_m^*(M), \quad M = 0, 1, \dots, L-1. \tag{4.10}$$

This is the cross-correlation operation between the received noise midamble sequence and the shifted version of the transmitted midamble sequence, as illustrate in Fig. 4.4.

## B. Tap identification

An ideal maximum-ratio combiner combines all the  $L$  channel components to make a decision, that is, the combiner assumes that there is one path at every time delay  $T$  and that channel parameters are perfectly known. In practice, that is not the case, which leads to performance degradation, since some of the tap correlators will contribute only noise [33]. Thus, the noise-only contributions should be excluded from the combiner. To exclude the noise-only taps, we only combine a fixed number of strongest paths.

Our aim in this section is to search for these strongest paths. As we see from (4.10)  $\hat{\alpha}_M = c \cdot \mathbf{r}_m^T \mathbf{s}_m^*(M)$  is a function of  $M$ , where,  $M = 0, 1, \dots, L-1$  denotes the tap delay in unit of  $T$  (refer to the tapped delay line channel model in Fig. 4.2). We rewrite the relation as

$$\hat{\alpha} = \varphi(MT), \quad M = 0, 1, \dots, L-1 \quad (4.11)$$

where,  $\hat{\alpha}$  is a function of  $M$  in unit of  $T$ . For easier identification of the peaks of this function, we raise the sample-rate to eight times the chip-rate (1 chip = 8 samples) in the tap weight calculation. Then (4.11) becomes

$$\hat{\alpha} = \varphi(N \cdot T/8), \quad N = 0, 1, \dots, 8L-1 \quad (4.12)$$

where,  $\hat{\alpha}$  is a function of  $N$  in unit of  $T/8$ . By identifying the strongest peaks of the function, we can find the signal paths and exclude the noise-only paths.

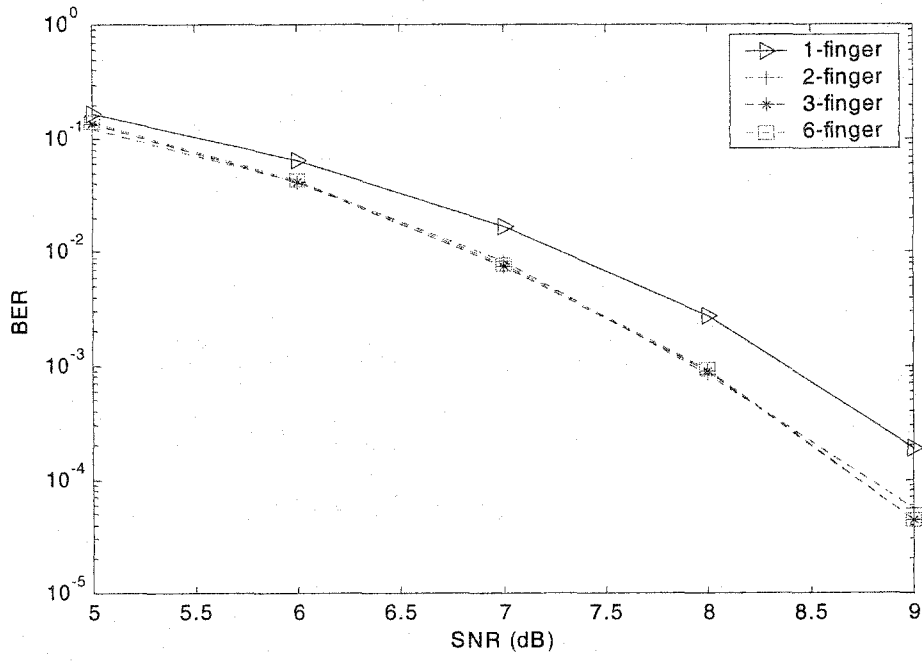
### **C. Simulation Results**

For the TD-SCDMA system performance comparison, the uplink BER is simulated according to the parameters shown in Table 4.1. We consider a one-user system with cross-correlation based RAKE receivers. We compare the performance using different number of combined fingers for ITU channels (refer to Tables 2.3 and 2.4), as shown in Fig. 4.5, where 1-finger means no combination. From the figures, we can see that under some ITU channel models, the multi-finger cross-correlation RAKE receiver does improve (see Fig. 4.5 (a) under Channel-A-vehicular model and (f) under Channel-B-indoor-to-outdoor model), but in others, it does not.

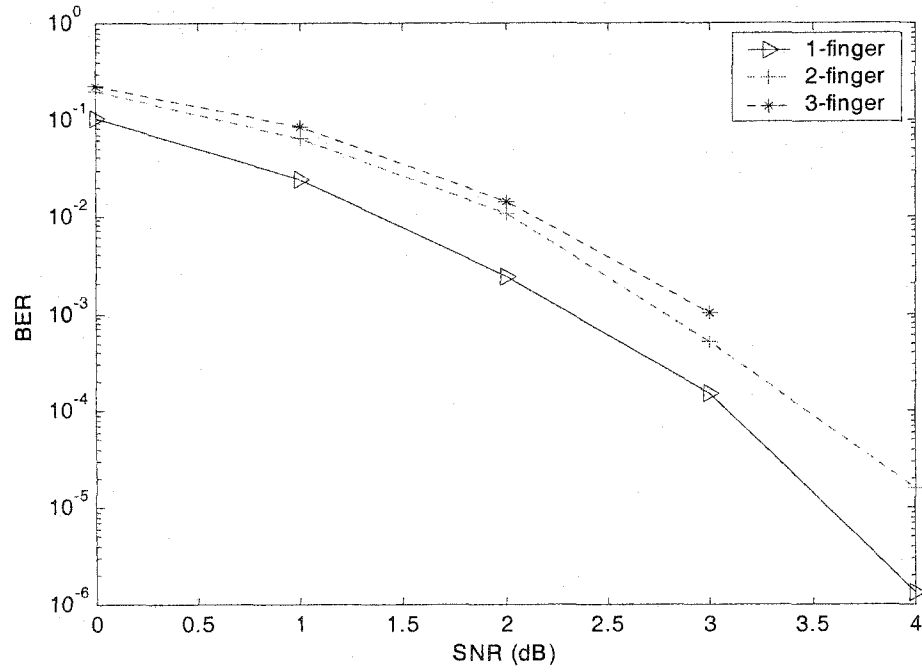
TABLE 4.1

## PARAMETERS FOR RAKE RECEIVERS

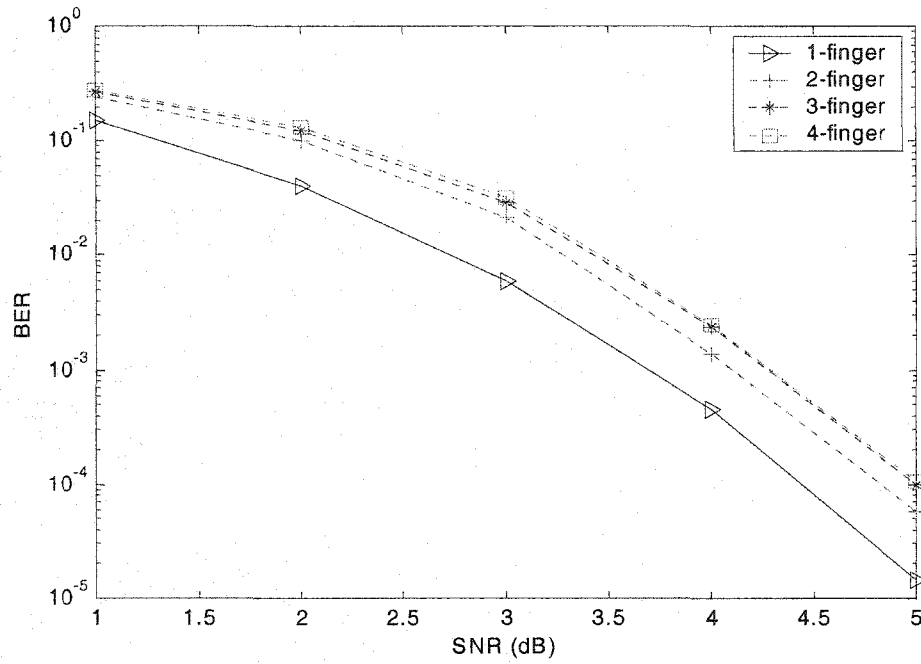
Parameter	Data	Units
Carrier Frequency	2000	MHz
Gross Data Rate	17600	bps
Information Bit Source	Random	
FEC Code Rate	1/2	
Channel Fading	Rayleigh	
Vehicle Speed	0	
Signal Constellation	QPSK	
Spreading Factor	16	
Channelization code	6	
Synchronization Step-Size	1/8	chip
No. of Paths (Fingers)	Up to 6 according to ITU model	
Transmission Time Interval (TTI)	10	ms



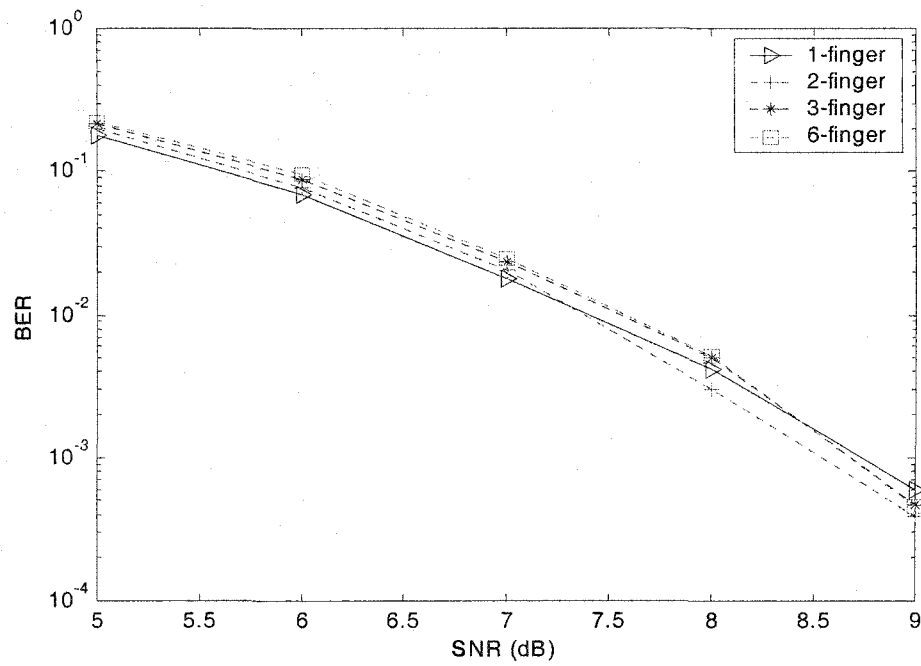
(a) ITU channel-A-vehicular model.



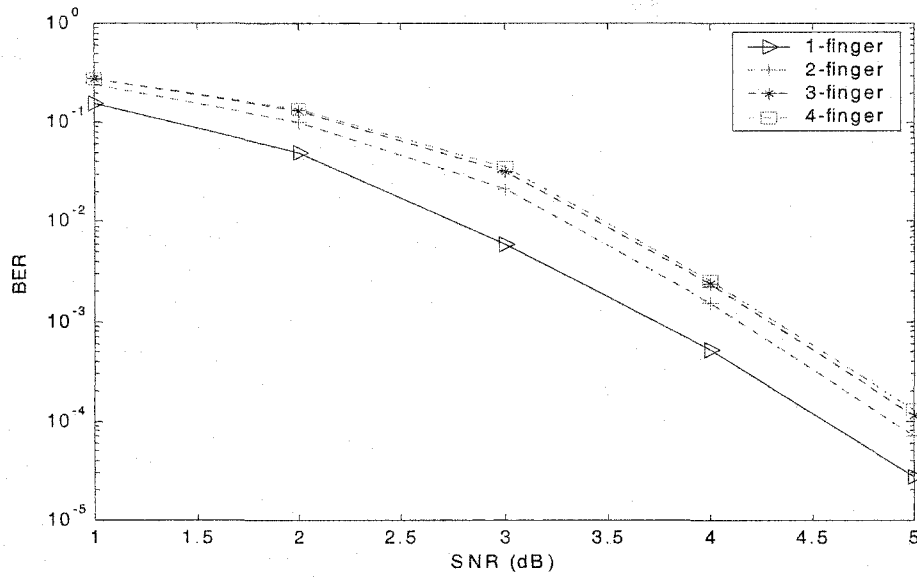
(b) ITU channel-A-indoor model.



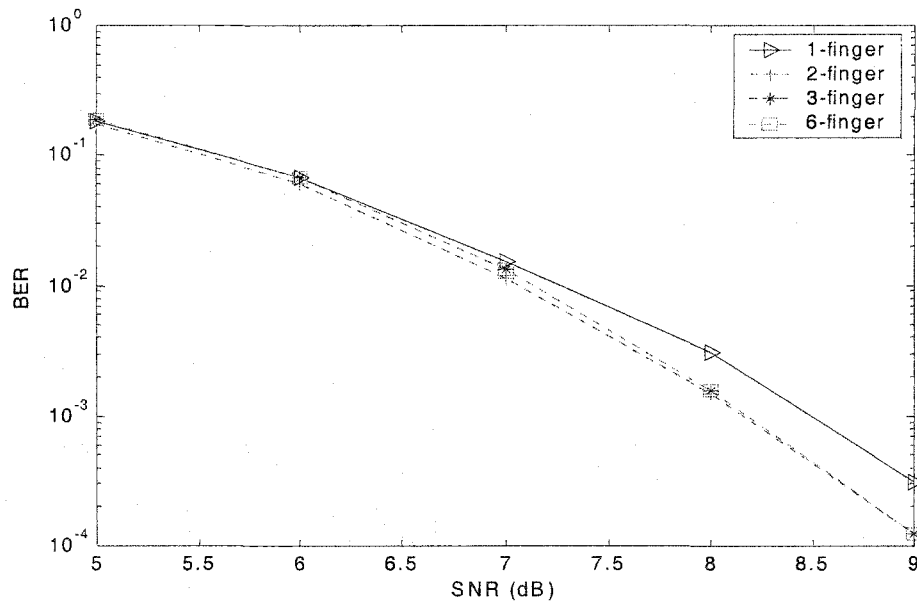
(c) ITU channel-A-indoor-to-outdoor model.



(d) ITU channel-B-vehicular model.



(e) ITU channel-B-indoor model.



(f) ITU channel-B-indoor-to-outdoor model.

Fig. 4.5. Performance of cross-correlation based RAKE receiver with different number of fingers.

Why does the cross-correlation based RAKE receiver not always work well in this system? The TD-SCDMA signal has an equivalent low-pass response with the bandwidth of the square-root raised cosine pulse-shaping filter, which is  $1/2 * 1/T_c$ , where  $T_c$  is the chip period. The cross-correlation RAKE receiver can achieve a resolution of  $T_c$  in the multipath delay profile. This means that the resolution in this system is 781.25 ns. But for the ITU channel models, most of the total multipath spread  $T_m$  is less than 781.25 ns. Thus, for the cross-correlation RAKE receiver the multipath appears to be a single path. The cross-correlation RAKE receiver cannot distinguish the various paths, and its performance is not very good in this system. This prompts us to consider the RAKE receiver with MMSE channel estimation whose channel resolution can be less than  $T_c$ .

#### 4.2.1.3.2 MMSE Channel Estimation

##### A. MMSE-based RAKE receiver method

MMSE channel estimation in a RAKE receiver is just a linear filter (shown in Fig. 4.6), which makes the filtered midamble signal  $\hat{r}_m(t)$  closest to the received midamble signal  $r_m(t)$  in a MMSE sense. We can adjust the tap weight coefficients  $\{\hat{\alpha}_k, k = 0, 1, \dots, L-1\}$  to minimize the error

$$e_m(t) = r_m(t) - \hat{r}_m(t). \quad (4.13)$$

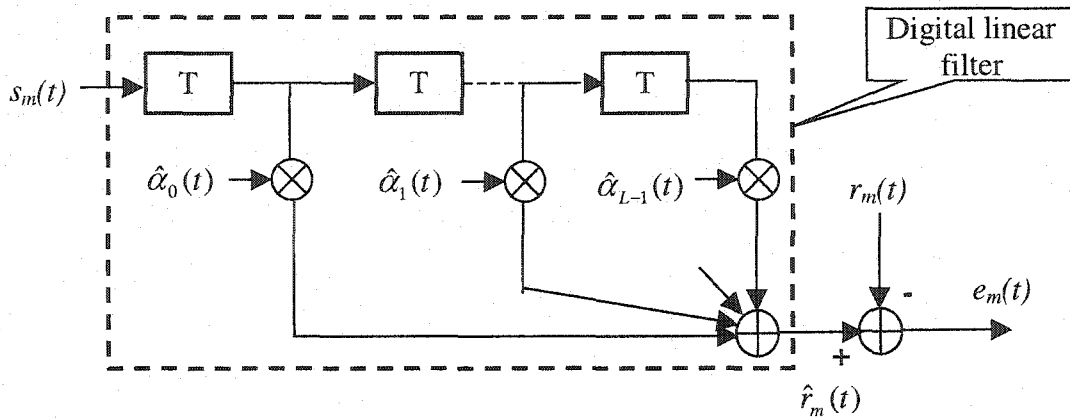


Fig. 4.6. MMSE channel estimation in a RAKE receiver.

Let  $J$  denote the performance index for the MMSE criterion, and  $J$  is defined as

$$\begin{aligned}
 J &= E(|e_m(t)|^2) \\
 &= E(|r_m(t) - \hat{r}_m(t)|^2)
 \end{aligned}
 \tag{4.14}$$

where,  $E$  is the statistical operation of expectation. Then minimizing the error  $e_m(t)$  in the MMSE sense is to minimize  $J$ . Thus, the estimated channel coefficients  $\{\hat{\alpha}_k, k = 0, \dots, L-1\}$  can be identified.

Since in practical systems, the expected value in (4.14) cannot be calculated, a time-average value over the observing period was used. Considering replacing the statistical expected value with the estimated value, minimizing  $J$  is equivalent to obtaining a least squares solution to the following over-determined system of equations

$$\mathbf{S}_m^* \hat{\boldsymbol{\alpha}} = \mathbf{r}_m,
 \tag{4.15}$$

where,  $\mathbf{S}_m$  is the transmitted midamble information matrix,  $\hat{\mathbf{a}}$  is the estimated channel coefficients vector, and  $\mathbf{r}_m$  is the received midamble vector. In particular, when considering a 4-tap-delay-line channel model, the matrix and vectors are

$$\mathbf{S}_m = \begin{bmatrix} s_m(0) & 0 & 0 & 0 \\ s_m(1) & s_m(0) & 0 & 0 \\ s_m(2) & s_m(1) & s_m(0) & 0 \\ s_m(3) & s_m(2) & s_m(1) & s_m(0) \\ \dots & \dots & \dots & \dots \\ s_m(143) & s_m(142) & s_m(141) & s_m(140) \end{bmatrix}, \quad (4.16)$$

$$\hat{\mathbf{a}} = [\hat{\alpha}_0 \quad \hat{\alpha}_1 \quad \hat{\alpha}_2 \quad \hat{\alpha}_3]^T, \quad (4.17)$$

and

$$\mathbf{r}_m = [r_m(0) \quad r_m(1) \quad r_m(2) \quad r_m(3) \quad \dots \quad r_m(143)]^T. \quad (4.18)$$

In this model,  $s_m(k)$  is the midamble symbol transmitted in the  $k$ th chip interval,  $\hat{\alpha}_k$  is the estimated channel coefficient in the  $k$ th multipath ( $\hat{\alpha}_0$  means the strongest path), and  $r_m(k)$  is the received midamble symbol in the  $k$ th chip interval. The least squares solution [36] for (4.15) is

$$\hat{\mathbf{a}} = (\mathbf{S}_m^H * \mathbf{S}_m)^{-1} * \mathbf{S}_m^H * \mathbf{r}_m. \quad (4.19)$$

Until now, the channel path separation is  $T_c$ , which means the channel resolution is  $T_c$ . Since in the ITU channel models, many paths are separated by less than  $T_c$ , we further modified the model to allow tap-delays from the set  $\{1, 1/2, 1/4, 1/8 \text{ chips}\}$ .

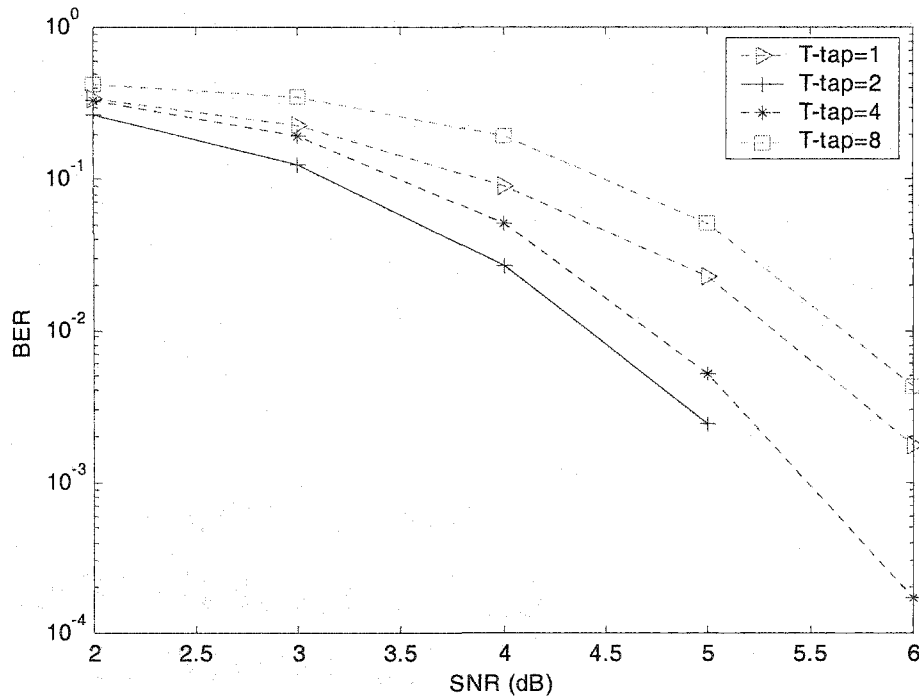
## B. Simulation results

For the TD-SCDMA system performance comparison, the uplink BER simulation is carried out according to the parameters shown in Table 4.1. We consider a one-user system with MMSE based RAKE receivers. First we compare the performance using different tap-delays from the set  $\{1, 2, 4, 8 \text{ samples, where } 1 \text{ sample} = 1/8 \text{ chips}\}$  under the same channel model, as shown in Fig. 4.7. In the figure, T-tap is tap duration in sample units ( $1 \text{ chip} = 8 \text{ samples}$ ), N-tap stands for number of taps, and T-1stfinger refers to the time delay of path  $\hat{\alpha}_0$  in samples compared to the strongest path. We can see that

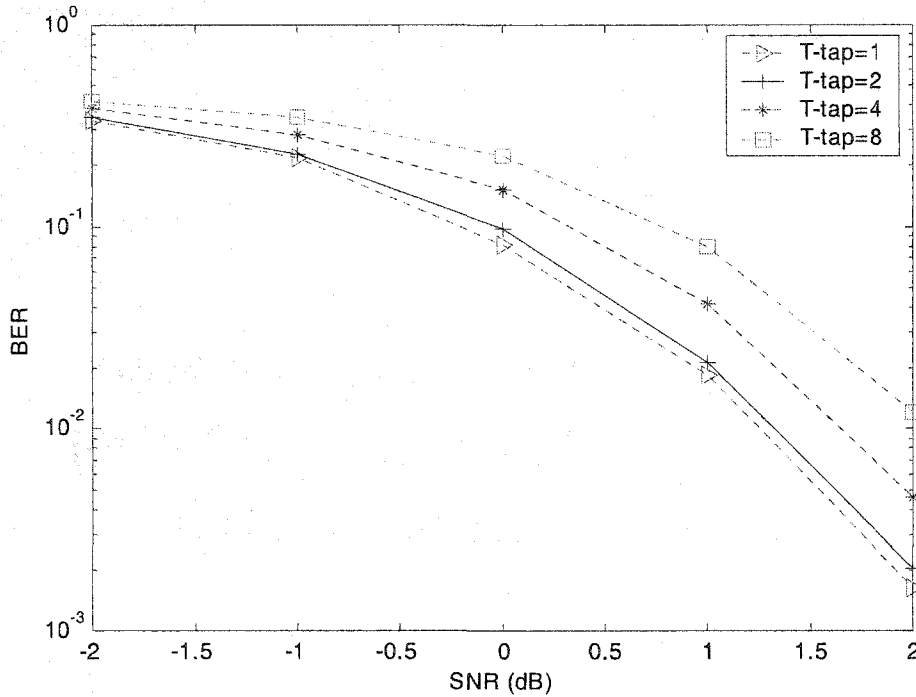
- Different tap-delays lead to different performance.
- Under Channel-A-vehicular model (Fig. 4.7 (a)), the best performance is under T-tap = 2 samples. Decreasing the T-tap from 8 to 2 leads to performance improvement. But continuing decreasing the T-tap to 1 only results in performance degradation since too many noise-only paths included can not balance the increasing resolution.
- Under Channel-A-indoor model (Fig. 4.7 (b)), the best performance is under T-tap = 1 sample.

- Under different channel models, the best T-tap is different.

We can explain this as follows. The MMSE based RAKE receiver does have fine resolution. The smaller the tap-delay, the finer the resolution. On one hand, finer resolution leads better performance, but decreasing the T-tap will include more noise-only paths. On the other hand, more noise-only paths result in performance degradation. So every channel model has a best T-tap for best performance.



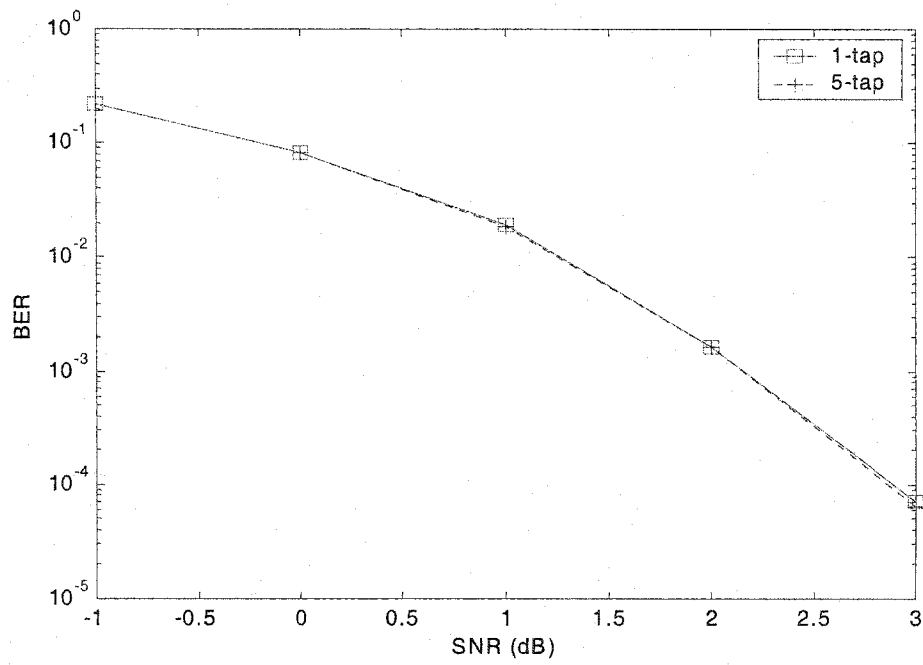
(a) ITU channel-A-vehicular model (N-tap=10,T-1stfinger=-4).



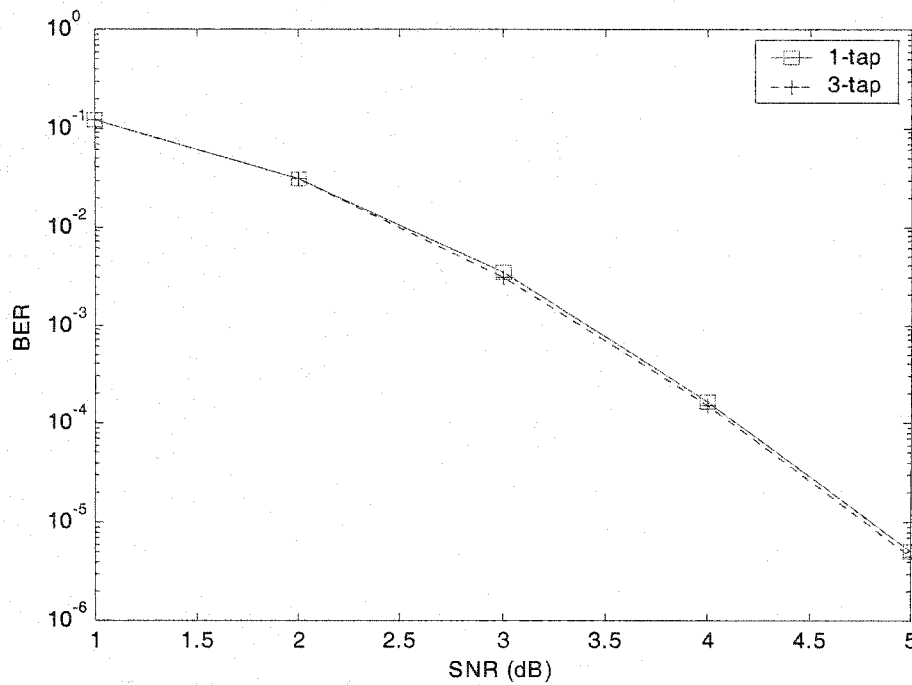
(b) ITU channel-A-indoor model (N-tap=5,T-1stfinger=-2).

Fig. 4.7. Performance of MMSE-based RAKE receiver with different tap-delays.

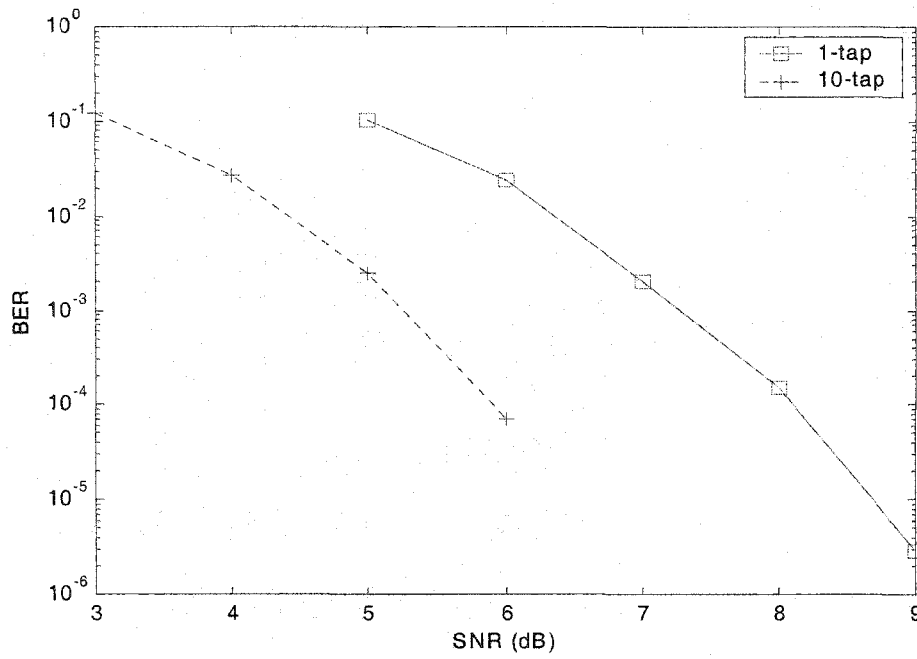
We also compare the performance using a different number of combined taps for ITU channels (refer to Tables 2.3 and 2.4), as shown in Fig. 4.8, where T-tap is tap duration in sample unit (1 chip = 8 samples), and T-1stfinger refers to  $\hat{\alpha}_0$  path time-delay in samples compared to the strongest path. From the figures, we can see that for some ITU channel models, the MMSE receiver does improve a lot, but for others, just slightly. The multi-finger MMSE receiver is always as good as or better than the one-finger receiver (one-finger receiver means no combination actually). However, that is not true for the cross-correlation based RAKE receiver as shown in Fig. 4.5.



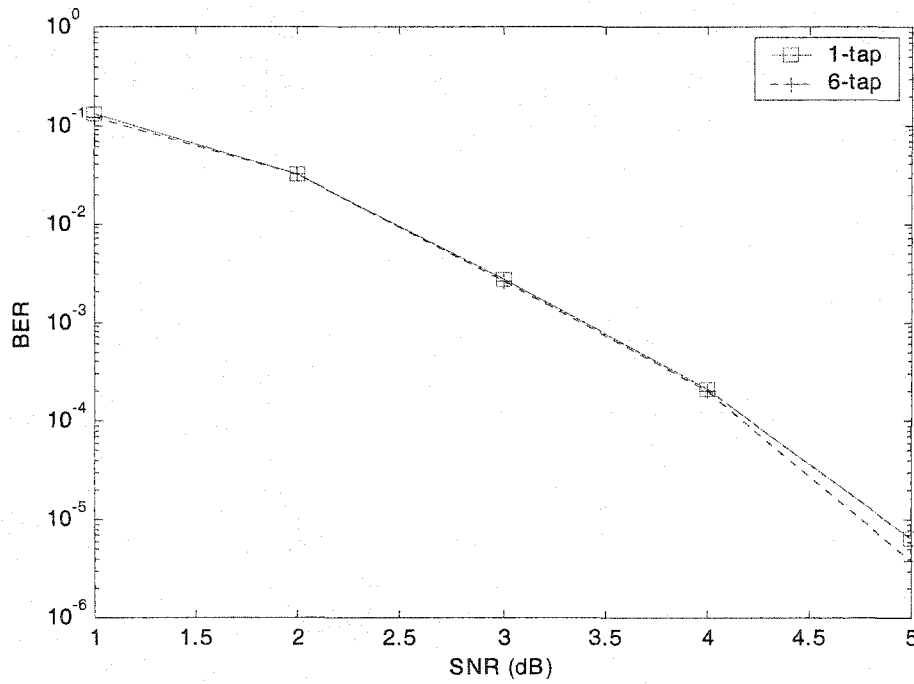
(a) ITU channel-A-indoor model (T-tap=1, T-1stfinger=-2).



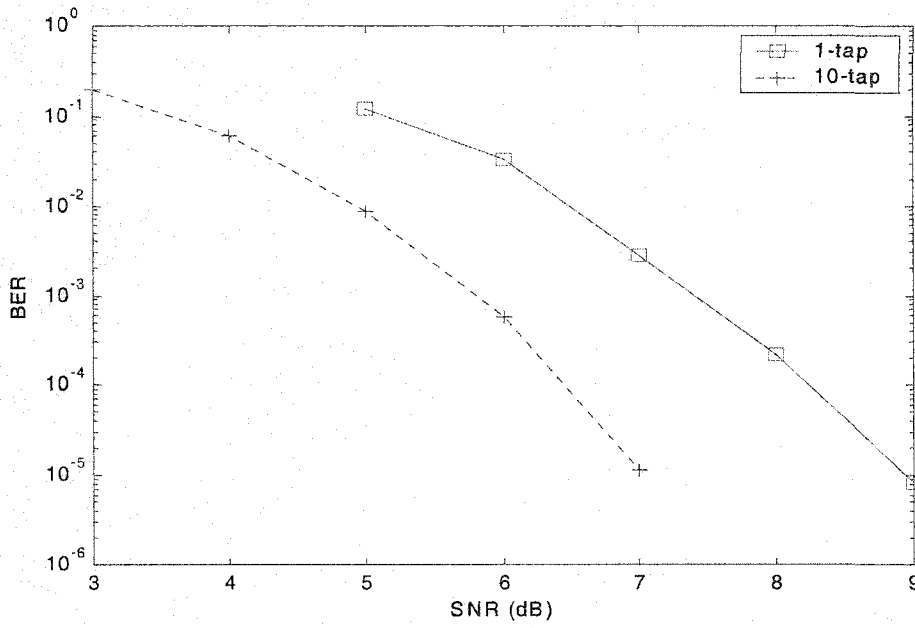
(b) ITU channel-A-indoor-to-outdoor model (T-tap=2, T-1stfinger=-1).



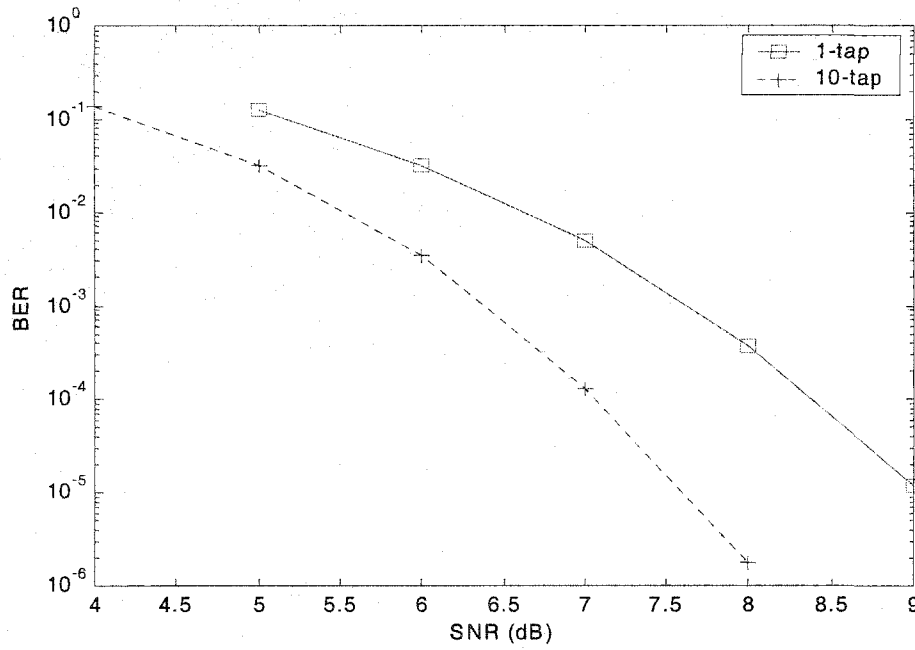
(c) ITU channel-A-vehicular model (T-tap=2, T-1stfinger=-4).



(d) ITU channel-B-indoor model (T-tap=1, T-1stfinger=-2)



(e) ITU channel-B-indoor-to-outdoor model (T-tap=2, T-1stfinger=4).

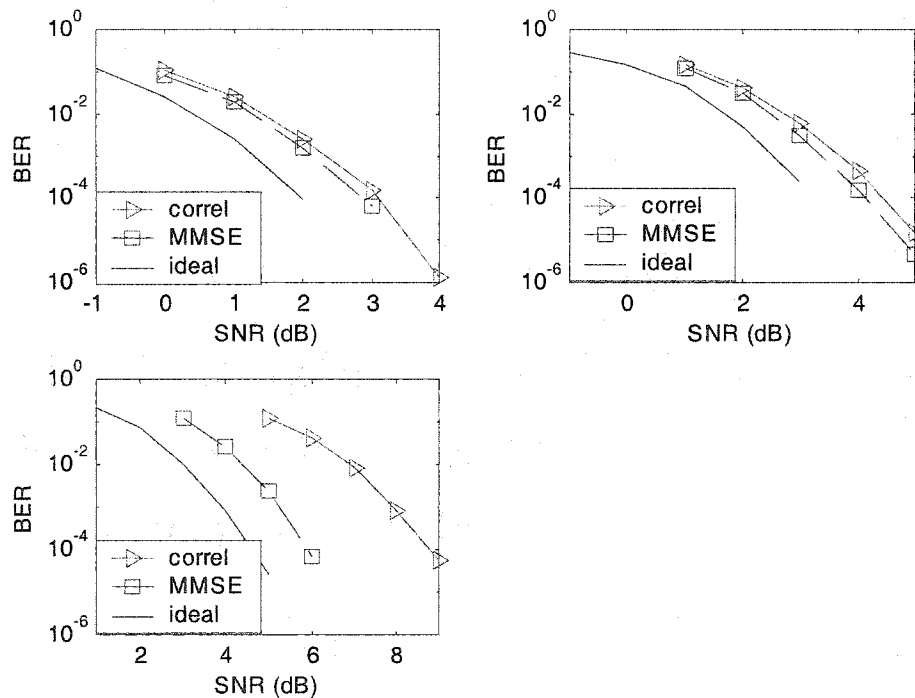


(f) ITU channel-B-vehicular model (T-tap=2, T-1stfinger=5).

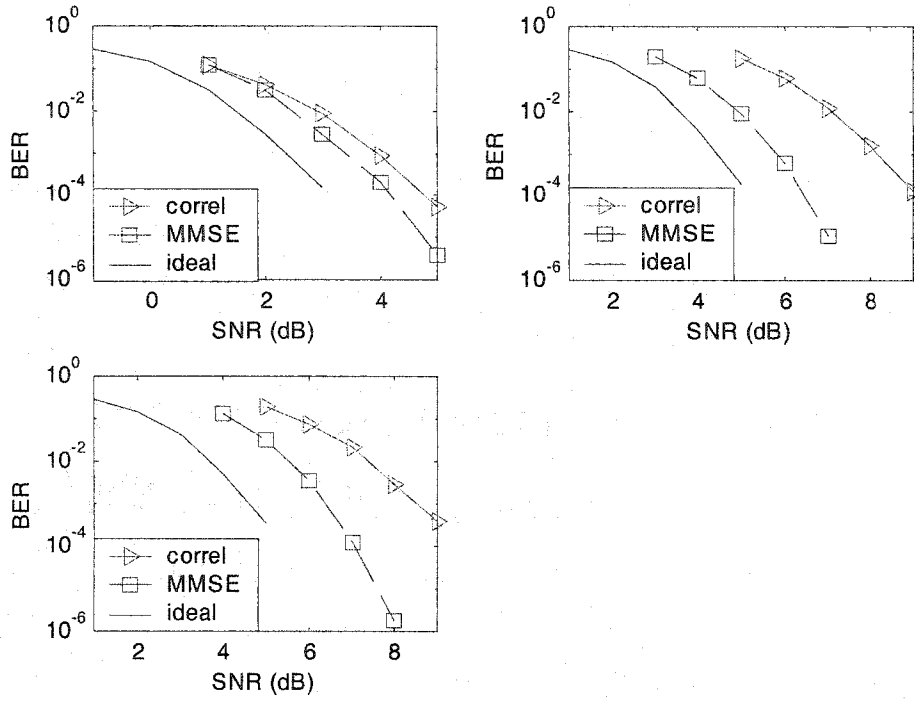
Fig. 4.8. Performance of MMSE-based RAKE receiver.

## 4.2.2 Simulation of the Uplink RAKE Receivers

For the RAKE receivers' comparison, the uplink BER simulation is carried out according to the parameters shown in Table 4.1. We consider a one-user RAKE receiver with ideal channel estimation, cross-correlation estimation and MMSE estimation, where an ideal RAKE receiver means we have known parameters for every path, namely time delay and coefficients. We compare the performance as shown in Fig. 4.9, where "ideal" means ideal channel coefficients, "cross" stands for cross-correlation estimator and "MMSE" indicates the use of the MMSE based estimation.



(a) ITU channel-A models.



(b) ITU channel-B models.

Fig. 4.9. Comparison of Cross-correlation / MMSE based receivers under ITU channel models.

From the figures, we can see that the MMSE based RAKE receiver is always better than the cross-correlation based RAKE receiver. For some ITU channel models, the MMSE based receiver does improve a lot, but for others, just slightly. There is about 1-dB distance between the ideal RAKE receiver and the MMSE-based RAKE receiver.

## 4.3 MMSE Equalizer

### 4.3.1 MMSE Equalizer Model

Multipath channel distortion can be compensated by a diversity method such as the RAKE receiver. In addition, channel distortion results in inter-symbol interference (ISI), which causes high error rates [33]. The compensator for the ISI is an equalizer. Our equalization method is based on a linear filter with adjustable coefficients. The equalizer coefficients are optimal when the MMSE is minimized.

The MMSE equalizer is different from the MMSE estimator in that the MMSE equalizer will not try to estimate the channel coefficients, but instead uses a finite length impulse response (FIR) filter as shown in Fig. 4.10 to compensate for the channel distortion. Here, we still use the midamble information to do the equalizer adjustment. The MMSE equalizer tries to make the filtered output signal  $\hat{s}_m(t)$  closest to the transmitted midamble signal  $s_m(t)$  in the MSE sense. The linear filter most often used for equalization is the transversal filter as shown in Fig. 4.11 [33]. Its input is the received midamble signal  $r_m(t)$  distorted by the multipath wireless channel, and its output is the estimate of the transmitted midamble signal  $\hat{s}_m(t)$ .

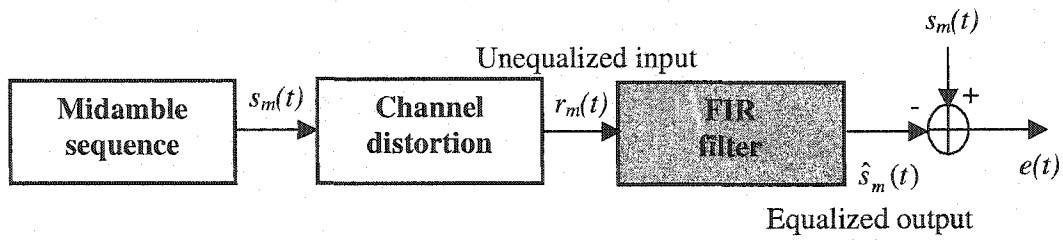


Fig. 4.10. Illustration of the MMSE equalizer.

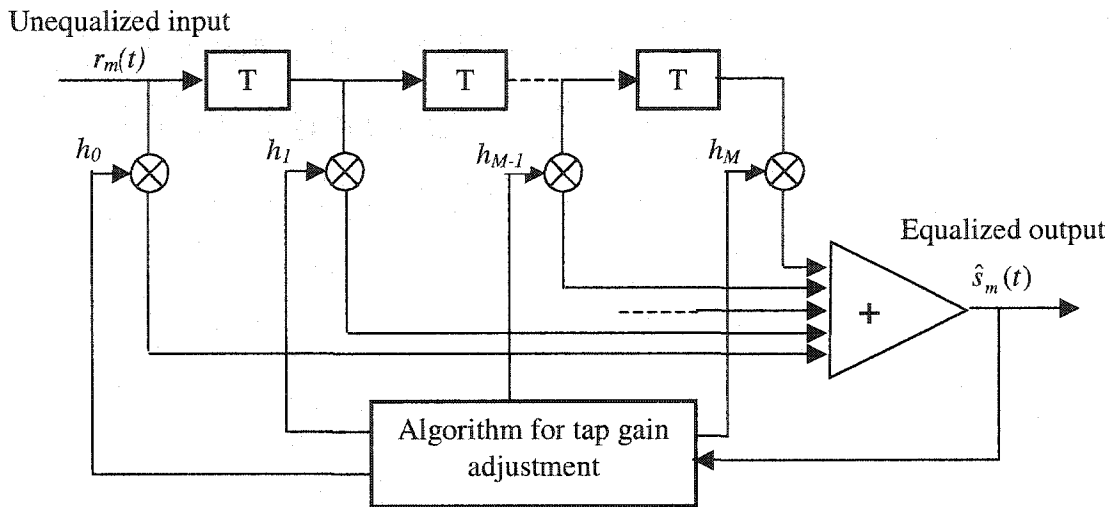


Fig. 4.11. Linear transversal filter for MMSE equalizer.

The estimate of the  $k$ th symbol can be expressed as

$$\hat{s}_m(kT) = \sum_{i=0}^M h_i r_m(k-i)T, \quad k = 0, 1, \dots, 143, \quad (4.20)$$

where,  $\{h_i\}$  are the  $M+1$  complex-valued tap weight coefficients of the filter. This estimate signal is not identical to the transmitted midamble signal  $s_m(t)$ . The error can be written as

$$e(kT) = s_m(kT) - \hat{s}_m(kT), \quad (4.21)$$

which can be simplified to

$$e(k) = s_m(k) - \hat{s}_m(k). \quad (4.22)$$

To minimize the error  $e(k)$  in the mean-square-error sense, we can obtain the optimized equalizer coefficients  $\{h_i\}$ .

#### 4.3.1.1 Fully Spaced Equalizer

When the equalizer taps are spaced at the chip rate, it is called a fully spaced equalizer. That means the tap-delay  $T$  in Fig. 4.11 is  $T_c$ , the duration of a chip. In discrete time digital form, (4.20) can be simplified as

$$\hat{s}_m(k) = \sum_{i=0}^M h_i r_m(k-i), \quad k = 0,1,\dots,143. \quad (4.23)$$

Writing it in matrix form, it can be expressed as

$$\hat{\mathbf{s}}_m = \mathbf{R}_m * \mathbf{h}^T, \quad (4.24)$$

where,  $\mathbf{R}_m$  is the received midamble information matrix,  $\mathbf{h}$  is the coefficient-vector of equalizer taps, and  $\hat{\mathbf{s}}_m$  is a estimated vector of the transmitted midamble information.

In particular, when considering a 4-tap-delay-line channel model, the matrix and vectors are

$$\mathbf{R}_m = \begin{bmatrix} r_m(0) & 0 & 0 & 0 \\ r_m(1) & r_m(0) & 0 & 0 \\ r_m(2) & r_m(1) & r_m(0) & 0 \\ r_m(3) & r_m(2) & r_m(1) & r_m(0) \\ \dots & \dots & \dots & \dots \\ r_m(143) & r_m(142) & r_m(141) & s_m(140) \end{bmatrix}, \quad (4.25)$$

$$\mathbf{h} = [h_0 \quad h_1 \quad h_2 \quad h_3]^T, \quad (4.26)$$

and

$$\hat{\mathbf{s}}_m = [\hat{s}_m(0) \quad \hat{s}_m(1) \quad \hat{s}_m(2) \quad \hat{s}_m(3) \quad \dots \quad \hat{s}_m(143)]^T. \quad (4.27)$$

Then minimizing  $e(k)$  in (4.22) is equivalent to obtaining a least squares solution to the following over-determined equations

$$\mathbf{R}_m * \mathbf{h}^T = \mathbf{s}_m, \quad (4.28)$$

where,  $\mathbf{s}_m$  is the transmitted midamble information vector. In the MSE sense, the optimized equalizer tap coefficient-vector is

$$\mathbf{h} = (\mathbf{R}_m^H * \mathbf{R}_m)^{-1} * \mathbf{R}_m^H * \mathbf{s}_m. \quad (4.29)$$

#### 4.3.1.2 Fractionally Spaced Equalizer

The chip rate equalizer can only compensate for the frequency response characteristics of the aliased-received signal. It cannot compensate for the channel distortion inherent in the sampling delay [33]. Given the shaping filter spread and channel path spread, we also considered half-chip rate, even quarter-chip rate

equalizers. That means the tap-delay  $T$  in Fig. 4.11 is  $T/2$  for half-chip rate or  $T/4$  for quarter-chip rate.

In contrast to the fully spaced equalizer, a fractionally spaced equalizer (FSE) is based on sampling the incoming signal at least as fast as the Nyquist rate. In the TD-SCDMA system, the transmitted signal consists of a pulse having a root-raise-cosine spectrum with a roll-off factor  $\beta = 0.22$ . Its spectrum extends to

$$F_{\max} = (1 + \beta)/(2T_c). \quad (4.30)$$

The signal can be sampled at the receiver at a rate

$$2F_{\max} = \frac{1 + \beta}{T_c}, \quad (4.31)$$

and then passed through an equalizer with tap spacing of  $T_c/(1 + \beta) = T_c/1.22$ . Considering that the TD-SCDMA system is already sampled at a rate of eight samples per chip, we chose to implement the fractionally spaced equalizer with tap spacings at  $T_c/2$  and  $T_c/4$ .

### 4.3.2 Simulation Results

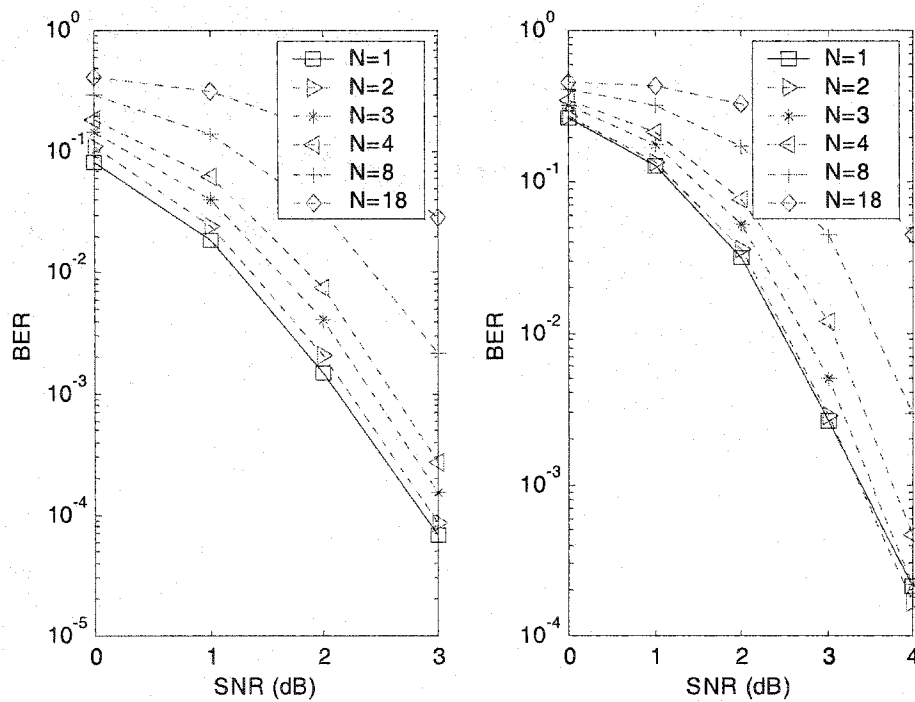
For the MMSE receivers' comparison, the uplink BER simulation is carried out according to the parameters shown in Table 4.2. We consider a one-user MMSE receiver with different number of taps or different tap spacings and ITU channels.

TABLE 4.2

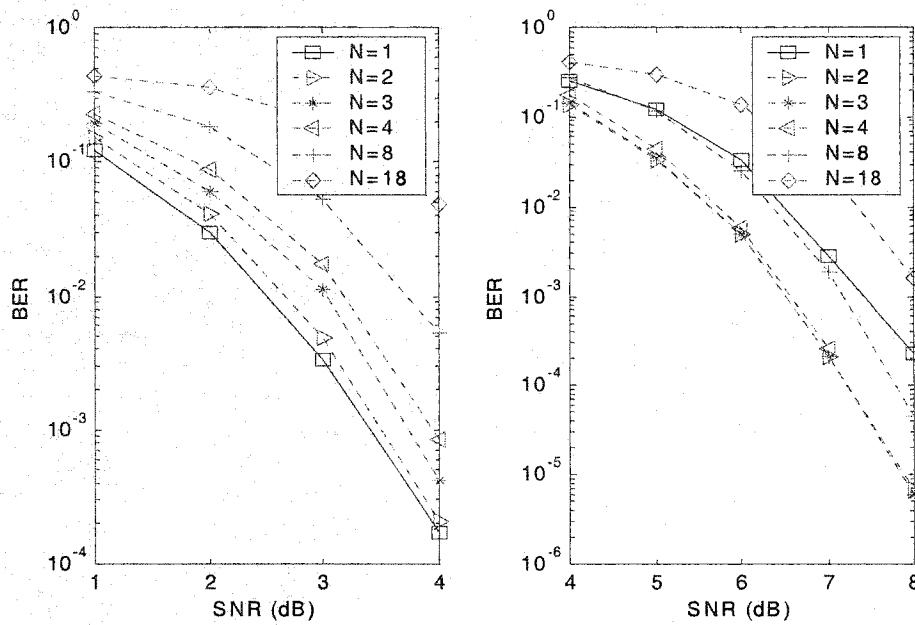
## PARAMETERS FOR MMSE RECEIVERS

Parameter	Data	Units
Carrier Frequency	2000	MHz
Gross Data Rate	17600	bps
Information Bit Source	Random	
FEC Code Rate	1/2	
Channel Fading	Rayleigh	
Vehicle Speed	0	
Signal Constellation	QPSK	
Spreading Factor	16	
Channelization Code	6	
Synchronization Step-Size	1/8	chip
No. of Paths (Fingers)	Up to 6 according to ITU model	
Equalizer Tap Separation	1,2,4,8	samples
Transmission Time Interval (TTI)	10	ms

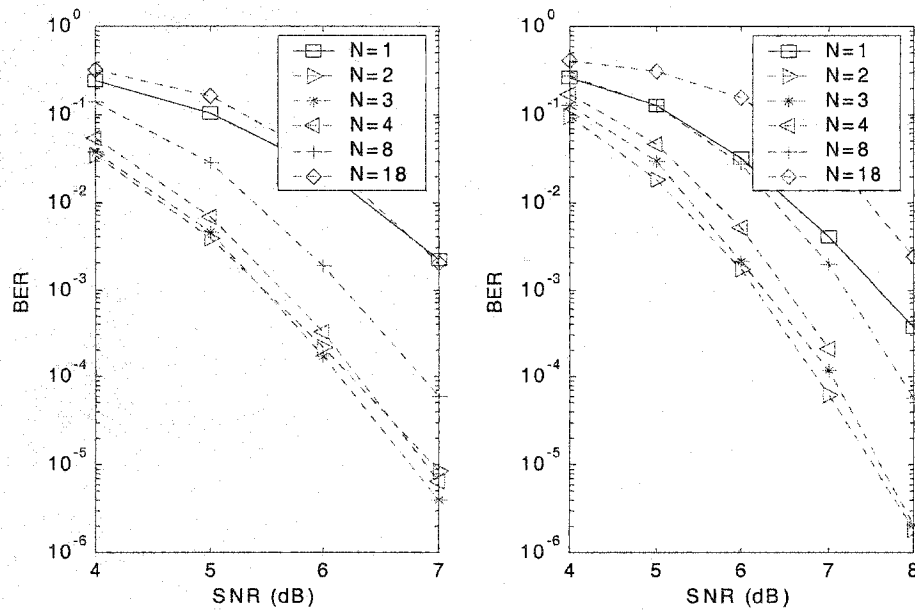
First, we consider half-spaced equalizer systems with different number of taps for ITU channel models, shown in Fig. 4.12, where  $T$  is the tap duration,  $T_{1\text{tap}}$  refers to the time-delay of tap  $h_0$ , and  $N$  is the length of the filter, i.e., number of taps. We can see from the results that: 1) in some channels, there is improvement by using the equalizer, but not for others ( $N = 1$  means no equalizer); 2) longer equalizers do not necessarily perform better; and 3) the best number of taps is very small, less than 5.



(a) ITU indoor-models (A model left, B model right).



(b) ITU indoor-to-outdoor models (A model left, B model right).

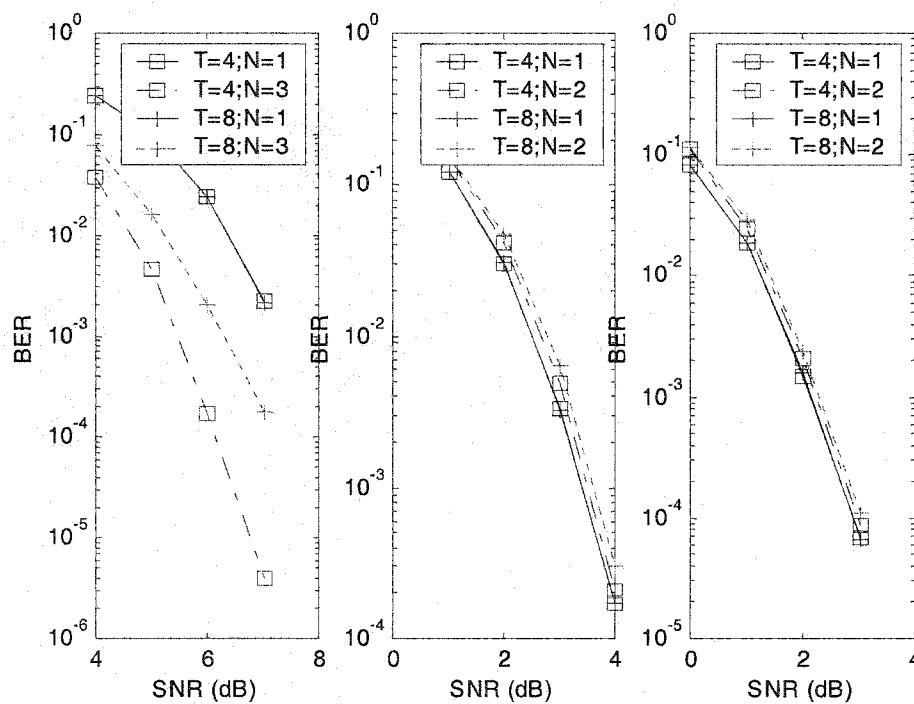


(c) ITU vehicular models (A model left, B model right).

Fig. 4.12. Comparison of MMSE equalizers with different equalizer length  $N$ .

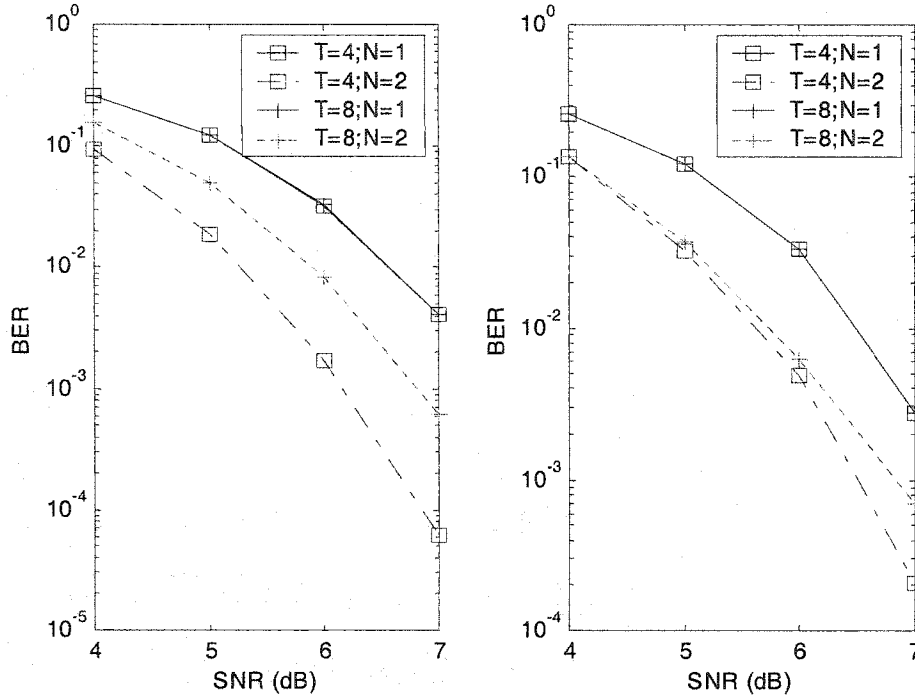
( $T_{1tap} = 0$ ,  $T = 1/2$  chip = 4 samples)

We compared the performance between the half-chip rate equalizer and the chip-rate equalizer, shown in Fig. 4.13. We see that: 1) the half-chip rate equalizer outperforms the chip-rate equalizer for all channels; and 2) for some channels, there is substantial difference, but for other channels, the half-chip rate equalizer just barely outperforms the chip-rate equalizer



(a) ITU Channel-A

(From left to right, vehicular, indoor-to-outdoor, and indoor model).

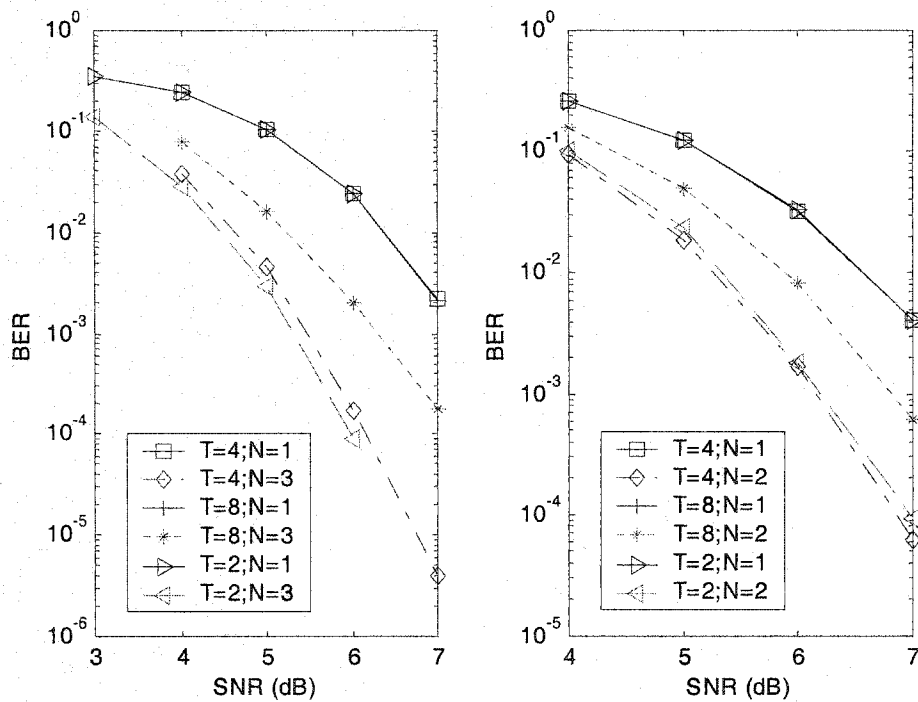


(b) ITU Channel-B (Vehicular left, indoor-to-outdoor right).

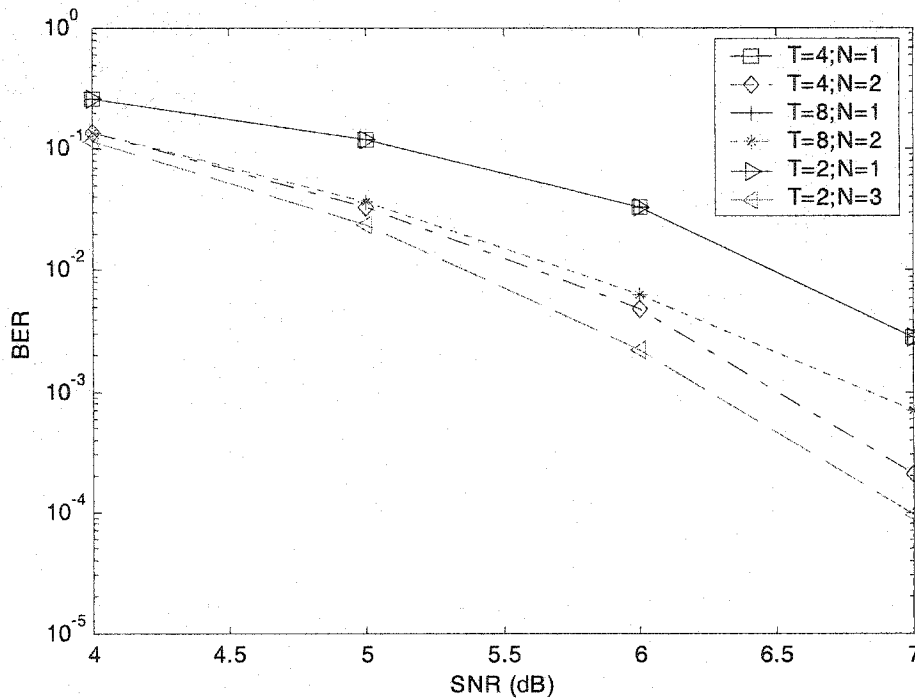
Fig. 4.13. Comparison of MMSE equalizers with differently spaced taps. ( $T_{1\text{tap}} = 0$ ,  $T = 1/2 \text{ chip} = 4 \text{ samples}$ )

For those channel models whose equalizer does improve the performance, we further evaluated the performance with a quarter-spaced equalizer. The simulation results are shown in Fig. 4.14, where  $T = 8 \text{ (samples)}$  means fully spaced,  $T = 4 \text{ (samples)}$  denotes the half-chip rate spaced equalizer, and  $T = 2 \text{ (samples)}$  stands for the quarter-chip rate spaced equalizer. We see that

- In some channels the quarter-chip rate equalizer outperforms the half-chip rate equalizer, but not for others.
- The fractionally-spaced equalizer outperforms the full-spaced equalizer for all channels.
- The performance of the quarter-chip rate and half-chip rate equalizers are close to each other.



(a) ITU vehicular-models (A model left, B model right).



b) ITU B-indoor-to-outdoor model.

Fig. 4.14. Comparison of MMSE equalizers with different rates.

## 4.4 Conclusion

After going through a mobile wireless communications channel [32], the signals lose their orthogonality, which leads to a performance loss. To compensate for this loss, RAKE and MMSE receivers were used and discussed.

For the RAKE receivers, the MMSE-based receiver always outperforms the cross-correlation based receiver, and there is about 1-dB difference between the MMSE-

based RAKE receiver and the ideal RAKE receiver with known channel coefficients. Even though the cross-correlation based RAKE receiver can exclude the noise-only paths, it does not always improve the performance since it cannot distinguish finer resolution paths with separation less than 1 chip. On other hand, the MMSE-based RAKE receiver always improves the performance.

For the MMSE receivers, the channel equalizer does improve the performance for some channels, but not for others. The fractionally spaced equalizer outperforms the fully spaced equalizer, and there is very little difference between the half-chip rate and the quarter-chip rate equalizers. The half-chip spaced equalizer is sufficient for this system.

As we mentioned before, the multi-path spread  $T_m$  of the channel is not large enough compared to the chip duration and the RAKE receiver has difficulty distinguishing these paths. Smart antenna techniques can effectively separate the multi-paths. A number of TD-SCDMA standard documents stress the need for smart antennas to obtain good performance.

# Chapter 5

## Antenna Arrays

### 5.1 Introduction

The TD-SCDMA system is an interference-limited system. This interference may come from multiusers, multipaths, or other sources. Even though the diversity provided by the RAKE receiver and channel equalization in the MMSE receiver can improve the performance, they have performance limitation because of the resolution limit in the multi-path time-delay and inclusion of many noise-only paths. These two receivers can only compensate for the multipath degradation in certain situations.

Antenna array systems can greatly improve the system performance by enhancing the detection and reception of certain desired signals and suppressing the interfering signals. Such system offers improved reception performance that would be difficult to achieve in any other way [37]. Antenna arrays can also efficiently combat multipath degradation. A number of TD-SCDMA standard documents stress the need for smart antennas to obtain good performance [38]-[40]. The principal reason derives from their ability to automatically sense the presence of interference noise

sources and to suppress these noises while simultaneously enhancing desired signal reception without knowledge of signal / interference environment by changing the beam-forming pattern.

## 5.2 System Model

We consider at the base station a linear array with four equispaced omni-directional antenna elements, and used a direct matrix inversion (DMI) algorithm and the MMSE criterion to estimate the array weight coefficients. The model of the antenna system is shown in Fig. 5.1.

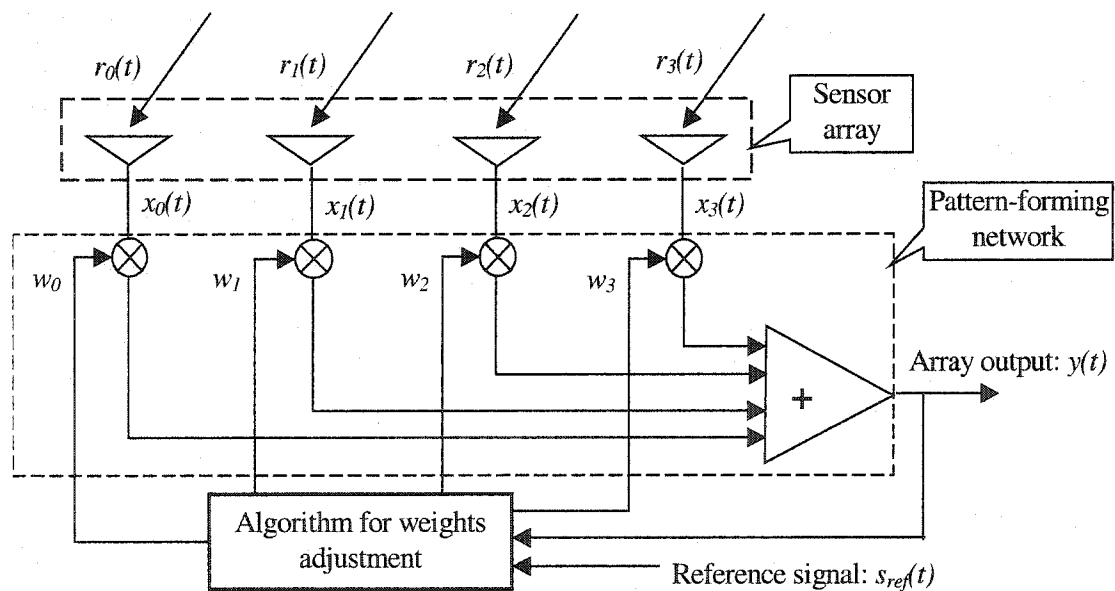


Fig. 5.1. Functional diagram of a four-element adaptive array system.

The signal vector  $r$  coming into the array will be contaminated by noise  $n$ . The array weight vector  $w$  is computed such that the noise at the output  $y$  is minimized subject to certain constraints. This array system consists of three functional blocks: the sensor array, the pattern-forming network, and the control unit to adjust the weight vector.

### 5.2.1 Sensor Array

We consider at the base station a linear array with four equispaced omni-directional antenna elements, as shown in Fig. 5.2. We assume the signal impinges on the array at an angle  $\theta$ , so that the signal phase lead at element  $j$  relative to element 0 is  $\psi_j = jd / \lambda \sin \theta$ ,  $j = 0, 1, 2, 3$ , where  $\lambda$  is the wavelength of the signal and  $d$  is sensor spacing.

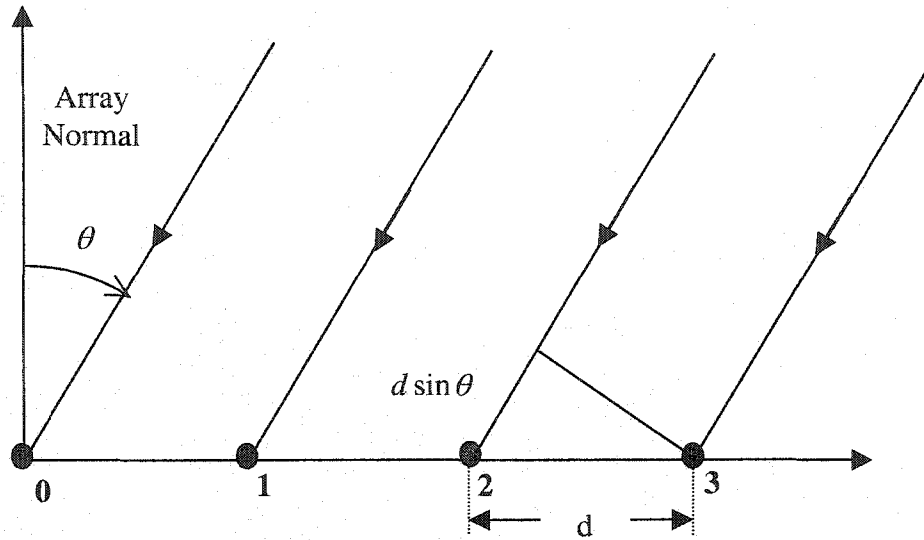


Fig. 5.2. Four-element equispaced linear array.

It is known that there is only small difference in the directional pattern between a single element and several closely spaced elements ( $d$  is less than  $\lambda/4$  apart). Consequently, arrays employing many elements very closely spaced are considered “inefficient”, if fewer array elements as desirable [37]. On the other hand, when element spacing  $d$  is large (larger than  $\lambda/2$ ), there are much many additional pattern nulls besides that in the desired direction. In that case, a desired signal can be located at (or near) one of the additional nulls. Then, degradation in the SNR array performance will occur. Therefore, a maximum element spacing of  $\lambda/2$  is usually used. We set the array element spacing in the antenna system at  $d = \lambda/2$ .

The effect of the element spacing on the beam pattern can be illustrated by a two-element array, as shown in Fig. 5.3. When the element spacing  $d$  is small ( $d = 0.2\lambda$  in the upper left in Fig. 5.3), the beam-pattern of the array is similar to that of the omni-directional single element antenna. When the element spacing  $d$  is large ( $d = 1.5\lambda$  in the lower left, and  $d = 2\lambda$  in the lower right in Fig. 5.3), there are many additional independent nulls in the beam-pattern. The spacing of  $d = 0.5\lambda$  (upper right of Fig. 5.3) is used in this work, neither like the omni-directional single element antenna, nor having many independent nulls.

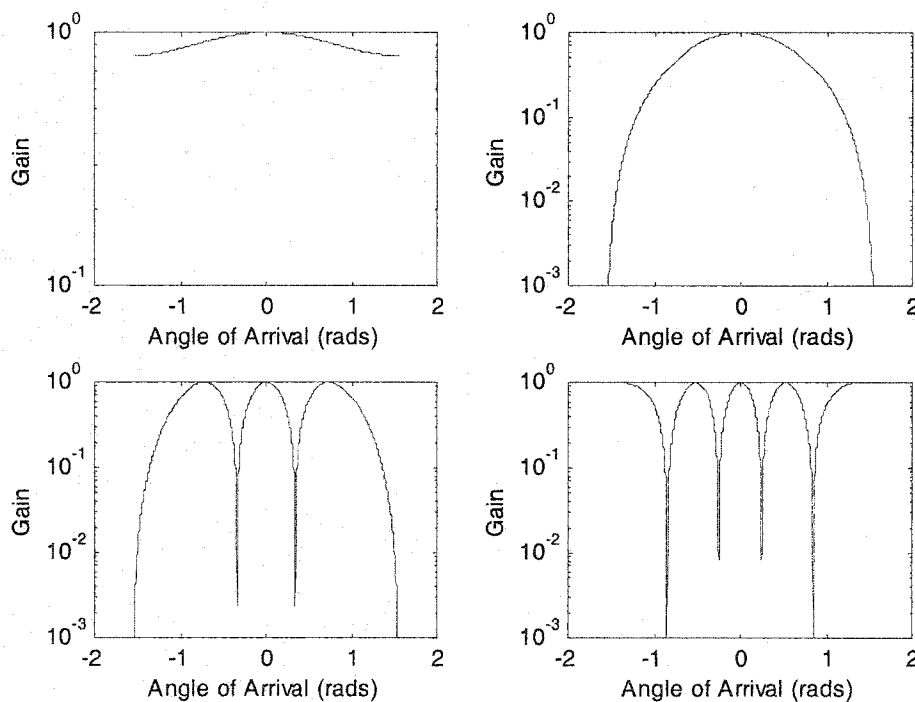


Fig. 5.3. Two-element linear array patterns. (upper left  $d = 0.2\lambda$ , upper right  $d = 0.5\lambda$ , lower left  $d = 1.5\lambda$ , and lower right  $d = 2\lambda$ ).

## 5.2.2 Pattern-Forming

The weighting vector  $\mathbf{w} = [w_0 \ w_1 \ w_2 \ w_3]$  in Fig. 5.1 has the effect of “steering” beam-pattern to the desired direction. To illustrate how the weighting vector affects the directional pattern for the four-element linear array, we assume that

$$\begin{aligned}\mathbf{w} &= [w_0 \ w_1 \ w_2 \ w_3] \\ &= [e^{j(0 \cdot \delta)} \ e^{j(1 \cdot \delta)} \ e^{j(2 \cdot \delta)} \ e^{j(3 \cdot \delta)}],\end{aligned}\tag{5.1}$$

which means that a phase shift (or an equivalent time delay) of  $\delta$  is inserted in the second element of the array, and a phase shift of  $(n-1)\delta$  in each succeeding  $n$ th element. The insertion of this sequence of phase shifts has the effect of shifting the principal lobe (or main lobe) by  $\theta_{main}$ , where

$$2\pi \cdot d \sin \theta_{main} / \lambda = \delta.\tag{5.2}$$

From (5.2), we can obtain,

$$\theta_{main} = \sin^{-1}[\lambda / d \cdot \delta / (2\pi)].\tag{5.3}$$

The resulting beam pattern can be “steered” by insertion of phase shifts in the weighting coefficients. This effect is illustrated in the lower plot of Fig. 5.4 for  $\delta = \pi/6$  and  $d = \lambda/2$  (therefore  $\theta_{main} = 0.1674$ ), which can be directly compared with the upper plot to see the main lobe shift resulting in the array pattern.

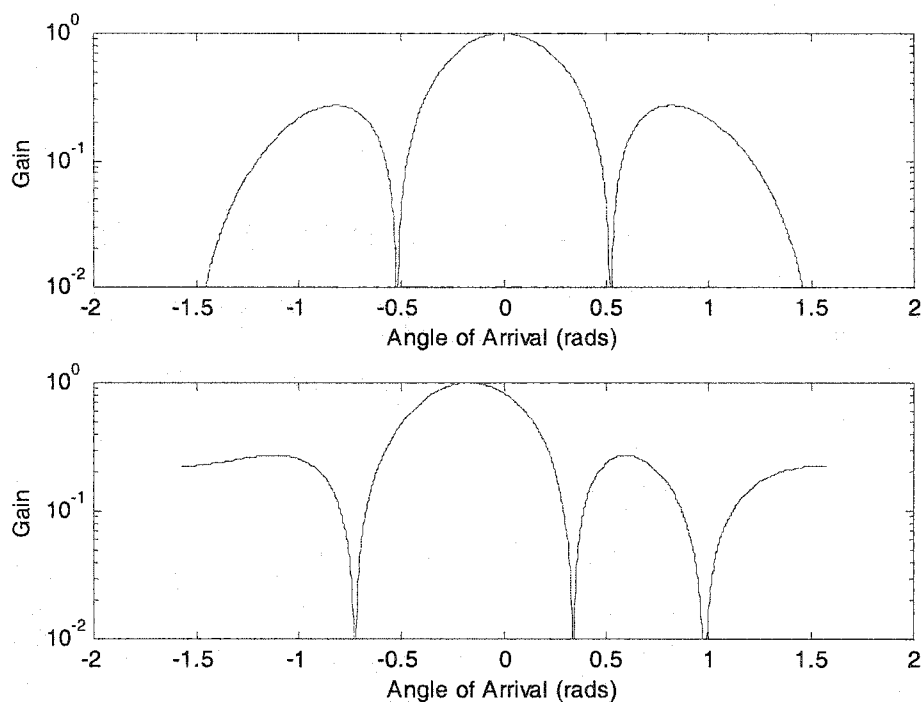


Fig. 5.4. Four-element linear array directivity pattern with  $d = \lambda/2$  and  $\delta = \pi/6$  in the upper,  $\delta = 0$  in the lower.

### 5.2.3 Control Unit for Weight Adjustment

The control unit is to adjust the weighting coefficient vector  $w$  such that the noise at the output  $y(t)$  is minimized according to the MSE criterion. For an easy illustration of how the control unit works, Fig. 5.1 is simplified to Fig. 5.5.

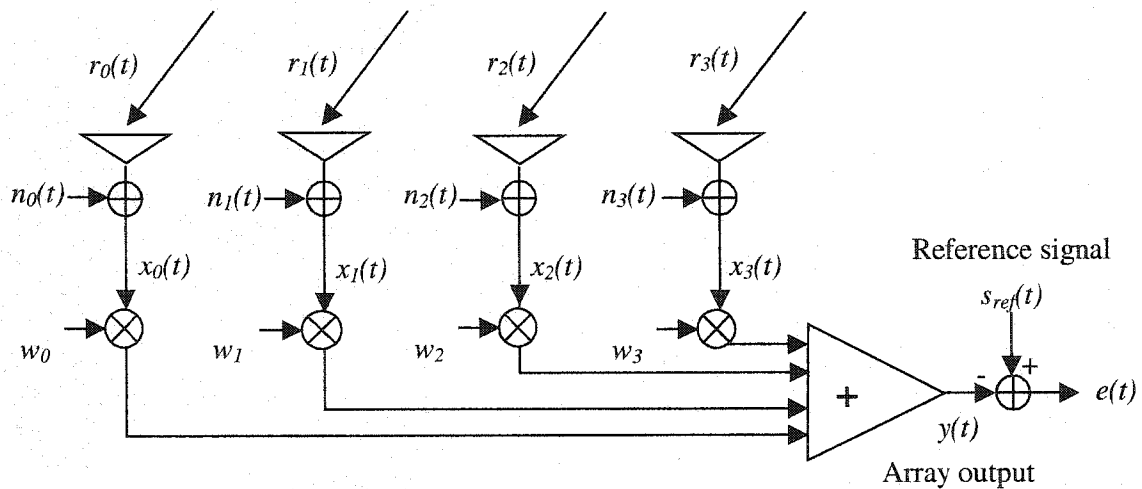


Fig. 5.5. Functional diagram of a four-element adaptive array system.

#### 5.2.3.1 Data Stream in the Control Unit

The signal vector  $r$  from one source (say, one user) at the input of the antenna array can be written as

$$\begin{aligned}
\mathbf{r} &= [r_0 \quad r_1 \quad r_2 \quad r_3]^T \\
&= [r_0 \quad r_0 e^{j\psi_1} \quad r_0 e^{j\psi_2} \quad r_0 e^{j\psi_3}]^T \\
&= r_0 \cdot [1 \quad e^{j\psi_1} \quad e^{j\psi_2} \quad e^{j\psi_3}]^T, \\
&= r_0 \cdot \mathbf{v}^T
\end{aligned} \tag{5.4}$$

where, the array propagation vector  $\mathbf{v}$  can be defined as

$$\mathbf{v} = [1 \quad e^{j\psi_1} \quad e^{j\psi_2} \quad e^{j\psi_3}]^T. \tag{5.5}$$

The signal  $\mathbf{r}$  coming into the array will be contaminated by noise  $\mathbf{n}$ , and  $\mathbf{n}$  can be defined as

$$\mathbf{n} = [n_0 \quad n_1 \quad n_2 \quad n_3]^T, \tag{5.6}$$

where,  $n_k$ ,  $k = 0,1,2,3$  are assumed to be AWGN noise. Thus, the signal  $\mathbf{x}$  before weighting can be expressed as

$$\begin{aligned}
\mathbf{x} &= [x_0 \quad x_1 \quad x_2 \quad x_3]^T \\
&= \mathbf{n} + \sum \mathbf{r}
\end{aligned} \tag{5.7}$$

where,  $\sum \mathbf{r}$  means summing all the signal from all sources (say, all the users). The output of the array illustrated in Fig. 5.5 can be expressed as

$$\begin{aligned}
y &= \mathbf{w}^T \mathbf{x} \\
&= \mathbf{w}^T (\mathbf{n} + \sum \mathbf{r})
\end{aligned} \tag{5.8}$$

The key function of the control unit is to minimize error signal  $e(t)$  in Fig. 5.5 according to the MSE criterion. The error signal is expressed as

$$e(t) = y(t) - s_{ref}(t). \tag{5.9}$$

### 5.2.3.2 Algorithm in the Control Unit— DMI

We use the mid-amble information to estimate the weight coefficient vector  $w$ . Since the data and the mid-amble are sent in different time slots (see the data burst structure shown in Fig. 5.6), recursive methods are not well suited if the mid-amble is used. Instead, we use a direct matrix inversion (DMI) algorithm and a MMSE criterion. This algorithm has the advantage of rapid convergence to the steady-state solution [37].

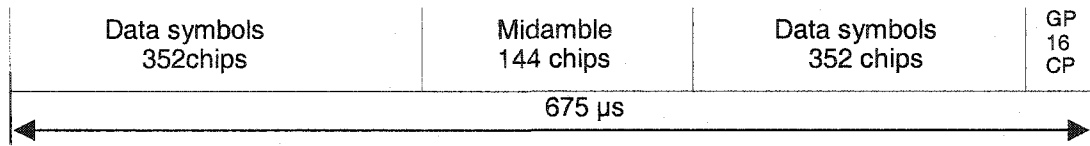


Fig. 5.6. Data burst structure.

Using the mid-amble sequences from all users, we adjust the weighting vector  $w$  so that the output sequence  $y(t)$  is closest to the desired user's mid-amble sequence in the MMSE sense. Consider two users, and let  $\mathbf{R}_I$  denote the mid-amble matrix of the interfering user, and  $\mathbf{R}_D$  the mid-amble matrix of the desired user. The matrixes can be expressed as

$$\mathbf{R}_I = \begin{bmatrix} r_{I0}(0) & r_{I1}(0) & r_{I2}(0) & r_{I3}(0) \\ r_{I0}(1) & r_{I1}(1) & r_{I2}(1) & r_{I3}(1) \\ \dots & \dots & \dots & \dots \\ r_{I0}(143) & r_{I1}(143) & r_{I2}(143) & r_{I3}(143) \end{bmatrix}, \quad (5.10)$$

and

$$\mathbf{R}_D = \begin{bmatrix} r_{D0}(0) & r_{D1}(0) & r_{D2}(0) & r_{D3}(0) \\ r_{D0}(1) & r_{D1}(1) & r_{D2}(1) & r_{D3}(1) \\ \dots & \dots & \dots & \dots \\ r_{D0}(143) & r_{D1}(143) & r_{D2}(143) & r_{D3}(143) \end{bmatrix}, \quad (5.11)$$

where,  $r_{Dk}(j)$  and  $r_{Ik}(j)$  are the desired and interfering user's midamble symbols coming into the  $k$ th antenna element at the  $j$ th chip duration, respectively. Similarly, let  $N$  be the AWGN noise matrix going out of the antenna elements, and  $X$  the data matrix coming out of the antenna elements and before weighting adjustment. Then,  $X$  can be written as

$$\mathbf{X} = \mathbf{R}_D + \mathbf{R}_I + \mathbf{N}. \quad (5.12)$$

The array output vector  $y$  during the midamble duration of 144 chips can be expressed as

$$\begin{aligned} \mathbf{y} &= (\mathbf{R}_D + \mathbf{R}_I + \mathbf{N}) \cdot \mathbf{w}^T \\ &= \mathbf{X} \cdot \mathbf{w}^T \end{aligned} \quad (5.13)$$

Since we want to suppress the interfering user's signal and AWGN noise, the transmitted midamble vector  $s_m$  of the desired user is chosen as the reference signal  $s_{ref}$ . It is expressed as

$$\begin{aligned} \mathbf{s}_{ref} &= \mathbf{s}_m \\ &= [s_m(0) \quad s_m(1) \quad \dots \quad s_m(143)]^T, \end{aligned} \quad (5.14)$$

where,  $s_m(k)$  is the midamble symbol of the desired user transmitted at the  $k$ th chip duration.

To minimize the error vector  $\mathbf{e} = \mathbf{y} - \mathbf{s}_{ref}$  during its 144-chip duration according to MSE criterion is equivalent to the least squares solution of the following over-determined set of equations in matrix form,

$$\mathbf{X} \cdot \mathbf{w}^T = \mathbf{s}_{ref}. \quad (5.15)$$

The DMI solution is

$$\mathbf{w} = (\mathbf{X}^H \mathbf{X})^{-1} \mathbf{X}^H \mathbf{s}_{ref}. \quad (5.16)$$

## 5.2.4 Array Performance Limits

The goal of this array system is to suppress the noise sources including the interfering signals, while simultaneously enhancing the desired signal reception. The operation of this adaptive array can be easily visualized in terms of the array beam sensitivity pattern [37]. Interference signal suppression is obtained by appropriately steering the beam pattern nulls and reducing side-lobe levels in the directions of the interference sources. The desired signal reception is maintained by preserving the desirable main-lobe features.

For its function to be fulfilled, the reference signal needs to be reasonably well correlated with the desired signal and uncorrelated with interference signals. The reference signal in the array system for TD-SCDMA is the transmitted mid-amble signal of the desired user, and the desired signal is the mid-amble signal itself.

Obviously, they are well correlated. The interference signal is the mid-amble of the interfering user. The mid-amble signals of different users are un-correlated to each other according to the standard.

The weighting vector  $w$  plays a key role in suppressing the interfering signal. The selection of an optimum weighing vector  $w$  is determined by canceling out correlated noise components in various element channels. Since the directional interferences, such as interfering user signals, in the various element channels are correlated, they can be suppressed. But for those non-correlated noises in the element channels, such as AWGN noise, no weighting vector can be found to cancel them out. So the pattern can put nulls in the directional interferences.

### **5.3 Simulation Results**

For the TD-SCDMA system simulation with an antenna array, the uplink BER is simulated according to the parameters shown in Table 5.1.

TABLE 5.1

## PARAMETERS FOR SYSTEM WITH ANTENNA ARRAY

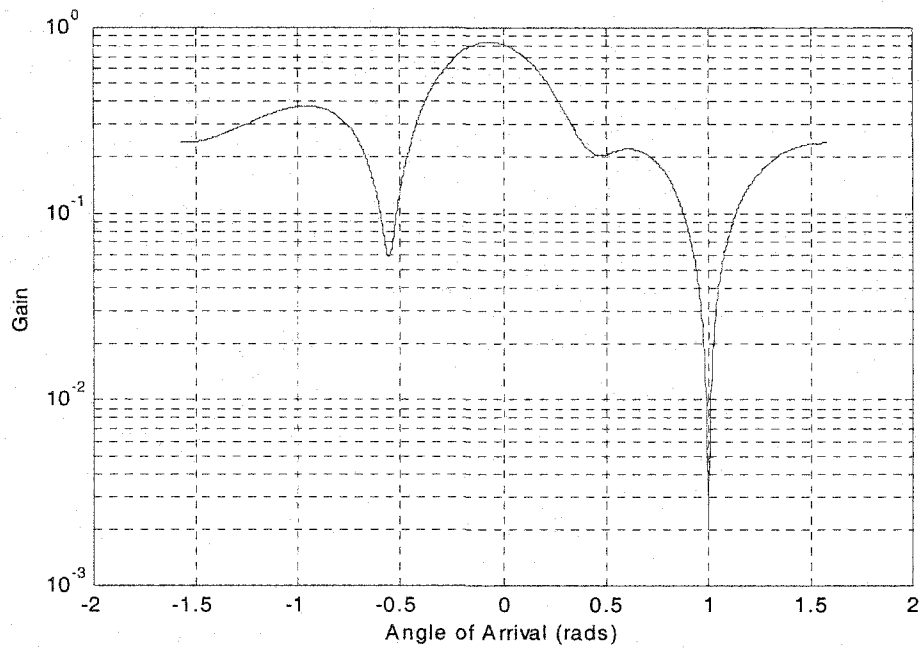
Parameter	Data	Units
Carrier Frequency	2000	MHz
Gross Data Rate	17600	bps
Information Bit Source	Random	
FEC Code Rate	1/2	
Channel Fading	Rayleigh	
Vehicle Speed	0	
Signal Constellation	QPSK	
Spreading Factor	16	
Synchronization Step-Size	1/8	chip
No. of Paths (Fingers)	Up to 6 according to ITU model	
Transmission Time Interval (TTI)	10	ms

### 5.3.1 Array Beam Pattern

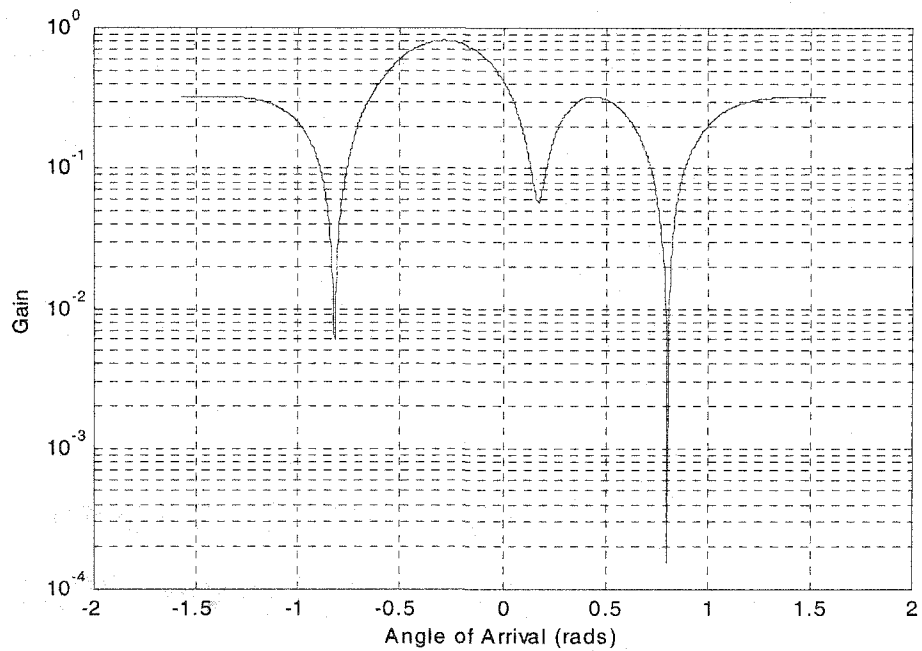
A linear array of four elements was simulated in the TD-SCDMA system. A maximum number of three nulls can be adjusted to improve the performance. A various number of interfering users ( $N < 3$ ,  $N = 3$ , or  $N > 3$ ) were simulated to study the beam pattern.

#### A. Beam pattern with $N < 3$

We first consider a two-user system, which means one interfering user  $N = 1$ . In one of our simulation examples, we consider the desired user located at angle 0 radians, and the interfering user at 1.0 radian, and obtained the array beam pattern shown in Fig. 5.7(a). In another example, we considered angles of  $-0.3$  radians (desired user) and 0.8 radians (interfering user), and obtained the pattern shown in Fig. 5.7 (b).



(a) Arriving angles of 0.0 (desired user) and 1.0 (interfering user) radians.



(b) Arriving angles of -0.3 (desired user) and 0.8 (interfering user) radians.

Fig. 5.7. Array beam pattern using DMI for a two-user system.

Then we consider a three-user system ( $N = 2$ ) with arriving angles of 0 (desired user), -0.4, and 0.3 radians, shown in Fig. 5.8. Notice that when the number of interfering users is  $N < 3$ , the algorithm automatically steers the beam in the desired direction and places nulls on the interferences.

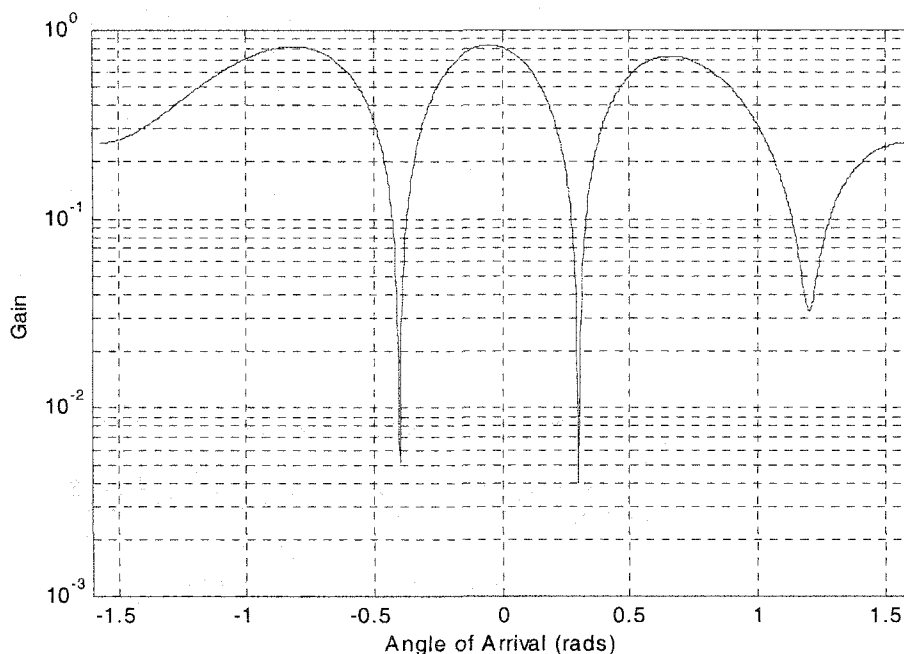


Fig. 5.8. Array beam pattern using DMI for three-user system with arriving angles of 0 (desired user), -0.4, and 0.3 radians.

### B. Beam pattern with $N = 3$

We consider a four-user system ( $N = 3$ ), with arriving angles of 0 (desired user), 0.3, -0.4, and 0.6 radians as shown in Fig. 5.9. Notice that when  $N = 3$ , the algorithm also automatically places nulls on the interferences.

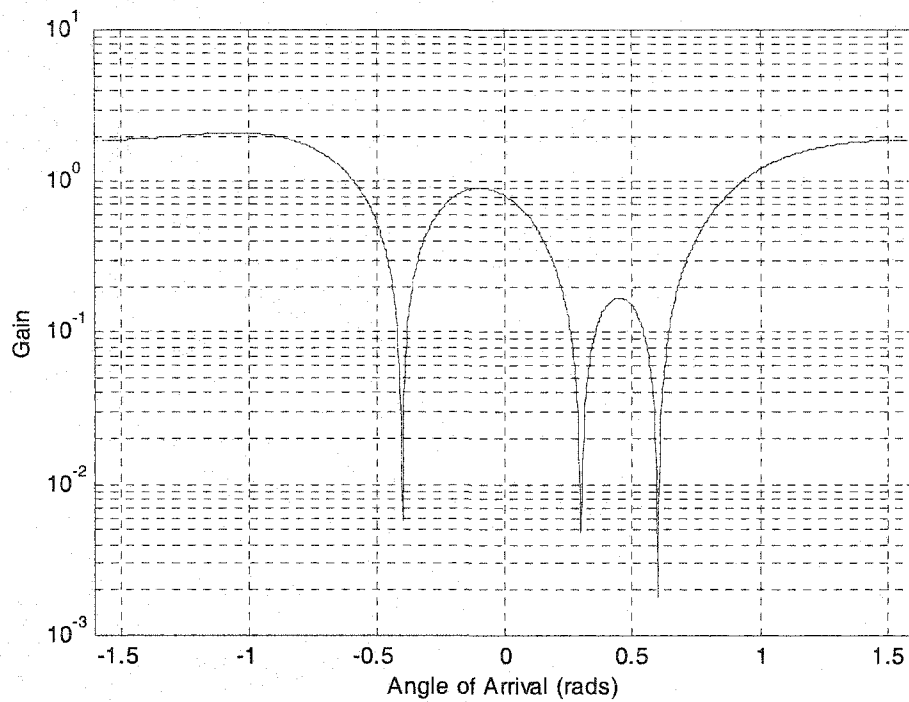
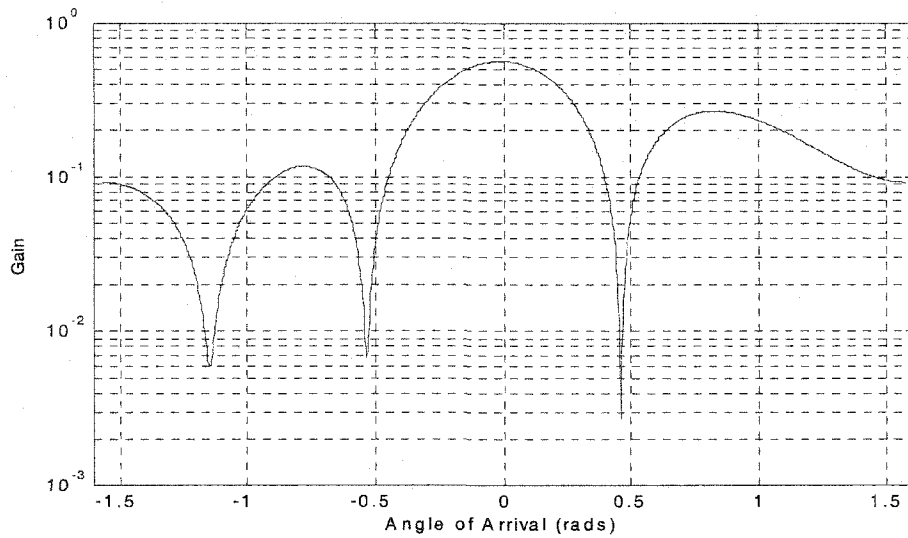


Fig. 5.9. Array beam pattern using DMI for four-user system with arriving angles of 0 (desired user), -0.4, 0.3, and 0.6 radians.

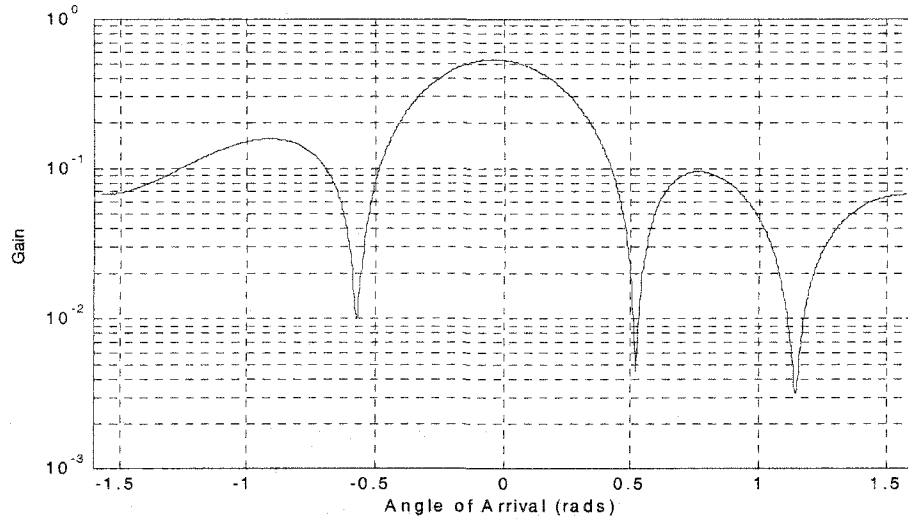
### C. Beam pattern with $N > 3$

The element spacing of a four-element linear array for the TD-SCDMA system is  $d = \lambda/2$ , which means only up to three array beam pattern nulls can be adjusted for array operation. Then what will happen when  $N > 3$ ? We consider two systems with five and eight users.

First we consider a five-user system ( $N = 4$ ), with arriving angles of 0 (desired user), 0.3, -0.4, 0.6, and -0.7 radians as shown in Fig. 5.10(a). Then we consider an eight-user system with arriving angles of 0 (desired user), 0.3, -0.4, 0.6, -0.7, 0.8, -0.9, and 1.0 radian as shown in Fig. 5.10(b). Notice that in Fig. 5.10 when  $N > 3$ , the algorithm can still automatically steer the beam in the desired direction (preserving the main-lobe around the angle of 0 radians), but does not place nulls on the interferences. Further, we can see that interference signal suppression is obtained by reducing side-lobe levels in the directions of the interference sources. Actually, none of the three nulls is at the interfering user's angle. This agrees with the theoretical analysis that the  $N$ -element linear array has  $N - 1$  degrees of freedom so that up to  $N - 1$  array beam pattern nulls can be independently adjusted for array operation.



(a) Five-user system with arriving angles of 0 (desired), 0.3, -0.4, 0.6, and -0.7 radians.



(b) Eight-user system with arriving angles of 0 (desired user), 0.3, -0.4, 0.6, -0.7, 0.8, -0.9, and 1.0 radian.

Fig. 5.10. Array beam pattern using DMI for five and eight-user system.

### 5.3.2 Performance Comparison

For performance evaluation with an antenna array, we do simulations of a multi-user system with the following numbers of interfering users  $N < 3$ ,  $N = 3$ , and  $N > 3$ . First we consider a two-user system ( $N < 3$ ) with the desired user located at angle 0 and the interference user at  $0.25\pi$  radians. We compare the performance with and without the antenna array, as shown in Fig. 5.11 under one path channel model. Then we do a four-user system simulation with the desired user located at angle 0 radians and the interference users at  $\{0.25\pi, -0.25\pi, 0.5\pi\}$  radians. Finally, we also considered an eight-user system simulation with desired user located at angle 0 radian and the interference users at  $\{0.25\pi, -0.25\pi, 0.5\pi, -0.5\pi, 0.75\pi, -0.75\pi, 0.9\pi\}$  radians. The performance comparison for a four and eight-user system simulation is shown in Fig. 5.12. We can see from the results that

- The performance gain is about 6 dB with a DMI smart antenna algorithm.
- With an array the four-user and eight-user systems perform about the same.
- Without an array the four-user system works better than the eight-user system, as expected because of less interference.

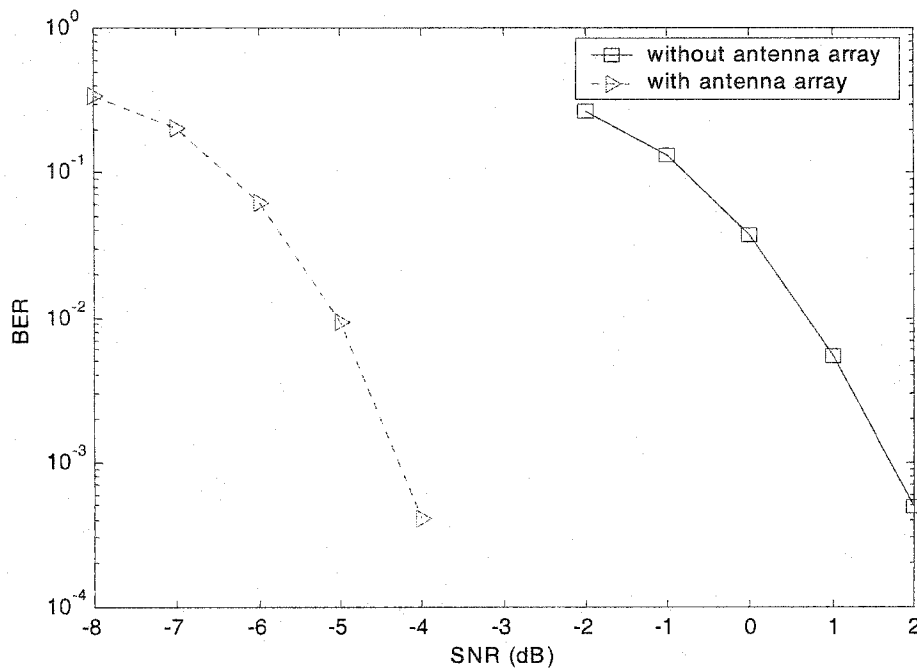


Fig. 5.11. Performance of two-user TD-SCDMA system with an antenna array.

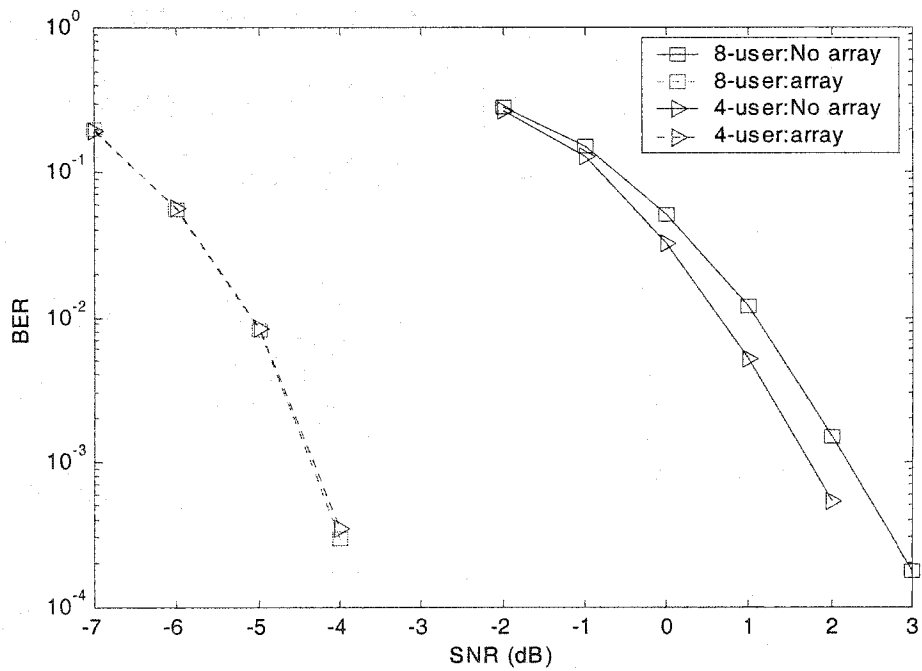


Fig. 5.12. Performance of a four and eight-user TD-SCDMA system with an antenna array.

## 5.4 Discussion and Conclusion

The linear array at base station with four equispaced omni-directional antenna elements can greatly improve the performance of a multi-user TD-SCDMA system by suppressing the noise sources including the interfering signal, while simultaneously enhancing the desired signal reception. The operation of this adaptive array can be easily visualized in terms of the array beam patterns. Interference signal suppression is obtained by appropriately steering beam pattern nulls and reducing side-lobe levels in the directions of the interference sources. The desired signal reception is maintained by preserving desirable main-lobe features.

For the TD-SCDMA system with array element spacing  $d = \lambda/2$ , only up to three nulls of the array beam pattern can be adjusted for array operation. When the number of interfering users  $N \leq 3$ , the algorithm automatically places nulls on the interferences. When the number of interfering users  $N > 3$ , the algorithm is not able to place nulls on the interferences, but reduces side-lobe levels in the directions of the interference sources. In both situations, the algorithm automatically steers the beam in the desired direction to enhance the desired signal reception. From the performance simulation results, we also can see that even though when the number of interfering users is  $N > 3$ , the beam pattern does not have nulls on the interferences, the performance still improves because of the reduction in side-lobe levels. In both situations, the performance improvement provided by the antenna array is about 6 dB.

## Chapter 6

### Conclusions

Third generation (3G) mobile systems are currently being deployed worldwide, and can satisfy the ever-increasing demand for high-speed data transmission. TD-SCDMA is one of the 3G systems. Among all the 3G systems being proposed, the advantages of TD-SCDMA lie in their outstanding spectrum efficiency, low transmission power, low cost, and flexibility for asymmetric traffic.

TD-SCDMA is unique in its uplink synchronization technique. The need for synchronization can be traced to the usage of the OVSF codes. It was shown that while for some pairs of codes the performance loss due to time misalignment is small, for some pairs there even exists a very small gain, but for other pairs it is very sensitive to small time shifts. For the system to meet performance specifications, synchronization is necessary. This can be achieved using standard techniques without introducing significant performance losses. The spreading OVSF codes used in this standard are the main reason for the need for uplink synchronization. These codes were selected because they preserve the orthogonality property in the same timeslot while using different spreading factors.

SCDMA techniques possess inherent protection against coherent interference since the orthogonal spreading OVSF codes are used. However, after going through a mobile wireless communications channel, which is characterized by time-varying multi-path channel fading, the signals lose their orthogonality property. This leads to a performance loss due to the increased cross correlation. The RAKE receiver and the MMSE receiver can compensate for this loss. As for RAKE receivers, the MMSE-based RAKE receiver always outperforms the cross-correlation based RAKE receiver, and there is about 1-dB difference between the MMSE-based RAKE receiver and the ideal RAKE receiver with known channel coefficients. Even though the cross-correlation based RAKE receiver can exclude noise-only paths, it does not always improve the performance since it cannot distinguish paths with separation less than 1 chip. On the other hand, the MMSE-based RAKE receiver always improves the performance. For the MMSE receivers, the channel equalizer does improve the performance for some channels, but not for others. The fractionally spaced equalizer outperforms the fully spaced equalizer, and the half-chip rate performs very close to the quarter-chip rate. The multi-path spread  $T_m$  of the channel is not large enough compared to the chip duration and the RAKE receiver has difficulty distinguishing these paths. This is the limitation of the RAKE receiver.

System performance can be improved greatly using antenna array system, which can enhance the detection and reception of desired signals and suppress interference. A linear array at the base station with four equispaced omni-directional antenna

elements were shown to improve the performance of multi-user TD-SCDMA systems. Operation of adaptive array can be understood in terms of array beam patterns. Interference signal suppression is achieved by appropriately positioning beam pattern nulls and reducing side-lobe levels in the directions of interference sources. Signal reception is maintained by preserving desirable main-lobe features. For the TD-SCDMA system with array element spacing  $d = \lambda/2$ , only up to three nulls of the array beam pattern can be adjusted for array operation. When the number of interfering users is  $N \leq 3$ , the algorithm automatically places nulls on the interferences. When the number of the interfering users is  $N > 3$ , the algorithm does not place nulls on the interferences, but reduces side-lobe levels in the directions of the interference sources. In both situations, the algorithm automatically steers the beam to optimize signal reception. From performance simulation, we also can see that even though when the number of interfering users is  $N > 3$ , the beam pattern does not have nulls on the interferences, performance still improves. This is because of the enhancing in main-lobe level. In both situations, the performance improvement is about 6 dB.

## References

- [1] J. Wang, F. Adachi, P. W. Baier, J. S. Lehnert, W. E. Stark, and M. B. Pursley, "Guest editorial wide-band CDMA I," *IEEE J. Select. Areas Commun.*, vol. 18, pp. 1341-1343, Aug. 2000.
- [2] S. Li, "TD-SCDMA radio transmission technology for IMT-2000," CATT Proposal to ITU for G3 RTT, Draft V.0.4, Sept. 1998.
- [3] S. Li and W. Chen, "SCDMA WLL system," (Feb. 2001). [Online] Available: [http://www.telecomn.com/english/china\\_comm/FOCUS4\\_9905.htm](http://www.telecomn.com/english/china_comm/FOCUS4_9905.htm).
- [4] S. Li, "The TD-SCDMA standard in IMT-2000," (Nov. 2000). [Online] Available: [http://www.telecomn.com.cn/gb/china\\_comm/Focus3\\_9912.htm](http://www.telecomn.com.cn/gb/china_comm/Focus3_9912.htm).
- [5] L. B. Milstein, "Wideband code division multiple access," *IEEE J. Select. Areas Commun.*, vol. 18, pp. 1352-1385, Aug. 2000.
- [6] H. Holma, S. Heikkinen, O. Lehtinen, and A. Toskala, "Interference considerations for the time division duplex mode of the UMTS terrestrial radio access," *IEEE J. Select. Areas Commun.*, vol. 18, pp. 1386-1393, Aug. 2000.
- [7] S. Sarkar, T. Chen, G. Leung, L. Blessent, and E. Tiedemann, "Cdma2000 reverse link: design and system performance," in *Proc. IEEE 52th Veh. Technol. Conf.*, 2001, pp. 2713-2719.
- [8] W. S. Wong and E. S. Sousa, "Performance optimization of single frequency broadcast systems in FDD-CDMA cellular bands for wireless multimedia services," in *Proc. IEEE 52th Veh. Technol. Conf.*, 2001, pp. 2728-2735.

- [9] S. Lim, C. H. Yoo, and S. Kim, "Performance evaluation of beamforming using pilot channel in cdma2000 reverse link," in *Proc. IEEE 53rd Veh. Technol. Conf.*, spring 2001, pp.2740-2744.
- [10] K. Satp, M. Abe, K. Horiguchi, H. Sugimoto, and T. K. Ren, "Evaluation of a turbo decoder performance on the cdma2000 reverse link," in *Proc. IEEE 51st Veh. Technol. Conf.*, Spring 2000, Tokyo, pp. 415 -419
- [11] M. Vollmer, M. Haardt, and J. Gotze, "Comparative study of joint-detection techniques for TD-CDMA based mobile radio systems," *IEEE J. Select. Areas Commun.*, vol. 19, pp. 1461-1475, Aug. 2001.
- [12] O. Prator, C. Unger, A. Zoch, and G. P. Fettweis, "Impact of channel estimation on the 3GPP-TD-CDMA," in *IEEE Global Telecommunications Conf.*, vol. 6, 2001, pp. 3365-3369.
- [13] G. Yang, C. Li, and J. Hu, "TD-SCDMA: way to the future," *IEEE Vehicular Technology Society News*, pp. 13-18, Aug. 2002.
- [14] H. Chen, C. Fan, and W. W. Lu, "China's perspectives on 3G mobile communications and beyond: TD-SCDMA technology," *IEEE Wireless Commun.*, pp. 48-59, Apr. 2002.
- [15] S. Kang, Z. Qiu, Y. Xiao, and S. Li, "Performance of active codes detection algorithms for the downlink of TD-SCDMA system," in *Proc. IEEE Int. Symp. Circuits Systems*, 2002, pp. I-613-I-616.

- [16] S. Kang, Z. Qiu, and S. Li, "The effect of channel estimation errors on joint detection algorithms in TD-SCDMA system," in *Proc. Int. Conf. Info-tech and Info-net*, 2001, pp. 303-308.
- [17] S. Li and J. Li, "TD-SCDMA standardization and prototype development," in *Fifth Asia-Pacific Conf. Commun. and Fourth Optoelectronics Commun. Conf.*, 1999, p. 1715.
- [18] S. Li, "Key technologies in SCDMA wireless access," in *Proc. Asia-Pacific Microwave Conf.*, 1997, pp. 169-172.
- [19] H. Lou, "Implementing the Viterbi algorithm," *IEEE Signal Processing Magazine*, vol. 12, pp. 42-52, Sept. 1995.
- [20] G. Yang, "Physical channels and mapping of transport channels," CWTS-WG1, TS C102, V3.3.0, Sept. 2000.
- [21] J. Zhang, "Multiplexing and channel coding," CWTS-WG1, TS C103, V3.1.0, Sept. 2000.
- [22] M.C. Jeruchim, P. Balaban, and K.S. Shanmugan, *Simulation of Communication System*. New York, NY: Plenum Press, 1992, pp. 344-350.
- [23] S. Li, "Radio transmission and reception," CWTS-WG1, TS C401, V3.2.0, Sept. 2000.
- [24] P. Dent, G.E. Bottomley, and T. Croft, "Jakes fading model revisited," *Electronics Letters*, vol. 29, pp. 1162-1163, June 1993.
- [25] W. C. Jakes, Jr., *Microwave Mobile Communications*. New York, NY: John Wiley & Sons, 1974.

- [26] R. F. W. Coates, G. J. Janacek, and K. V. Lever, "Monte Carlo simulation and random number generation," *IEEE J. Select. Areas Commun.*, vol. 6, pp. 58-66, Jan. 1988.
- [27] G. D. Forney, Jr., "Maximum-likelihood sequence detection in the presence of Intersymbol interference," *IEEE Trans. Inform. Theory*, vol. 18, pp. 363-378, May 1972.
- [28] M.R.G. Butler, S. Armour, P.N. Fletcher, A.R. Nix, and D. R. Bull, "Viterbi decoding strategies for 5 GHz wireless LAN systems" in *Proc. IEEE 54th Veh. Technol. Conf.*, 2001, pp. 77-81.
- [29] J.K. Holmes, *Coherent Spread Spectrum Systems*. New York, NY: John Wiley & Sons, Inc., 1982.
- [30] G. Yang, "Physical layer procedure," CWTS-WG1, TS C105, V3.2.0, Sept. 2000.
- [31] R. C. Dixon, *Spread Spectrum Systems*, 2nd ed.. New York, NY: John Wiley & Sons, Inc., 1984.
- [32] A. Wautier, J. Dany, C. Mourot, and V. Kumar, "A new method for predicting the channel estimate influence on performance of TDMA mobile radio systems" *IEEE Trans. Veh. Technol.*, vol. 44, pp. 594-602, Aug. 1995.
- [33] J. G. Proakis, *Digital Communications*, 3rd ed.. Singapore: McGraw-Hill, 1995.
- [34] G. Chen, X. Yu, and J. Wang, "Adaptive channel estimation and dedicated pilot power adjustment based on the fading-rate measurement for a pilot-aided

- CCDMA system" *IEEE J. Select. Areas Commun.*, vol. 19, pp. 132-140, Jan. 2001.
- [35] M. R. Baissas and A. M. Sayeed, "Pilot-based estimation of time-varying multipath channels for coherent CDMA Receivers", *IEEE Trans. Signal Processing*, vol. 50, pp. 2037-2049, Aug. 2002.
- [36] M. H. Hayes, *Statistical Digital Signal Processing and Modeling*. New York, NY: John Wiley & Sons, Inc., 1996, pp.33-34.
- [37] R. A. Monzingo and T. W. Miller, *Introduction to Adaptive Arrays*. New York, NY: John Wiley & Sons, Inc., 1980.
- [38] J. Liu, Y. Yuan, L. Xu, R. Wu, Y. Dai, Y. Li, L. Zhang, M. Shi, and Y. Du, "Research on smart antenna technology for terminals for the TD-SCDMA system", *IEEE Commun. Magazine*, vol. 41, pp. 116-119, June 2003.
- [39] E. Mitjana, X. Song, L. Lu, M. Haardt, C. Gessner, G. Lehmann, and M. Vollmer, "Performance of smart antenna in TD-SCDMA system", in *International Conf. on Commnu. Technol. Proc.*, 2000, pp. 152-155.
- [40] Q. Wu and X. Xiao, "Intelligent antenna arrays for the TD-SCDMA uplink", in *Proc. International Conf. On Signal Processing*, 2002, pp. 25-28.